

CHANNEL CHARACTERIZATION FOR BROADBAND POWERLINE COMMUNICATIONS

By

CHRISPIN TSHIKOMBA MULANGU



A Thesis Submitted in Fulfillment of the Academic Requirements for the Degree of Doctor of Philosophy in the School of Engineering: Electrical, Electronic and Computer Engineering, University of KwaZulu-Natal.

2014

Supervision:

PROFESSOR T.J.O. AFULLO, Pr. Eng., R. Eng. (Kenya), PhD.

PROFESSOR N.M. IJUMBA, Pr. Eng., R. Eng. (Kenya), R. Eng. (Tanzania), C. Eng., PhD.

As the candidate's supervisor, I have approved this thesis for submission.

Signed:.....

Date:.....

Preface

The research work in this thesis was done by Chrispin Tshikomba Mulangu, under the supervision of Professor Dr. Thomas J. O. Afullo and Professor Dr. Nelson M. Ijumba in the school of Electrical, Electronic and Computer Engineering at the University of KwaZulu-Natal, Durban, South Africa. The work was sponsored by ESKOM South Africa as part of the HVDC Centre at the University of KwaZulu-Natal.

The work performed in this thesis has been published in various fora, among them, PIERS 2012 conference in Malaysia, the IEEE-APC 2012 conference in Cape Town and, at ICET 2013 conference, Los Angeles, USA. Also, part of the research has been published in the transactions of the SAIEE Africa Research Journal and another part submitted for publication in the transaction of the IERI.

The author certifies that this thesis represents his own original and unaided work except where specifically indicated in the text and that it has not been submitted to any other university for degree purposes.

Acknowledgments

I wish to express my sincere gratitude to my supervisors Professor Dr. Thomas J. O. Afullo and Professor Dr. Nelson M. Ijumba, for their supervision and inspiration at the University of KwaZulu-Natal.

I also wish to thank all those who reviewed this thesis and suggested substantial improvements, most notably Mr. Peter Akuon and Mr. Abraham Nyete.

I also wish to express my sincere appreciation to my family, especially my dear wife, Suzanne Buki and lovely children, Christelle Mulangu and Elie Mulangu, and those who love and care for me.

Finally, I am thankful to the Almighty God who has given me strength and wisdom to pursue this dream.

Declaration

I, **Chrispin Tshikomba Mulangu**, declare that

1. The research reported in this thesis, except where otherwise indicated, is my original research.
2. This thesis has not been submitted for any degree or examination at any other university.
3. This thesis does not contain other persons' data, pictures, graphs or other information, unless specifically acknowledged as being sourced from other persons.
4. This thesis does not contain other persons' writing, unless specifically acknowledged as being sourced from other researchers. Where other written sources have been quoted, then:
 - a. Their words have been re-written but the general information attributed to them has been referenced
 - b. Where their exact words have been used, then their writing has been placed in italics and inside quotation marks, and referenced.
5. This thesis does not contain text, graphics or tables copied and pasted from the Internet, unless specifically acknowledged, and the source being detailed in the thesis and in the references sections.

Signed

.....

Date

.....

Abstract

The main limiting factor in broadband powerline communications is the presence of impedance discontinuities in the wired channel. This phenomenon is present in both outdoor and indoor powerline communication (PLCs) channels. It has been established that the impedance of the electrical loads and line branching are the main causes of impedance discontinuities in PLC channel networks.

Accurate knowledge of the expected impedances of the corresponding discontinuity points would be vital in order to characterize the channel for signal transmission. However, the PLC channel network topologies lead to different branching structures. Additionally, the existence of a myriad of electrical loads, whose noise and impedance vary with frequency, are a motivation for a rigorous design methodology in order to achieve a pragmatic channel model.

In order to develop such a channel model, an approach similar to the one applied in radio propagation channel modeling is adopted, where specific attenuation determined at a point is used in predicting the attenuation for the entire power cable length. Therefore, the powerline is modeled with the assumption of a randomly spread multitude of scatterers in the vicinity of the channel with only a sufficient number of impedance discontinuity points. The line is considered as a single homogeneous element with its length divided into a grid of small areas with dimensions that range from 0.5 to 3 mm. Thus, each small area transmits an echo and the forward scattered response gets to the receiver. With this approach, point specific attenuation along the line is proposed and used to derive the channel transfer function.

Measurement results show that both the analytical specific attenuation model developed in this work and the channel transfer function are feasible novel ideas in PLC channel network characterization. It is seen from the measurements that the signal attenuation is directly proportional to the number of branches, and this is in line with the findings of previous researchers.

A comparison between the measured values and the simulation results of the frequency response shows a very good agreement. The agreement demonstrates applicability of the models in a practical environment. Thus we conclude that the models developed do not require knowledge either of the link topology or the cable models but requires an extensive measurement campaign.

Table of Contents

Preface	i
Acknowledgments.....	ii
Abstract.....	iv
Table of Contents.....	v
List of Symbols.....	vii
List of Figures.....	viii
List of Tables	xii
1 Introduction.....	1
1.1 Problem formulation.....	2
1.2 Motivation and Objectives.....	2
1.3 Outline of the thesis.....	3
1.4 Contributions	4
1.5 Publications in Journal and Conference Proceedings	5
2 Propagation Mechanism and Characteristics in PLC Channels	6
2.1 Introduction	6
2.2 Propagation Mechanism	6
2.3 Transmission line Discontinuities and Signal Attenuation.....	6
2.3.1 Transmission Line Parameters	7
2.3.2 Signal Attenuation.....	11
2.3.3 Refractivity of a Metal	16
2.3.4 Theory of Dielectric Material.....	16
2.3.5 Scattering parameters	17
2.4 PLC Channel Characteristics.....	20
2.4.1 Multipath Characteristics	20
2.5 PLC Channel Noise Modeling.....	23
2.6 Modulation Techniques	25
2.6.1 Single- Carrier Modulation	25
2.6.2 Spread Spectrum Modulation.....	26
2.6.3 Multi Carrier Modulation.....	26
2.7 Coding Schemes	27
2.8 Powerline Communications Standard	28
2.9 Chapter Conclusion	29
2.10 References	29
3 Modeling of Broadband Powerline Communication Channels.....	33
3.1 Introduction	33

3.2	Transmission Line Parameters.....	34
3.3	Transfer channel Function.....	36
3.4	Proposed Transfer Function.....	40
3.5	Chapter Conclusion	45
3.6	References	45
4	Semi-empirical Model for Indoor Broadband Powerline Communication Channels	47
4.1	Introduction	47
4.2	Scattering Points Size Distribution for Indoor Broadband PLC Channels.....	47
4.2.1	Multipath Propagation Model	48
4.2.2	Scattering Points Approximation Model.....	52
4.3	Estimation of Specific Attenuation due to Scattering Points for Broadband PLC Channels	
	57	
4.3.1	Specific Attenuation Model and Optimization.....	57
4.4	Phase shift Due to Number of Branching Nodes in the PLC Channels.....	65
4.5	Frequency Response for PLC Channel.....	70
4.6	Chapter Conclusion	74
4.7	References	75
5	Channel Model Validation Using Measurements	79
5.1	Introduction	79
5.2	Measurement Devices.....	79
5.2.1	Network Analyzer	79
5.2.2	Oscilloscope	80
5.2.3	Signal Generator.....	80
5.3	Measurement Techniques	81
5.3.1	Input Impedance Measurements.....	81
5.3.2	Attenuation Measurements.....	92
5.4	Analysis of Powerline Attenuation Models.....	93
5.5	PLC Channel Network Measurements	95
5.6	Chapter Conclusion	97
5.7	References	97
6	Conclusions and Recommendation for Future Work.....	98
6.1	Conclusions	98
6.2	Recommendation for Future work.....	100
	References.....	101

List of Symbols

Symbols	Meaning
θ	Angle
γ	Attenuation coefficient
k	Wave number in free space
f	Frequency
a	Complex dielectric constant of water
b	Relative permittivity
L	Inductor
C	Capacitor
λ	Wavelength
R	Resistor
T	Transmission coefficient
v	Terminal velocity of raindrops
c	Speed velocity of the light
Γ	Reflection coefficient
Z_0	Characteristic impedance
Z_L	Load impedance
Z_{in}	Input impedance
α	Propagation constant
$H(f)$	Channel transfer function

List of Figures

Figure 2.3-1 Two-conductor transmission line.	6
Figure 2.3-2 Propagation of the electromagnetic wave into different dielectric media.	7
Figure 2.3-3 Equivalent-circuit model of transmission line section	8
Figure 2.3-4 The reflection coefficient of the coaxial transmission line.	11
Figure 2.3-5 Specific attenuation of coaxial copper line with inner conductor radius $a = 0.8$ mm and a copper outer conductor of inner radius b varies from 1.5 to 10 mm.	13
Figure 2.3-6 Specific attenuation of coaxial copper line with inner conductor of radius $a = 2$ mm and a copper outer conductor of radius b varying from 4.5 to 10 mm.	13
Figure 2.3-7 Specific attenuation of coaxial copper line with inner conductor of radius $a = 2$ mm and an outer conductor of radius b varying from 4.5 to 10 mm.	14
Figure 2.3-8 Specific attenuation for coaxial transmission line with inner conductor of radius $a = 0.8$ mm and an outer conductor of radius $b = 2$ mm.	14
Figure 2.3-9 Specific attenuation for coaxial transmission line with inner conductor of radius $a = 2$ mm and an outer conductor of radius $b = 4.5$ mm.	15
Figure 2.3-10 Specific attenuation for transmission line, [Ahola, (2002)].	15
Figure 2.3-11: Complex dielectric	17
Figure 2.3-12: S-parameter measurements with the network analyzer	19
Figure 2.4-1 Block diagram of PLC channel	21
Figure 2.4-2: Powerline network with multiple branches at a single node [Anatory <i>et al.</i> , (2005)].	22
Figure 2.4-3 PLC channel transfer function, [Zimmerman <i>et al.</i> , (2002)].	22
Figure 2.5-1 Generations of background and corona noise	24
Figure 2.6-1 Spread spectrum system digital communication system	26
Figure 2.6-2 OFDM Transceiver process	27
Figure 2.7-1 Block diagram of ARQ system	28
Figure 2.7-2 Interleaving method for burst error channel	28
Figure 2.7-3 Block diagram of OFDM with BCM	28
Figure 3.1-1 Two-conductor distributed transmission line.	34
Figure 3.3-1 One tap cable multipath signal propagation	36
Figure 3.3-2 Multipath model from [Zimmerman <i>et al.</i> , (2002)]	38
Figure 3.3-3 Series resonant circuit	39
Figure 3.3-4 Transfer function of the series resonance model	39
Figure 3.3-5 Simulation network model	40
Figure 3.4-1 Transfer function model	41
Figure 3.4-2 Phase response of the transmission Line	42
Figure 3.4-3 Amplitude response with a and D varying	43

Figure 3.4-4 Phase response with r and D varying	43
Figure 3.4-5 Amplitude response with resistance loads increased.....	44
Figure 3.4-6 Phase response with resistance loads increased.	44
Figure 4.2-1 PLC channel network analysis	49
Figure 4.2-2 Reflection and transmission at a branching node.....	50
Figure 4.2-3 Variance and mean of Y with $Z_o = 50\Omega$ and $de = U - 25\Omega, 25\Omega$	52
Figure 4.2-4 Indoor PLC channel model	52
Figure 4.2-5 Scattering point size distribution for PLC channel with twenty branching nodes	54
Figure 4.2-6 Scattering point size distribution for PLC channel with ten branching nodes	54
Figure 4.2-7 Scattering point size distribution for PLC channel with fifteen branching nodes.....	55
Figure 4.2-8 Scattering point size distribution for PLC channel with four branching nodes.....	56
Figure 4.2-9 Probability density function of scattering points for PLC channel	56
Figure 4.3-1 Comparison of estimated specific attenuation model for PLC channel	59
Figure 4.3-2 Regression fitting for specific attenuation in dB.....	59
Figure 4.3-3 Optimized model for specific powerline attenuation.	60
Figure 4.3-4: Model for 4 and 6 branching nodes at 10-100 MHz.	61
Figure 4.3-5: Models for 5 and 10 branching nodes at 10-100 MHz.....	61
Figure 4.3-6: Models for 13 and 21 branching nodes at 10-100 MHz.....	62
Figure 4.3-7: Models for 4 and 8 branching nodes at 10-100 MHz.....	62
Figure 4.3-8 Specific attenuation at 10, 16.7 and 21.5 MHz with number of branching nodes	64
Figure 4.3-9 Specific attenuation at 27.8, 35.9 and 46.4 MHz with number of branching nodes	64
Figure 4.3-10 Specific attenuation at 59.9, 77.4 and 100 MHz with number of branching nodes	65
Figure 4.4-1 Specific Phase shift for scattering points (2 branching nodes) using lognormal distribution.....	66
Figure 4.4-2 Specific Phase shift for scattering points (8 branching nodes) using lognormal distribution.....	67
Figure 4.4-3 Specific Phase shift for scattering points (15 branching nodes) using lognormal distribution.....	67
Figure 4.4-4 Specific Phase shift for scattering points (20 branching nodes) using lognormal distribution.....	68
Figure 4.4-5 Specific Phase shift for scattering points (8 branching nodes) using lognormal distribution.....	68
Figure 4.4-6 Phase shift for scattering points using lognormal distribution	69
Figure 4.5-1: Two-port network model of two-wire transmission line.....	70
Figure 4.5-2: A Cascade two-port networks model of two-wire transmission line	70
Figure 4.5-3: Network configuration for two-wire transmission line	71
Figure 4.5-4: Network configuration for two-wire transmission line equivalent	72

Figure 4.5-5: Network configuration for two-wire transmission line as ABCD matrix	72
Figure 4.5-6: The frequency response of a 40 m two-wire transmission with two-branch of length 5 m each terminated by a load of 50Ω	72
Figure 4.5-7: The frequency response of a 40 m two-wire transmission with two open-circuited branches of length 5 m each.....	73
Figure 4.5-8: The phase shift of a two-wire transmission with two open-circuited branches of length 5 m each.	73
Figure 5.1-1 Schematic diagram for measurements.....	79
Figure 5.1-2 System setup for measurements	79
Figure 5.3-1: PVC insulated flexible cable.....	81
Figure 5.3-2: Measurements setup using network analyzer.....	82
Figure 5.3-3: Measurement set up of the propagation speed of transmission line	84
Figure 5.3-4: Snap shot of the sending end (yellow) and receiving end (blue) of the signal in a 100 m long transmission line	84
Figure 5.3-5: Net input impedance measured when the cable end is open-circuited as a function of frequency in the range of 10 – 100 MHz.	85
Figure 5.3-6: Complex input impedance measured when the cable end is open as a function of frequency in the range of 10 – 100 MHz.	85
Figure 5.3-7: Input impedance measured when the cable end is short-circuited as a function of frequency in the range of 10 – 100 MHz. the length of the cable is 100 m.	86
Figure 5.3-8: The real (continuous) and imaginary (dashed) of input impedance measured when the cable end is short-circuited as a function of frequency in the range of 10 – 100 MHz; the length of the cable is 100 m.	86
Figure 5.3-9: Characteristic impedance of the cable as a function of frequency in the range of 10 – 100 MHz; the length of the cable is 100 m.	87
Figure 5.3-10: Phase of the characteristic impedance of the cable as a function of frequency in the range of 10 – 100 MHz; the length of the cable is 100 m.	87
Figure 5.3-11: Network configuration	88
Figure 5.3-12: Input impedance measured when the cable end is open as function of frequency in the range of 10 – 100 MHz; the length of the cable is 40 m with bridge taped with 5 m branch each.....	89
Figure 5.3-13: Input impedance measured when the cable end is open as function of frequency in the range of 10 – 100 MHz; the length of the cable is 40 m with bridge taped with 5 m branch each.....	89
Figure 5.3-14: Input impedance measured when the cable end is short-circuited as a function of frequency in the range of 10 – 100 MHz; the length of the cable is 40 m with bridge taped with 5 m branch each.	90

Figure 5.3-15: The real (continuous) and image (dashed) of input impedance measured when the cable end is short-circuited as function of frequency in the range of 10 – 100 MHz; the length of the cable is 40 m with bridge taped with 5 m branch each. 90

Figure 5.3-16: Characteristic impedance of the cable as function of frequency in the range of 10 – 50 MHz; the length of the cable is 40 m with bridge taped with 5 m branch each..... 91

Figure 5.3-17: Phase of the characteristic impedance of the cable as function of frequency in the range of 10 – 100 MHz; the length of the cable is 40 m with bridge taped with 5 m branch each..... 91

Figure 5.3-18: The specific attenuation of two configuration transmission line. 92

Figure 5.4-1: The specific attenuation of a transmission line without branches, calculated from measured data and estimated model derived from scattering model. 94

Figure 5.4-2: The specific attenuation of a transmission line with two branching points, calculated from measured data and estimated model derived from scattering model. The length of the cable is 40 m with bridge taped with 5 m branch each. 94

Figure 5.5-1: Channel transfer response with 50Ω load at the branches end..... 95

Figure 5.5-2: Channel transfer response with the branches open-circuited. 96

Figure 5.5-3: The phase shift of a bridged tap with the branches open-circuited. 96

List of Tables

Table 2.3-1 Distributed parameters of two-wire and coaxial transmission lines	10
Table 2.4-1 Parameters of the multipath model.	22
Table 3.3-1 parameters of the multipath model [Zimmerman <i>et al.</i> , (1999), Zimmerman <i>et al.</i> , (2002)].	37
Table 3.3-2 Set of parameters of series resonance circuits model	40
Table 3.3-3 Set of parameters of proposed model	40
Table 4.2-1 Model parameters	56
Table 4.3-1 Attenuation parameters for different number of branching nodes at 10 – 100 MHz.....	63
Table 4.3-2 Power law attenuation parameters for different frequencies.	63
Table 4.4-1 Phase Shift parameters for frequency range of 10-100 MHz	69
Table 5.3-1: Measured S_{11} data	83

Chapter One

Introduction

The powerline communication (PLC) channel exhibits unfavorable transmission properties. It is characterized by a frequency selective transfer function, attenuation that increases with length and frequency, and severe narrowband interference [Biglieri, (2003)]. In order to overcome these difficulties, a lot of effort has been undertaken to characterize and model the powerline channel [Meng *et al.*, (2004), Barmada, (2006)]. A complete understanding of the behaviour of broadband PLC channel is important when setting up the channel transmission lines or when simulating the performance of such complicated communication technologies [Amirshahi, (2006), R'oka, (2008), Katayama *et al.*, (2006), Mujčić *et al.*, (2004)]. Today, several models have been proposed for characterizing the PLC channel like those in [Dlh'a'n and Farka' (2008), Guillet *et al.*, (2009)]. An interesting approach was introduced in [Zimmermann *et al.*, (2002), Philipps, (2000)] that describes the PLC channel by its multipath behaviour.

The multipath propagation of the powerline communication channel (PLC) arises from the presence of several branches and impedance mismatches that cause multiple reflections. Each path is comprised of scattering points that are reflected a specific number of times at specific points of discontinuity along its routes. The scattering points are located where impedance mismatch occurs. In such models, not only the desired signal, but also one or more delayed and attenuated versions of the transmitted signal get to the receiver. Further, a detailed discussion of scattering points' spatial allocation, in which path amplitude distributions and path arrival time distributions are proposed to follow the lognormal distribution for different number of branches is well presented in Papaleonidopoulos *et al.*, (2003). In their investigation, Güzelgöz *et al.*, (2011) established that the first arrival path is distinguishable from the other paths in the sense that it experiences less reflection and less attenuation along its propagation path, giving it a favorable position with regard to signal detectability. In their study, the statistics of the first arrival path were initially investigated. It was shown that the first arrival path can be defined by Log-Normal probability density function (PDF). It was also observed that the mean of the approximating Log-Normal variable decreases with an increasing number of branches between transmitter and receiver, while its variance increases. The same observation was made when the maximum number of branches that extend out of a branching node is increased.

However, despite these unique approaches, the PLC channel remains an important research area of interest because the existing solutions to the inherent problems need to be refined further, and as such,

we still do not have a universally accepted model of the PLC channel like the COST models for the mobile radio channel.

In this thesis, the first arrival path is investigated and the powerline is modeled as one single element with its length divided into a grid of small areas with dimensions ranging from 0.5 to 3 mm where each small area transmits an echo and the forward scattered response gets to the receiver. The scattering point is assumed to be small and spherical in shape, and then Mie scattering technique is applied in order to determine the point specific attenuation based on forward scattering.

1.1 Problem formulation

The powerline network is the most ubiquitous network compared to similar networks in the world, and that it reaches every socket in the household, which makes the installation of the PLC channel system relatively cost-effective, since no additional wire infrastructure needs to be laid out. However, as research shows, the PLC channel presents a very harsh environment for high-frequency communication signals, with three critical channel parameters: noise, impedance, and attenuation, being highly unpredictable and variable in time, frequency, and location. Therefore a concerted effort is needed to accurately characterize the powerline. In addition, while some effort has been made to model the low and medium voltage lines, mainly from a narrowband perspective, further inputs are needed to characterize broadband powerlines. This work therefore seeks to investigate and develop general models for the channel transfer function from a broadband point of view.

Thus, for this study, the questions that face the researcher are:

- (i) What is the appropriate model for the PLC medium that takes into account the channel loading, attenuation, multipath, and impedance mismatch?
- (ii) How would this model be used to determine an optimal communications option for PLC?

1.2 Motivation and Objectives

The majority of people in developing countries stay in rural areas where some of them have access to electricity; but majority of them do not have access to the internet. Deployment of dedicated mobile and wireless network communications is not economically feasible because the return on investment is low for service providers due to the low purchasing power of the populace which is mainly poor. Therefore, the PLC channel would be a more attractive technology in such a case since its convenient outlets (power sockets) serve as connection ports from each room in a home, office or factory for the services such as internet, video conference, Voice over IP, Video streaming, and E-commerce

connectivity, etc. Additionally, the fact that this communication technology uses the existing power network renders it very cost effective.

PLC technologies are grouped into narrowband PLC (NB-PLC), operating usually below 500 kHz, and broadband PLC (BB-PLC), operating usually at frequencies above 1.8 MHz, [Galli *et al.*, (2011)]. Recent studies are focused mainly on the frequencies up to 30 MHz, [Zimmermann, (2002)]. This is due to the increasing demand for broadband data transmission, which utilizes BB-PLC. This is the focus of the current research work where we propose models that are valid up to 100 MHz.

In summary, this research involves the evaluation and testing of the foregoing models with the desire of developing a universal PLC channel model with the following objectives:

1. To investigate and develop the transfer characteristics for powerline communications at low voltages.
2. To use simulations to verify existing models and develop similar models by varying different parameters in those models.
3. To use analytical models to verify the simulation models.
4. To verify the analytical models with measurements on a test bed.

1.3 Outline of the thesis

The outline of the thesis is as follows:

Chapter one starts with a short introduction touching on the progress made in PLC technology channel modelling, challenges facing the PLC channel and the characteristics of the transmission medium. This is then followed by the problem formulation, motivation and objectives and finally the outline of the thesis.

Chapter two gives a summary of the propagation mechanism in PLC channels. This revolves around the PLC channel characteristics; which includes the multipath characteristics and the path amplitude statistics of PLC channels. This chapter focuses on reflection and transmission coefficients at the branching and termination points, attenuation in PLC channels and analysis of the first arrival path.

In Chapter three, we focus more on developing a new PLC channel model and investigating the impact of load, line length and diameter of the transmission line on the channel transfer function over the frequency range of 1-20 MHz.

In Chapter four, we investigate the influence of the number of branching nodes and then provide a unique scattering distribution model for PLC channels. The model is based on the validation of the assumption of a randomly spread multitude of scatterers in the vicinity of the channel that only requires a sufficient number of impedance discontinuity points. We consider the line as one single element, and its length is divided into a grid of small areas or scattering points with dimensions ranging from 0.5 to 3 mm. We also study Mie scattering theories and their application to branching nodes in order to determine the attenuation in PLC channels and a power law model is proposed where only the number branching nodes is needed to estimate the specific attenuation.

In Chapter five, measurements are done to ascertain the accuracy of the models developed in Chapter three and four, and come up with an appropriate channel transfer function using different ‘live’ power network configurations.

1.4 Contributions

As the title of the thesis implies, “*Channel Characterization for Broadband Powerline Communications*,” all the chapters in this thesis are aimed at making significant contributions to this topic. Below is the summary of the significant contributions in this work:

- Proposition of empirical PLC channel attenuation models that depict the number of nodes dependency on attenuation along a powerline network path per length operating at different frequencies up to 100 MHz.
- Development of PLC channel attenuation model along the powerline network with a number of branching nodes. The PLC channel model is regarded as comprising of scattering points or small area scattering based on the validation of the assumption of a randomly spread multitude of scatterers in the vicinity of the channel that only requires a sufficient number impedance discontinuity points. But due to the fact that the requirement of having a minimum number of branches within two branching nodes has to be met, the PLCs power law model is proposed.
- Formulation of theoretical PLC channel attenuation models for the prediction of specific attenuation on powerline network first arrival path link from the scattering properties of scattering points or small area scattering and Log-normal small area scattering size distribution models. This is achieved by utilizing the Mie scattering theory for metallic spheres on the scattering points, and mathematical integration analysis. Furthermore,

preliminary study of scattering points' size distribution for different number of branching nodes for PLC channels has also been investigated.

1.5 Publications in Journal and Conference Proceedings

The work in this thesis has been published in the following conference proceedings and journals:

1. C. T. Mulangu, T. J. O. Afullo and N. M. Ijumba, "Modelling of Broadband Powerline Communication Channels," *SAIEE*, Vol. 102 (4) December 2011.
2. C. T. Mulangu, T. J. O. Afullo and N. M. Ijumba, "Semi-empirical Model for Broadband Powerline Communication Channels," submitted to *IERI Journal of Information Engineering Letters*, accepted for publication, June. 2013.
3. C. T. Mulangu, T. J. O. Afullo and N. M. Ijumba, "Attenuation Model for Indoor Multipath Broadband PLC Channels," *IEEE-ICEAA*, Cape town, South Africa, September, 2012, ISBN: 978-1-4673-0405-4.
4. C. T. Mulangu, T. J. O. Afullo and N. M. Ijumba, "Novel Approach for Powerline Communication channel Modelling," *IEEE Power & Energy Society, POWER AFRICA 2012*, Johannesburg, South Africa, July, 2012, ISBN: 978-1-4673-2548-6.
5. C. T. Mulangu, T. J. O. Afullo and N. M. Ijumba, "Scattering Points Size Distribution for Indoor Broadband PLC Channels," *PIERS, Malaysia, March, 2012*, ISSN: 1559-9450.
6. C. T. Mulangu, T. J. O. Afullo and N. M. Ijumba, "Estimation of Specific Attenuation due to Scattering Points for Broadband PLC Channels," *PIERS, Malaysia, March, 2012*, ISSN: 1559-9450.

Chapter Two

Propagation Mechanism and Characteristics in PLC Channels

2.1 Introduction

In this chapter, we focus on the propagation mechanisms of the signal through the powerline network at high frequency range, such as: reflection, transmission and scattering. In PLC channels, a transmitted signal travelling from the source to the receiver suffers reflections at impedance discontinuities along its path to the receiver. Therefore, only part of the signal that is sent at the transmitter reaches the receiver. This signal comprises of different signal components that are delayed and attenuated in different degrees.

2.2 Propagation Mechanism

Reflection occurs when the propagating wave impinges upon an object whose dimensions are very large compared to its wavelength. Güzelgöz *et al.*, (2011) observed that the first arrival path signal is easily distinguishable from the other paths in the sense that it experiences less reflection and less attenuation along its propagation path, giving it a favorable position in terms of detectability. On the contrary, scattering is one of the most difficult phenomena to analyze in closed form and it usually occurs when the propagating wave impinges upon an object whose dimensions are very small compared to the wavelength of the propagating signal.

2.3 Transmission line Discontinuities and Signal Attenuation

The main loss mechanisms of low voltage power cables at signal frequencies used in powerline communications are dielectric losses, resistive losses and coupling losses. The radiation losses are significant if the separation of the conductors is an appreciable fraction of the wavelength (Tomasini, 2001). Figure 2.3-1 below shows a generator of voltage v_s and internal impedance R_s connected to the load impedance Z_L through a length d of a transmission line of characteristic impedance Z_0 . We wish to determine the voltage v_L and current at the load in terms of the generator voltage.

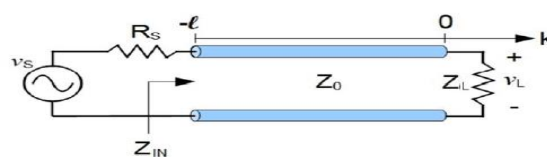


Figure 2.3-1 Two-conductor transmission line.

2.3.1 Transmission Line Parameters

A transmission line can be defined as any structure or medium that guides electromagnetic (EM) waves from one location to another. The transmission line has two conductors carrying current to support an EM wave, which is transverse electromagnetic (TEM) or quasi-TEM mode. For the TEM mode:

$$\vec{E} = -Z_{TEM} \hat{a}_n \times \vec{H}, \quad \vec{H} = \frac{1}{Z_{TEM}} \hat{a}_n \times \vec{E}, \quad \text{and} \quad Z_{TEM} = \eta = \sqrt{\frac{\mu}{\epsilon}}. \quad (2.1)$$

where, E is electric field, H is magnetic field and Z is the impedance of the wave.

The current and the EM wave have different characteristics. When an EM wave propagates into different dielectric media, partial reflection and partial transmission will occur as shown in Figure 2.3-2. And, this propagation obeys Snell's law, that is:

$$\frac{\sin \theta_t}{\sin \theta_i} = \frac{n_1}{n_2} = \frac{v_{p2}}{v_{p1}} = \frac{\eta_2}{\eta_1} = \sqrt{\frac{\epsilon_{r1}}{\epsilon_{r2}}} \quad \text{and} \quad \theta_i = \theta_r. \quad (2.2)$$

where θ_i is the angle subtended between the incident ray and the normal to the interface, and θ_t is the angle subtended between the refracted ray and the normal to the interface. The quantities n_1 and n_2 are termed as the refractive indices of media 1 and 2, respectively. The law of refraction follows directly from the fact that the speed v with which light propagates through a dielectric medium is inversely proportional to the refractive index of the medium. Now, v_{p1} is the speed of light in medium 1, whereas v_{p2} is the speed of light in medium 2. The refractive index n is rooted in the material relative permittivity ϵ_r . η_1 and η_2 are termed the wave impedance of media 1 and 2.

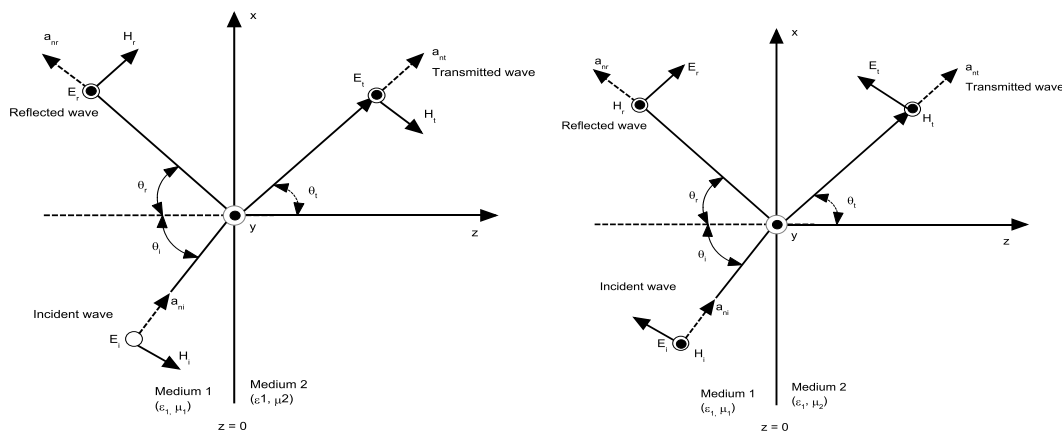


Figure 2.3-2 Propagation of the electromagnetic wave into different dielectric media.

The reflection coefficient: $\Gamma = \frac{E_{r0}}{E_{i0}}$ and the transmission coefficient: $\tau = \frac{E_{t0}}{E_{i0}}$ of EM waves can be expressed as follows for both perpendicular and parallel polarization:

In the case of perpendicular polarization,

$$\begin{cases} \Gamma_{\perp} = \frac{\eta_2 / \cos \theta_t - \eta_1 / \cos \theta_i}{\eta_2 / \cos \theta_t + \eta_1 / \cos \theta_i} = \frac{n_1 \cos \theta_i - n_2 \cos \theta_t}{n_1 \cos \theta_i + n_2 \cos \theta_t} = \frac{\sin(\theta_t - \theta_i)}{\sin(\theta_t + \theta_i)} \\ \tau_{\perp} = \frac{2\eta_2 / \cos \theta_t}{\eta_2 / \cos \theta_t + \eta_1 / \cos \theta_i} = \frac{2n_1 \cos \theta_i}{n_1 \cos \theta_i + n_2 \cos \theta_t} = \frac{2 \cos \theta_t \sin \theta_i}{\sin(\theta_t + \theta_i)} \end{cases} \quad (2.3)$$

In the case of parallel polarization,

$$\begin{cases} \Gamma_{\parallel} = \frac{\eta_2 \cos \theta_t - \eta_1 \cos \theta_i}{\eta_2 \cos \theta_t + \eta_1 \cos \theta_i} = \frac{n_1 / \cos \theta_t - n_2 / \cos \theta_i}{n_1 / \cos \theta_t + n_2 / \cos \theta_i} = \frac{\tan(\theta_t - \theta_i)}{\tan(\theta_t + \theta_i)} \\ \tau_{\parallel} = \frac{2\eta_2 \cos \theta_t}{\eta_2 \cos \theta_t + \eta_1 \cos \theta_i} = \frac{2n_1 / \cos \theta_t}{n_1 / \cos \theta_t + n_2 / \cos \theta_i} = \frac{2 \cos \theta_t \sin \theta_i}{\sin(\theta_t + \theta_i) \cos(\theta_t - \theta_i)} \end{cases} \quad (2.4)$$

In case of normal incidence,

$$\begin{cases} \Gamma_{\perp} = \Gamma_{\parallel} = \frac{\eta_2 - \eta_1}{\eta_2 + \eta_1} \\ \tau_{\perp} = \tau_{\parallel} = \frac{2\eta_2}{\eta_2 + \eta_1} \end{cases}, \text{ where } \eta_1 = \sqrt{\frac{\mu_1}{\epsilon_1}} \text{ and } \eta_2 = \sqrt{\frac{\mu_2}{\epsilon_2}} \quad (2.5)$$

The model parameters are derived from the equivalent-circuit model of a transmission line section so as to obtain the transfer function of the channel, as shown in Fig.2.3-3, and Equations (2.6) and (2.7) below.

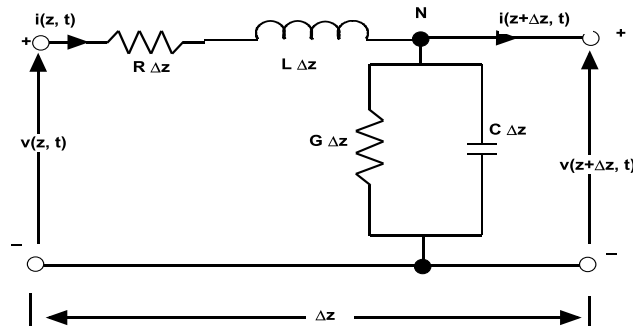


Figure 2.3-3 Equivalent-circuit model of transmission line section

The quantities $v(z,t)$, $v(z+\Delta z,t)$, $i(z,t)$ and $i(z+\Delta z,t)$ denote the instantaneous voltages and currents at locations z and $z+\Delta z$. R , L , G and C are the per unit length resistance (Ω/m), inductance (H/m), conductance (S/m) and capacitance (F/m), respectively.

Transmission line equations: In higher frequency range, the transmission line model is utilized to analyze EM power flow.

$$\left\{ \begin{array}{l} -\frac{v(z+\Delta z,t) - v(z,t)}{\Delta z} = Ri(z,t) + L \frac{\partial i(z,t)}{\partial t} \\ -\frac{i(z+\Delta z,t) - i(z,t)}{\Delta z} = Gv(z,t) + C \frac{\partial v(z,t)}{\partial t} \end{array} \right. \Rightarrow \left\{ \begin{array}{l} -\frac{\partial v}{\partial z} = Ri + L \frac{\partial i}{\partial t} \\ -\frac{\partial i}{\partial z} = Gv + C \frac{\partial v}{\partial t} \end{array} \right. \quad (2.6)$$

If we set $(z,t) = \text{Re}[V(z)e^{j\omega t}]$, $i(z,t) = \text{Re}[I(z)e^{j\omega t}]$, then, we can write the following:

$$\left\{ \begin{array}{l} -\frac{dV}{dz} = (R + j\omega L)I(z) \\ -\frac{dI}{dz} = (G + j\omega C)V(z) \end{array} \right. \Rightarrow \left\{ \begin{array}{l} \frac{d^2V(z)}{dz^2} = (R + j\omega L)(G + j\omega C)V(z) = \gamma^2V(z) \\ \frac{d^2I(z)}{dz^2} = (R + j\omega L)(G + j\omega C)I(z) = \gamma^2I(z) \end{array} \right. \quad (2.7)$$

where, the propagation coefficient γ is given by:

$$\gamma = \alpha + j\beta = \sqrt{(R + j\omega L)(G + j\omega C)} \quad (2.8)$$

where α is the attenuation coefficient and β is the phase coefficient.

This implies that :

$$V(z) = V_0^+ e^{-\gamma z} + V_0^- e^{\gamma z}, \quad I(z) = I_0^+ e^{-\gamma z} + I_0^- e^{\gamma z} \quad (2.9)$$

and, the characteristic impedance is given by:

$$Z_0 = \frac{V_0^+}{I_0^+} = -\frac{V_0^-}{I_0^-} = \frac{R + j\omega L}{\gamma} = \frac{\gamma}{G + j\omega C} = \sqrt{\frac{R + j\omega L}{G + j\omega C}} \quad (2.10)$$

Table 2.3-1 below shows the distributed parameters of two-wire and coaxial transmission lines. Here, μ and σ are the permeability and conductivity of the metal conductors, respectively; a and b are the radius of the central and outer conductors for the coaxial line, respectively; D is the separation distance between conductors.

The voltage reflection coefficient of the load impedance Z_L is given by:

$$\Gamma = \frac{Z_L - Z_0}{Z_L + Z_0} = |\Gamma|e^{j\theta_\Gamma}, \quad (2.11)$$

and the transmission coefficient by:

$$\tau = 1 + \Gamma \quad (2.12)$$

Figure 2.3-4 shows MATLAB simulations of the reflection coefficient of a coaxial transmission line of 100 m length in the frequency range 10 to 100 MHz.

In the case of a lossless and distortionless transmission line, the propagation speed of the electromagnetic wave v_p is given by:

$$v_p = \frac{1}{\sqrt{LC}} = \frac{1}{\sqrt{\mu_o \mu_{r,i} \epsilon_o \epsilon_{r,i}}} \quad (2.13)$$

Table 2.3-1 Distributed parameters of two-wire and coaxial transmission lines

Parameter	Two-wire line	Coaxial line	Units
R	$2 \left(\frac{R_s}{2\pi a} \right) = \frac{1}{\pi a} \sqrt{\frac{\pi f \mu}{\sigma}}$	$\frac{1}{2\pi} \left(\frac{1}{a} + \frac{1}{b} \right) \sqrt{\frac{\pi f \mu}{\sigma}}$	Ω/m
L	$\frac{\mu}{\pi} \cosh^{-1}(D/2a)$	$\frac{\mu}{2\pi} \ln(b/a)$	H/m
G	$\frac{\pi \sigma}{\cosh^{-1}(D/2a)}$	$\frac{2\pi \sigma}{\ln(b/a)}$	S/m
C	$\frac{\pi \epsilon}{\cosh^{-1}(D/2a)}$	$\frac{2\pi \epsilon}{\ln(b/a)}$	F/m

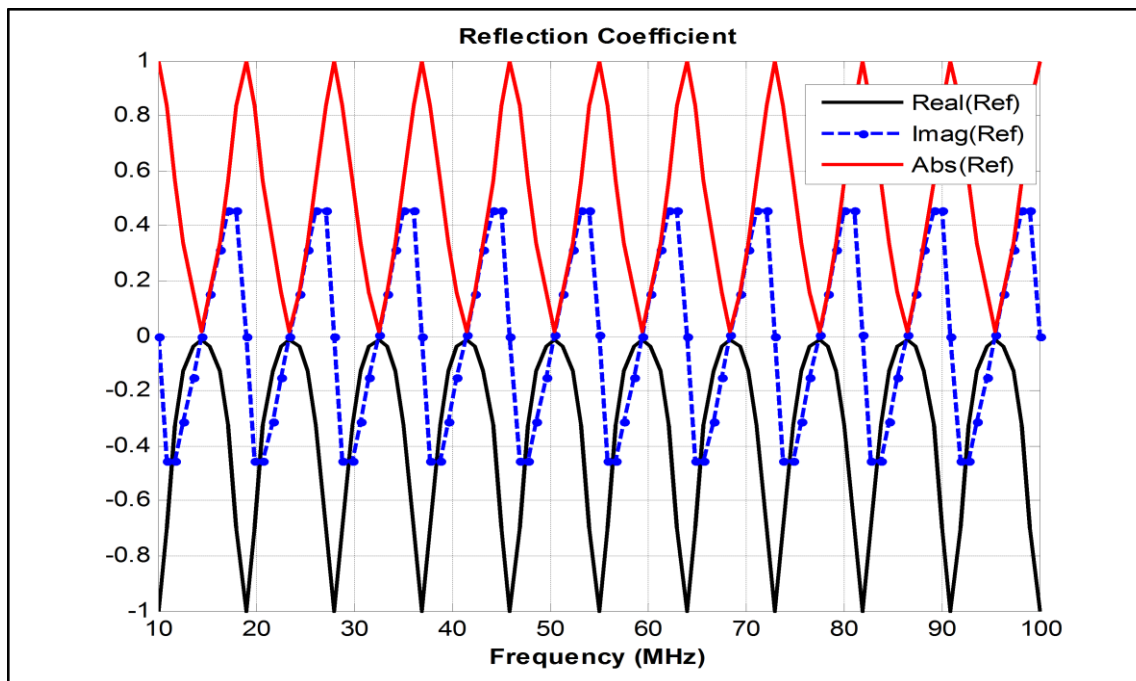


Figure 2.3-4 The reflection coefficient of the coaxial transmission line.

where both μ_o and ε_o are the permeability and permittivity of a vacuum respectively. The relative permeability μ_r and permittivity ε_r are the parameters of the insulation material of the transmission line. For PVC insulation, ($\varepsilon_r = 2.26$) and $v_p = 0.6c_0$, where, c_0 is the speed of the light.

The distribution of the current on the cross-sectional area of the conductor is described with a variable penetration or skin depth, δ , given by :

$$\delta = \frac{1}{\sqrt{\frac{1}{2} \omega \mu_0 \mu_{r,c} \sigma_c}} \quad (2.14)$$

where ω is the angular frequency of the signal propagating in the transmission line, $\mu_{r,c}$ is the relative permeability of the conductor material, and σ_c is the conductivity of the conductor material.

2.3.2 Signal Attenuation

Transmission line discontinuities are caused by mechanical connections, changes in cable type or load appliances and cause coupling losses. The amount of coupling losses depend, for example, on the topology of the distribution network, the signal frequency, the characteristics of the cabling and the characteristics of the devices connected to the distribution network. The resistive losses of the

conductor are caused by the finite conductivity of conductors. At high frequencies, the current is forced to flow on the surface of the conductor due to skin effect; the resistive losses increase as a function of frequency with the relation of $\sim\sqrt{f}$.

Dielectric losses occur in the insulation material. The polarised molecules inside the insulation material are synchronised to the frequency of the electric field. The friction between the molecules causes power losses each time the electric field changes polarity. In addition, the resistivity of the insulation material is finite. The existence of leakage currents in the insulation material also causes losses. The losses of the insulation material are expressed by the loss tangent or dissipation factor, $\tan\delta$.

Figures 2.3-5 and 2.3-6 below show the attenuation (in dB/m) versus the characteristic impedance of a coaxial transmission line using polyethylene ($\epsilon_r = 2.26$) as the dielectric medium, that has a solid copper inner conductor of radius $a = 2$ mm and a copper outer conductor of inner radius b . The outer conductor is much thicker than the skin depth, and the ratio b/a varies from 1.5 to 10 and negligible losses are assumed. The attenuation decreases as the characteristic impedance increases; and this is explained in Fig. 2.3-7 which shows that characteristic impedance increases when copper outer conductor of inner radius b varies from 4.5 to 10 mm. The attenuation is inversely proportional to the characteristic impedance. Fig. 2.3-8 and 2.3-9 show the attenuation as function of frequency. Fig. 2.3-8 shows the specific attenuation for coaxial transmission line with inner conductor of radius $a = 0.8$ mm and a copper outer conductor of inner radius $b = 2$ mm. The highest attenuation is 0.35 dB and the lowest is 0.245 dB whilst in Fig. 2.3-9, the specific attenuation for coaxial transmission line with inner conductor of radius $a = 2$ mm and a copper outer conductor of inner radius $b = 4.5$ mm, has the highest attenuation of 0.258 dB and the lowest of 0.23 dB. This shows that there is higher conductor attenuation for a cable with an inner conductor of radius $a = 0.8$ mm and a copper outer conductor of inner radius $b = 2$ mm, than for a cable of an inner conductor of radius $a = 2$ mm and a copper outer conductor of inner radius $b = 4.5$ mm.

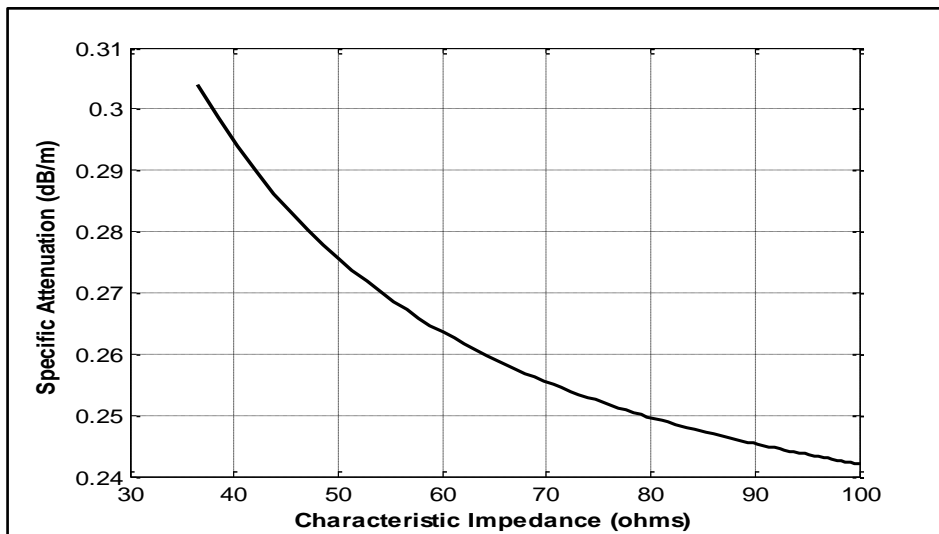


Figure 2.3-5 Specific attenuation of coaxial copper line with inner conductor radius $a = 0.8$ mm and a copper outer conductor of inner radius b varies from 1.5 to 10 mm.

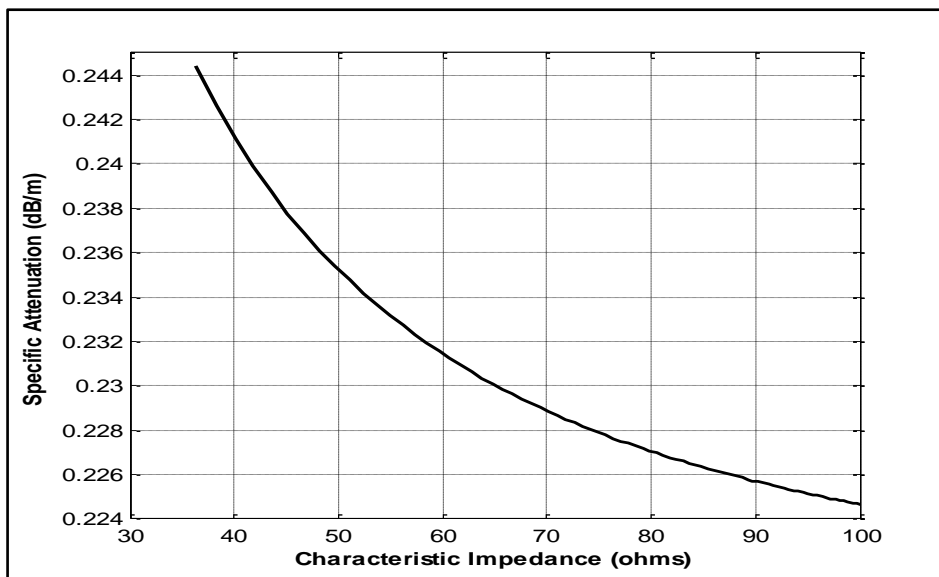


Figure 2.3-6 Specific attenuation of coaxial copper line with inner conductor of radius $a = 2$ mm and a copper outer conductor of radius b varying from 4.5 to 10 mm.

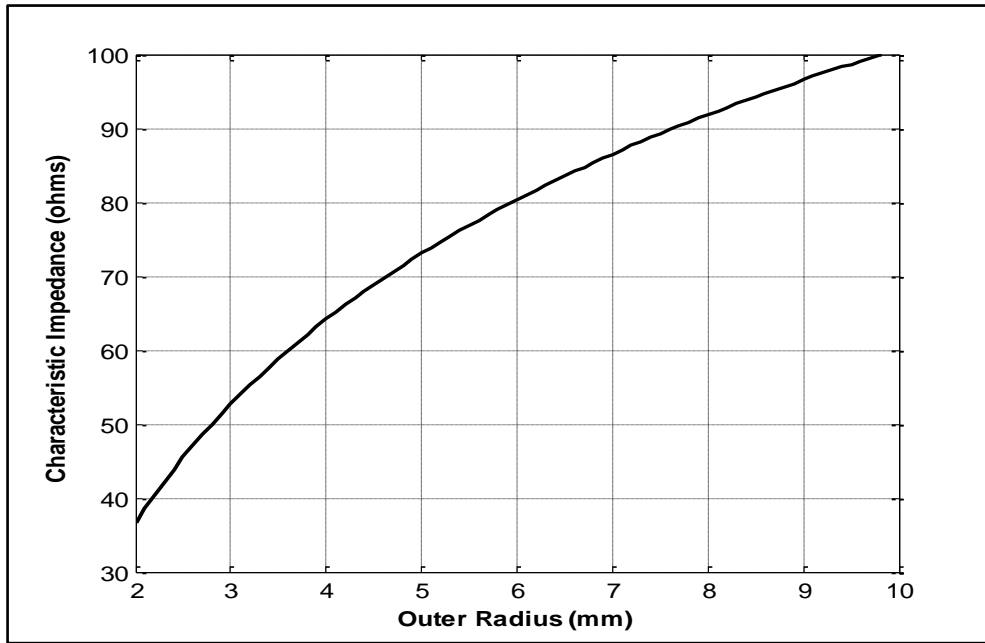


Figure 2.3-7 Specific attenuation of coaxial copper line with inner conductor of radius $a = 2$ mm and an outer conductor of radius b varying from 4.5 to 10 mm.

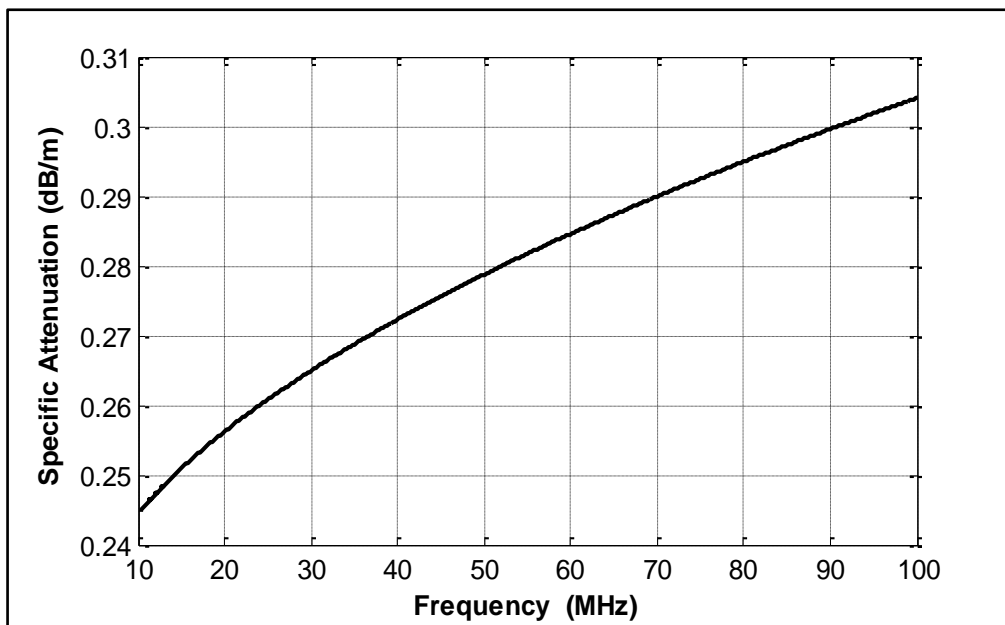


Figure 2.3-8 Specific attenuation for coaxial transmission line with inner conductor of radius $a = 0.8$ mm and an outer conductor of radius $b = 2$ mm.

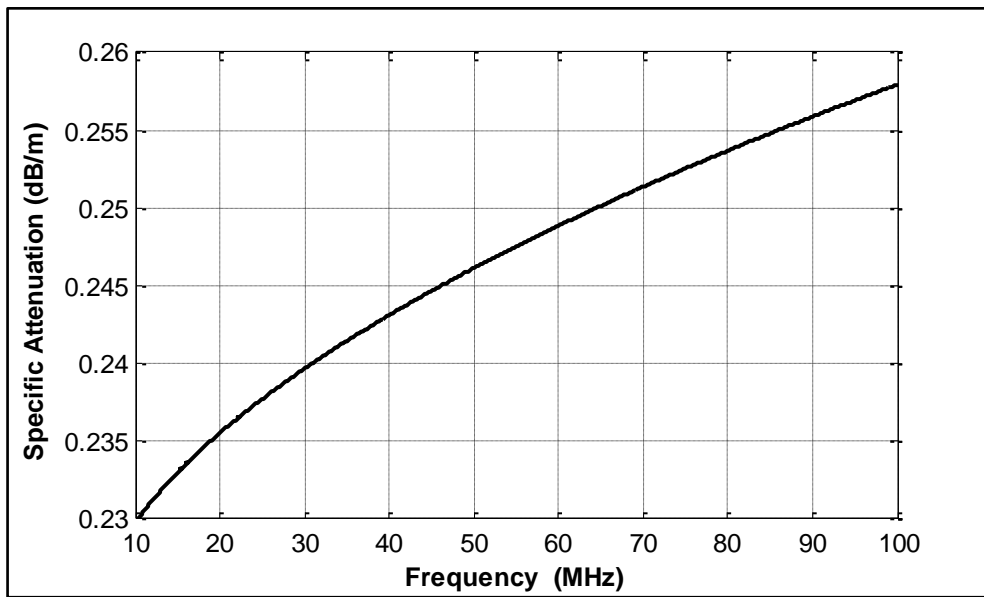


Figure 2.3-9 Specific attenuation for coaxial transmission line with inner conductor of radius $a = 2$ mm and an outer conductor of radius $b = 4.5$ mm.

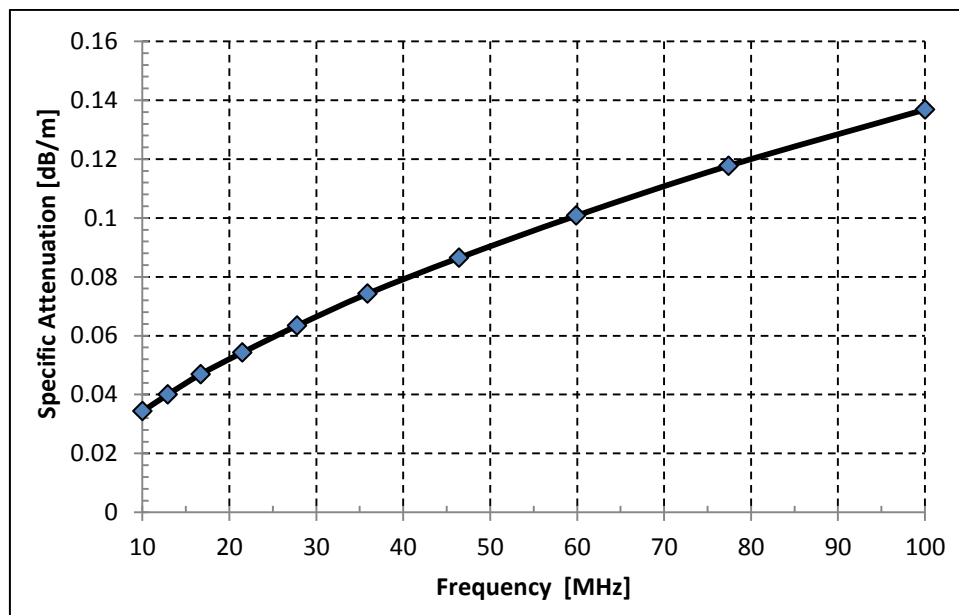


Figure 2.3-10 Specific attenuation for transmission line, [Ahola, (2002)].

Ahola, (2001) presented a formula for the specific attenuation as a function of frequency using the power curve fitting algorithm as shown in Fig. 2.3-10:

$$\alpha(f) = 0.5 * 10^{-6} f^{0.6} \quad (2.15)$$

where f is the frequency, [Hz].

2.3.3 Refractivity of a Metal

In a transmission line, the metal of complex electric permittivity $\epsilon = m_1^2$ is embedded in a dielectric medium of permittivity $\epsilon_2 = m_2^2$. A scattering point in this medium is illuminated by a plane wave of angular frequency $\omega = 2\pi c/\lambda = kc/m_d$ and $k = 2\pi/\lambda$ is the wave number, λ the wavelength in the medium. The refractive index with respect to the medium is given by:

$$m = \sqrt{\frac{\epsilon_1 \cdot \mu_1}{\epsilon_2 \mu_2}} \quad (2.16)$$

where, ϵ_1 and μ_1 are the permittivity and permeability of the metal; and ϵ_2 and μ_2 are the permittivity and permeability of the medium.

The complex refractive index $m(f)$, being a function of frequency f , is related to the complex relative dielectric permittivity $\epsilon(f)$ of metal at lower frequencies as given in Feynman *et al.*, (1964):

$$m(f) = \sqrt{\sigma/2\epsilon_0\omega} (1 - i) \quad (2.17)$$

where, σ is the electric conductivity of the conductor and ϵ_0 is the permittivity of the free space. At lower frequencies, from Equation (2.17), we observe that the real and imaginary parts of refractive index $m(f)$, have the same magnitude. With such a large imaginary part of $m(f)$, the wave is rapidly attenuated in the metal, [Feynman *et al.*, (1964)]. In the case of copper, for frequencies less than 10^{12} Hz (Plasma frequency), $\sigma = 5.76 \times 10^7 (\text{ohm} - \text{meter})^{-1}$, [Feynman *et al.*, (1964)].

2.3.4 Theory of Dielectric Material

The polyvinyl chloride (PVC) is the insulating material of choice for LV power cables. However, rubber or polyethylene is used for higher temperature grading needs in the insulation of power cables. The insulating and conducting materials have a critical influence on the power cable characteristics in the high frequency range. However, it is almost impossible to make any realistic and practical definition of the overall PVC dielectric characteristics, since they rely mainly on factors like the exact insulating material composition, frequency range of operation, temperature ranges and variations, etc, [Liu, *et al.*, (2001)].

The parameters of greatest interest are the conductivity, σ , and the permittivity, ϵ , since these govern the dielectric attenuation. Permittivity is a complex quantity, whereby:

$$\epsilon = \epsilon' - j\epsilon'' = \frac{D}{E}, \quad (2.18)$$

where D is the electric flux density, E the electric field strength, ϵ' is the dielectric constant, $\epsilon_0 (= 8.854191 \times 10^{-12} \frac{F}{m})$ is the permittivity of free space, ϵ'_r is the relative dielectric constant, $\epsilon'' = \epsilon_0 \epsilon''_r$ is the dielectric loss factor and ϵ''_r is the relative dielectric loss factor of the dielectric. The real and imaginary parts of the permittivity may be represented as a set orthogonal axes as in Fig. 2.3-11.

Dielectric loss can also be expressed in terms of the loss tangent, that is:

$$\tan\delta = \frac{\epsilon''}{\epsilon'} = \frac{\sigma}{\omega\epsilon'_r\epsilon_0} \quad (2.19)$$

According to Lin, (1991) the ϵ'_r of PVC is in the range of 3.49 – 3.41 for 10 MHz to 100 MHz. Dielectric losses of PVC insulation material are about 50-100 times larger than those of polyethylene (Harper, 1975).

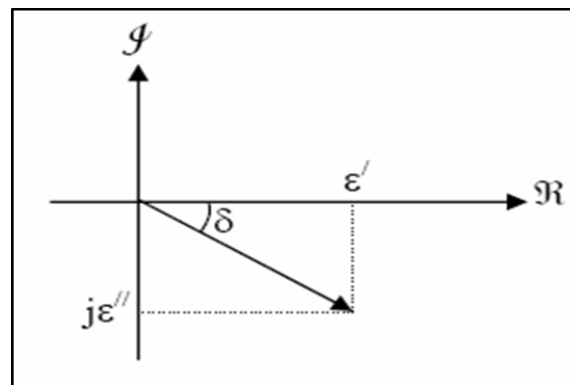


Figure 2.3-11: Complex dielectric

2.3.5 Scattering parameters

"Scattering parameters" or "S-parameters" are used in electrical engineering, electronic engineering, and communications systems engineering to describe the electrical behaviour of linear electrical networks when under various steady state stimuli by small signals. They are among a family of parameters used in electronics engineering, other examples being: Y-parameters, Z-parameters, H-parameters, T-parameters and ABCD-parameters. Although applicable at all frequencies, S-parameters are mostly measured and specified for networks operating at radio and microwave frequencies. For a generic multi-port network, it is assumed that all ports except the one or a pair under consideration are terminated with loads identical to the system impedance and each of the ports is allocated a number "n" ranging from 1 to N, where N is the total number of ports. For port n, the

associated S-parameter definition is in terms of incident and reflected 'power waves', a_n and b_n respectively. These power waves are normalised versions of the corresponding incident and reflected travelling voltage waves, V_n^+ and V_n^- respectively, in accordance with transmission line theory. They are related to the system impedance Z_0 , as given in the expressions below:

$$a_n = \frac{V_n^+}{\sqrt{Z_0}} \quad (2.20)$$

and,

$$b_n = \frac{V_n^-}{\sqrt{Z_0}} \quad (2.21)$$

For all ports of the entire network, the reflected power waves may be defined in terms of the S-parameter matrix and the incident power waves by the following matrix equation:

$$\begin{pmatrix} b_1 \\ b_2 \\ \vdots \\ b_n \end{pmatrix} = \begin{pmatrix} S_{11} & S_{12} & \dots & S_{1n} \\ S_{21} & S_{22} & \dots & \dots \\ \dots & \dots & \dots & \dots \\ S_{n1} & \dots & \dots & S_{nn} \end{pmatrix} \begin{pmatrix} a_1 \\ a_2 \\ \vdots \\ a_n \end{pmatrix} \quad (2.22)$$

The S-parameter matrix for the 2-port network is probably the most common and it serves as the basic building block for the higher order matrices. In this case the relationship between the incident, reflected power waves and the S-parameter matrix is given by:

$$\begin{pmatrix} b_1 \\ b_2 \end{pmatrix} = \begin{pmatrix} S_{11} & S_{12} \\ S_{21} & S_{22} \end{pmatrix} \begin{pmatrix} a_1 \\ a_2 \end{pmatrix} \quad (2.23)$$

Expanding the matrices into equations gives:

$$b_1 = S_{11}a_1 + S_{12}a_2 \quad (2.24)$$

and

$$b_2 = S_{21}a_1 + S_{22}a_2 \quad (2.25)$$

Each equation gives the relationship between the incident and reflected power waves at each of the networks ports 1 and 2 in terms of the network's individual S-parameters, S_{11} , S_{12} , S_{21} and S_{22} . If one considers an incident power wave a_1 at port 1, there may result from it waves exiting from either port 1 itself (b_1) or port 2 (b_2). However if, according to the definition of S-parameters, port 2 is terminated with a load (Z_0) identical to the system impedance then b_2 will be totally absorbed making a_2 equal to zero. Therefore, we have:

$$S_{11} = \frac{b_1}{a_1} \quad (2.26)$$

and

$$S_{21} = \frac{b_2}{a_1} \quad (2.27)$$

Similarly, if port 1 is terminated in the system impedance then a_1 becomes zero, giving:

$$S_{12} = \frac{b_1}{a_2} \quad (2.28)$$

and

$$S_{22} = \frac{b_2}{a_2} \quad (2.29)$$

If the 2-port network under consideration is a non-reciprocal device such as an amplifier operating at small signal levels in its linear region and ports 1 and 2 are the input and output respectively, each of the S-parameters is equal to the following common amplifier parameters:

- S_{11} : which is the input port voltage reflection coefficient
- S_{12} : which is the reverse voltage gain
- S_{21} : which is the forward voltage gain
- S_{22} : which is the output port voltage reflection coefficient

All such S-parameters are complex quantities so they are expressed in magnitude and phase and, in general, are dependent on frequency. Therefore the frequency must be defined together with the system impedance for S-parameter measurements across a device under test (DUT) as shown in Fig. 2.3-12 below.

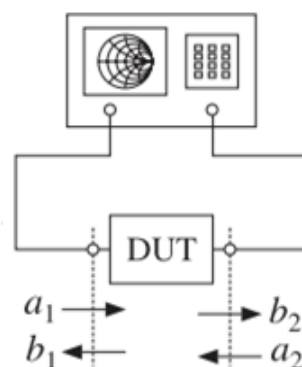


Figure 2.3-12: S-parameter measurements with the network analyzer

2.4 PLC Channel Characteristics

2.4.1 Multipath Characteristics

Several authors have addressed the issue of channel modeling for narrow-band and broadband powerline communications, for low, medium, and high voltage lines. The characterization of the PLC channel transmission environment focuses on the multi-path signal propagation, the signal attenuation, the noise scenario and electromagnetic compatibility.

Meng *et al.* (2004) presented a wonderful approach to develop the transfer characteristics of a broadband powerline communication channel in which the low voltage powerline is approximated as a transmission line with two intrinsic parameters, namely the characteristic impedance and the propagation constants for a lumped-circuit model. This model is tested against practical measurements conducted on existing powerlines. In an addition, Bermuda *et al.*, (2006) presented an innovative channel model for the broadband characterization of powerlines in the presence of time-varying loads. The model is characterized by taking into account both measured and geometrical channel characteristics, with the channel described by a two-port scattering matrix derived from a wavelet-based expansion of the input and output quantities. The upper and lower bounds for the channel response in the presence of varying loads are also derived, thus resulting in a statistical characterization of the channel. The proposed method can be used for both known and unknown or indeterminate network topologies.

In another input to multipath modelling, R'oka and Urminsk' (2008) presented experimental measurements for verification of the parametric model for PLC reference channels in the real PLC channel environment. The information presents a broad knowledge base for the design of the PLC channel modem that can be used for practical deployment of the PLC channel data transmission systems. Amirshahi and Kavehrad (2006) also presented a channel model suitable for multi-wire overhead medium voltage lines. The model is used to evaluate the multipath channel response and associated capacity limit in several power distribution grids for applications in broadband over PLC.

All in all, according to Biglieri (2003), the challenges that PLC channels face consists of investigating the power network's characteristics as a communication channel under the following study areas:

- (i) Frequency-varying and time-varying attenuation of the medium
- (ii) Dependence of the channel model on location, network topology and connected loads
- (iii) High inference due to noisy loads
- (iv) High nonwhite background noise

- (v) Various forms of impulse noise
- (vi) Electromagnetic compatibility (EMC) issues that limit available transmitted power.

Figure 2.4-1 is an illustration of what plagues the PLC channel. Biglieri (2003) and Chen and Chiueh (2002) observed that there is no universal PLC channel model that has been accepted like is with the case of COST models for mobile radio channels.

Having different paths or lengths and terminated loads tapered to the main path, the impedance of the PLC channel significantly varies with the frequency in the range of a few ohms to a few kilo-ohms. When assumed to be linear, the PLC channel presents notches due to reflections and cancellations caused by impedance mismatches, and as a consequence, the signal propagates in different ways. Therefore, the PLC channel is better presented as a multipath environment with frequency-selective attenuation. In addition, there is a change in the frequency response when an electrical device is switched on or off, thus the PLC channel is time-varying. Attenuation of the signal in a powerline consists of all the coupling losses which are very high in powerline in the range from 40dB/km to 100 dB/km resulting in a very low SNR at the receiver.

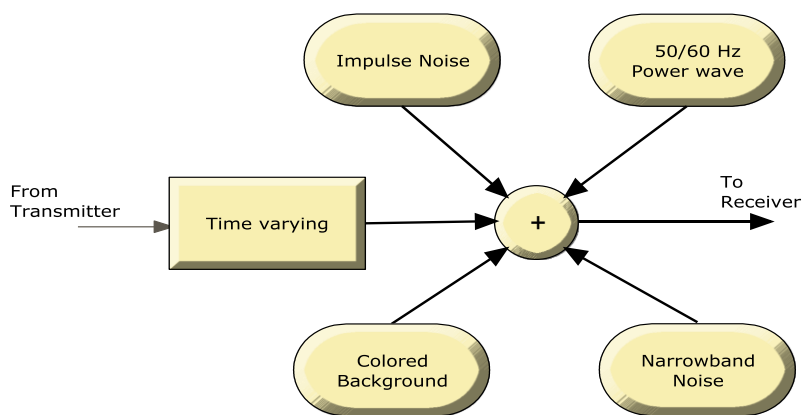


Figure 2.4-1 Block diagram of PLC channel

During the literature survey, we replicated some of the results obtained by the researchers mentioned above. Here we present the multipath model proposed by Zimmerman *et al.*, (2002) in Fig. 2.4-3 with four paths. Table 2.4-1 shows the parameters of the model.

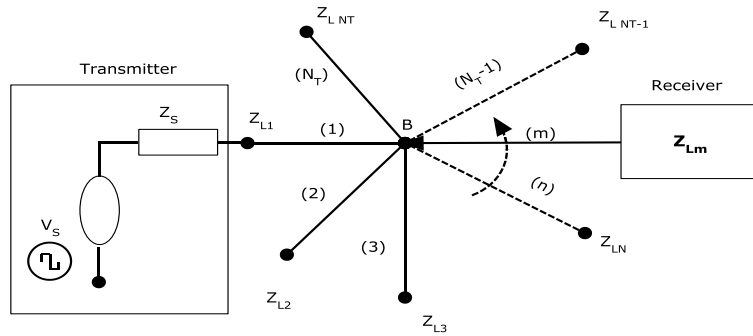


Figure 2.4-2: Powerline network with multiple branches at a single node [Anatory *et al.*, (2005)].

In Figure 2.4-2, NT is the total number of branches connected say at node ‘1’ and terminated in any arbitrary load. Let n, m, M and Lm , represent any branch number, any referenced (terminated) load, number of reflections (with total L number of reflections), respectively, [Anatory *et al.*, (2005)].

Table 2.4-1 Parameters of the multipath model.

Path No.	1	2	3	4
delay in μs	1.0	1.25	1.76	2.64
equivalent length in m	150	188	264	397
Weighting factor g_i	0.4	-0.4	-0.8	-1.5
$k = 0,5$	$a_0=0$		$a_0=8 \cdot 10^{-6}$	

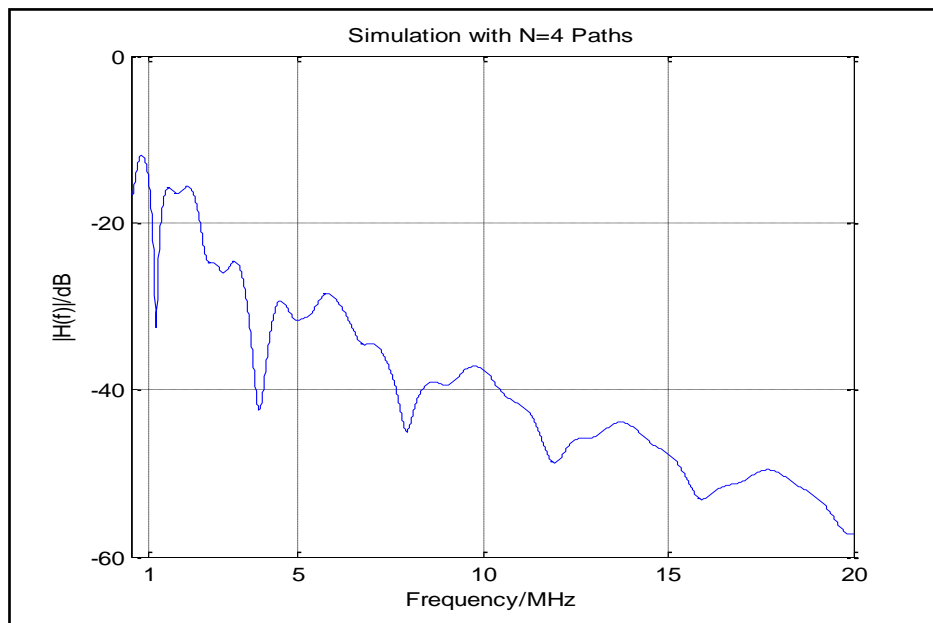


Figure 2.4-3 PLC channel transfer function, [Zimmerman *et al.*, (2002)].

2.5 PLC Channel Noise Modeling

The main sources of disturbance in the PLC channel environment are coloured background noise, narrow-band interference, and impulsive noise. The coloured background noise is caused by a summation of numerous noise sources with low powers. Its power spectral density (PSD) varies with frequency in the range 0 to 30 MHz, and significantly increases in the lower frequencies, and also with the time in terms of minutes or even hours (see for example R'oka and Urminsk' (2008)). Narrowband noise is caused by amplitude modulation (AM) radio broadcasts, and can thus be modelled using modulated sinusoids. There are three main types of impulsive noise [R'oka and Urminsk' (2008)]:

- Periodic impulsive noise asynchronous with the main frequency — caused by switching on and off of power supplies and AC/DC power converters. Its spectrum is a discrete line spectrum with a repetition rate in the range between 50 and 200 kHz.
- Periodic impulsive noise synchronous with the main frequency - caused by rectifiers located in the power supplies operating synchronously with the main cycle. Its PSD decreases with frequency and the repetition rate is 50 Hz to 110 Hz.
- Asynchronous impulsive noise - caused by impulses generated by the switching transient events in the network. It is considered as the worst noise in the PLC channel environment because of its magnitude that can easily reach several dB (even 50 dB and higher) over other noise types.

Katayama *et al.*, (2006) proposed a mathematically accurate model of narrowband powerline noise based on experimentation. The noise was expressed as a Gaussian process. The noise waveform generated with this model showed a good agreement with that of the actual measured noise.

Mujčić *et al.*, (2004) also presented an experimental modeling of corona noise over a 400 kV overhead powerline. The algorithm for measuring variations in the corona noise level was described on the basis of noise samples as shown in Fig. 2. 5-1. An appropriate computer model of the corona noise compliant with the measurement results was then proposed.

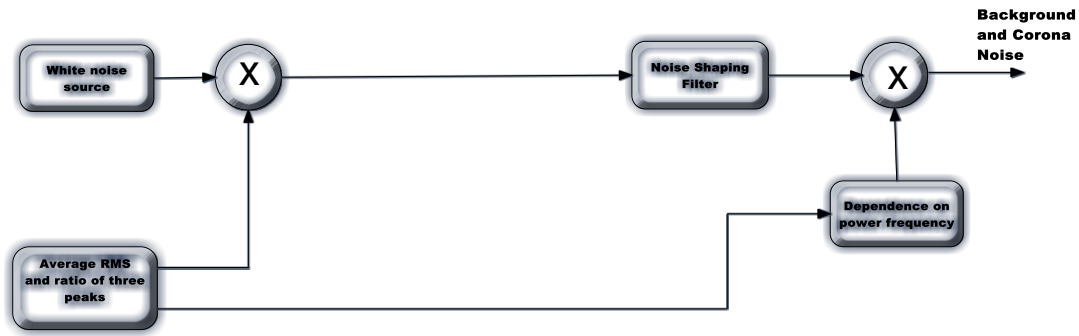


Figure 2.5-1 Generations of background and corona noise

The first step in modeling relative corona noise is by expressing it by a mathematical function. The dependence of an instantaneous corona noise voltage to the 50 Hz power frequency can be approximated by three cosine signals with a period $T_1=1/(3*50)$ seconds and amplitude $U_{i\ max}$, given by [Mujčić *et al.*, (2004)]:

$$U_i(t) = \frac{U_{imax}}{2} \left[1 - \cos\left(\frac{2\pi}{T_1} t\right) \right] \quad 0 < t < T_1 \quad (2.30)$$

where the voltage U_{imax} stands for the maximum RMS value on a particular phase of a powerline and the voltage U_{imin} stands for the minimum RMS value. From the known dependence of the instantaneous corona noise voltage on the 50 Hz power frequency, the average RMS value is defined as:

$$U_{Nrms} = \sum_{i=1}^3 \sqrt{\frac{1}{3T_1} \int_0^{T_1} |U_i(t)|^2 dt} \quad (2.31)$$

Equation (2.32) shows the modification of (2.30) to incorporate the background noise, U_{min} as:

$$U_i(t) = \frac{U_{imax}-U_{min}}{2} \left[1 - \cos\left(\frac{2\pi}{T_1} t\right) \right] + U_{min} \quad 0 < t < T_1 \quad (2.32)$$

In fact, the author proposed a model where the background and corona noise are synthesized by filtering the white noise source and multiplying it by function U which describes its dependence on the power frequency. The impact of weather conditions is represented by a different block average RMS and a ratio of three peaks. The average RMS and the ratio of the three peaks block have two outputs. The first output is the average RMS of the corona noise which multiplies samples of the white noise. The second output holds values of relative corona noise amplitudes U_{imax} on a particular phase for the block dependence on the power frequency.

The noise-shaping filter can be described by:

$$H(z) = \frac{1}{1 + \sum_{i=1}^n a_i z^{-i}} \quad (2.33)$$

where a_i is set of coefficients.

Dlh'a'n and Farka', (2008) analyzed the capability of Orthogonal frequency division multiplexing (OFDM) as an error correcting code if used for transmission over channel with asynchronous impulsive noise. New decoding algorithms of OFDM-RS code are presented with emphasis on low implementation complexity. The decoding and error correcting capability of these new algorithms has been evaluated in a series of simulations. As a test channel model for simulations, the PLC channel was selected.

Guillet *et al.*, (2009) also studied the parameters of impulsive and other noise types generated by load commutation in the powerline network. They proposed a new approach for controlling the commutation instant of the load; which reduces the asynchronous impulsive noise emitted by a resistive load by up to 15 dB.

2.6 Modulation Techniques

Biglieri (2003) noted that the selection of an appropriate modulation scheme for the PLC channel must account for three major factors, namely:

- (i) The presence of noise and impulsive disturbances, causing a relatively low signal-to-noise ratio.
- (ii) The time-varying, frequency-selective nature of the channel.
- (iii) Regulatory constraints with regard to EMC and EMI that limit the transmitted power.

This therefore calls for the choice of either a robust solution or an adaptive modulation and coding scheme. Some of the possible modulation schemes are discussed below.

2.6.1 Single- Carrier Modulation

Most basic modulation schemes make use of a single carrier at a frequency f_o . On the other hand, the information is encoded in terms of amplitude, phase, or frequency changes of the carrier. However, since PLC channel introduces strong intersymbol interference (ISI), powerful detector and equalization techniques are called for. The deep frequency notches present in the channel transfer

function prevent the use of linear equalizers, as the noise enhancement they cause is a serious drawback on such a noisy channel.

2.6.2 Spread Spectrum Modulation

The basic digital elements of a spread spectrum digital communication system are illustrated in Fig. 2.6-1. From this figure, we see that the channel encoder, decoder, modulator and demodulator are the basic elements of a conventional digital communication system. In addition to these elements, a spread spectrum system employs two identical pseudorandom sequence generators, one which interfaces with the modulator at the transmitting end and the second, which interfaces with the demodulator at the receiving end. These two generators produce a pseudorandom or pseudonoise (PN) binary-valued sequence that is used to spread the transmitted signal in frequency at the modulator and despread the received signal at the demodulator. Spread spectrum techniques (SST) are a good choice for PLC channel due to their immunity against selective attenuation and all kinds of narrowband interference. An additional interesting feature of SST, especially with regard to EMC, is the low power spectral density of the transmitted signal. Moreover, media access can be accomplished by code-division multiple access (CDMA), offering multiple access without global coordination or synchronization. However spread spectrum requiring low SNR has bad modulation efficiency.

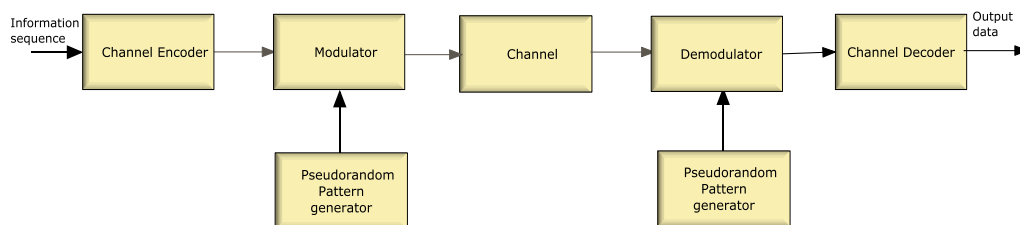


Figure 2.6-1 Spread spectrum system digital communication system

2.6.3 Multi Carrier Modulation

The basic concept of this technique is the conversion of incoming data flow into a set of independent sub-channels, each of them used to modulate different carriers that are transmitted simultaneously. Multicarrier techniques include two most common forms of modulations which are OFDM and discrete multitone (DMT). In the discrete implementation of OFDM, often called DMT, the ISI can be completely eliminated through the use of a cyclic prefix. The sub channels in OFDM need not be contiguous, so a large continuous block of spectrum is not needed for high rate multicarrier communications.

In wireless communications, some studies on the impact of multipath on OFDM systems are investigated in Okada *et al.*, (1993) and Vandendorpe *et al.*, (1993). Nevertheless, because the channel characteristics of wireless communications are different from those of powerline communications, study of the multipath effect on the PLC channel is needed with regard to this modulation technique. The OFDM modulation process is well adapted to such environment because first, it uses in its scheme a cyclic prefix which brings a good immunity against inter symbol interference and then, the equalizer is easy to implement. Fig. 2.6-2 shows the transmission OFDM process.

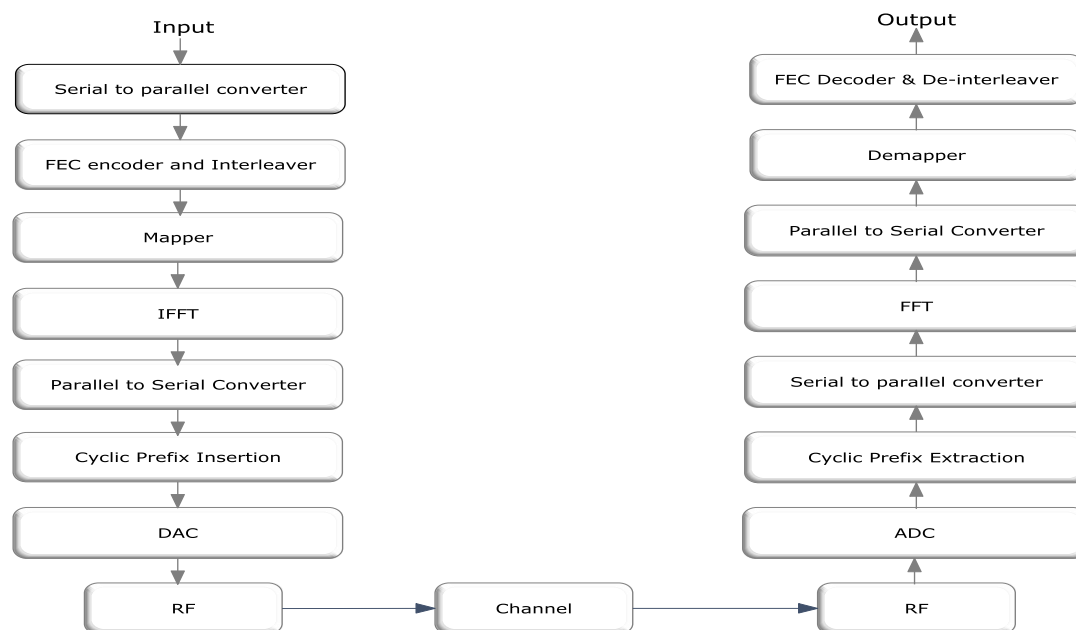


Figure 2.6-2 OFDM Transceiver process

2.7 Coding Schemes

PLC channel is a hostile channel that needs forward error correction (FEC) coding, interleaving, automatic repeat request (ARQ) for reliability of data communication, as shown in Fig.2.7-1. The encoded bits are applied to the modulator for transmission and received signals are then demodulated and decoded. It also includes transmit and receive controllers that exchange information via feedback channels.

The basic idea behind coding and interleaving is to randomize the location of errors that occur in bursts, since most codes designed for AWGN channels do not work well when there is a long sequence of errors. Thus, the interleaver disperses the location of errors occurring in bursts such that only a few simultaneous errors occur, which can typically be corrected by most AWGN codes.

The spreading out of burst errors is accomplished by an interleaver and the error correction is accomplished by the code as shown in Fig.2.7-2.

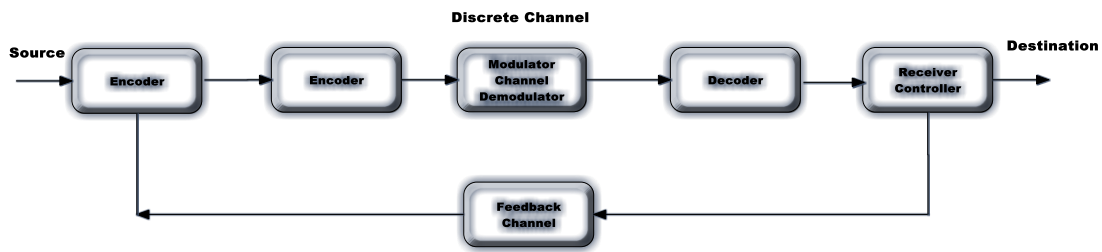


Figure 2.7-1 Block diagram of ARQ system



Figure 2.7-2 Interleaving method for burst error channel

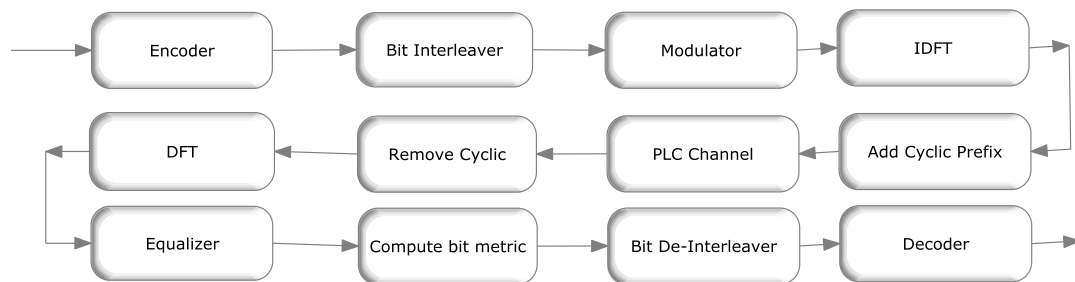


Figure 2.7-3 Block diagram of OFDM with BCM

OFDM can be successfully joined with coding by using bit interleaved coded modulation as shown in Fig. 2.7-3.

2.8 Powerline Communications Standard

The European committee for electrotechnical standardization (CENELEC) on powerline communications differs from the standards applied in the USA or in Japan. The European standard is presented in the European standard EN 50 065-1 (CENELEC, 1991), where the frequency band A (9 – 95 kHz) is reserved for the use in distribution companies and the frequency bands B (95 – 125 kHz), C (125 – 140 kHz) and D (140 – 148.5 kHz) are reserved for domestic use. A special carrier sense multiple access (CSMA) protocol is defined for the frequency band C (125 – 140 kHz). The characteristic of the standard (CENELEC, 1991) is the limiting of the maximum output voltage of the

transmitter. It does not primarily define the power spectral density of the transmitted signal. For the American or Japanese standard, the frequencies almost up to 500 kHz can be used for powerline communications.

2.9 Chapter Conclusion

In this chapter, we have addressed the characterization of the PLC channel environment while focusing on multi-path signal propagation, signal attenuation, noise and electromagnetic compatibility issues. We have observed that the PLC channel is a horrible channel with high attenuation up to 60 dB/km in the frequency range from 1 to 20 MHz. We have also considered man-made noise in the channel. The presence of different types of noise calls for the use of either a robust solution or adaptive modulation and coding schemes so as to attain optimal performance of the PLC channel.

Until now, there is no universally accepted model for the transfer function of powerline channel as there are many parameters that need to be known or measured before determining the transfer function. In the next chapter, several channel PLC models from multipath propagation principles have been suggested. We then propose a channel model based on Monte Carlo approach to get the transmission line parameters with the cable length taken into consideration.

2.10 References

Güzelgöz, S., H. B. Çelebi, and H. Arslan, (2011),” Statistical Characterization of the Paths in Multipath PLC Channels,” *IEEE Trans. On Power Delivery*, vol. 26, No. 1, January.

Lindell, G (2001), “On Coding and Modulation for the Powerline Communication Channel,” *Proceeding of ISPLC*, Sep., pp. 14-17.

Mulangu, C.T and T. J. Afullo, (2009) “Variability of the Propagation Coefficients Due to Rain for Microwave Links in Southern Africa,” *Radio Sci.*, Vol. 44.

Mätzler, C. (2002b), MATLAB Functions for Mie Scattering and Absorption, Version 2, *IAP Res. Rep. No. 08*, University of Bern, Switzerland, June.

Bohren, C. F and D. R. Huffman, (2004), “*Absorption and scattering of light particles*,” Wienheim, John Wiley.

Philipps, H., (1999), “Modelling of Powerline Communication Channels,” *in Proc. ISPLC*, pp. 14-21.

Zimmermann, M., K. Dostert, (1999), "A multi-path signal propagation model for the powerline channel in the high frequency range," *ISPLC*, pp. 45-51, Lancaster U.K.

Papaleonidopoulos, I.C., C.N. Capsalis, C.G. Karagiannopoulos and N.J. Theodorou, (2003), "Statistical Analysis and Simulation of Indoor Single-Phase Low Voltage Powerline Communication Channels on the basis of Multipath Propagation," *IEEE Trans. Consumer Electronics*, Vol.49, No. 1, pp. 89-99, February.

T. S. Rappaport, (1996). *Wireless Communications: Principles and Practice*. Upper Saddle River, NJ: Prentice-Hall.

Mätzler, C. (2002a), Effects of Rain on Propagation, Absorption And Scattering of Microwave Radiation Based on The Dielectric Model of Liebe, *IAP Res. Rep. No. 02-10*, University of Bern, June.

Anatory, J., N. Theethayi, R. Thottappillil, M.M. Kissaka and N.H. Mvungi, (2005). "The effects of Interconnections and Branched Network in the Broadband Power line Communications," *International Gathering of Radio Science*, India, 23rd –29th October.

Meng, H., S. Chen, Y.L. Guan, C. Law, P.L. So, E. Gunawan and T.T. Lie, (2004), "Modeling of Transfer Characteristics for the Broadband Power Line Communication Channel," *IEEE Trans. Power Delivery*, Vol. 19, No. 3, July, pp. 1057-1064.

Barmada, S. and A. Musolini, (2006), " Innovative Model for Time-Varying Power Line Communication channel Response Evaluation," *IEEE Journal on Selected Areas in Communications*, Vol. 24, No. 7, July, pp1317-1326.

R'oka and Urminsk', (2008) "Experimental Measurements for Verification of the Parametric Model For Reference Channels In the Real PLC channel Environment," *Journal of Electrical Engineering*, Vol. 59, No.3, pp. 146-152.

Amirshahi, P. and M. Kavehrad (2006) "High-Frequency Characteristics of Overhead Multiconductor Power Lines for Broadband Communications," *IEEE Journal on Selected Areas in Communications*, Vol. 24, No. 7, July, pp. 1292-1303.

Biglieri, B. (2003) "Coding and Modulation for a Horrible Channel," *IEEE Communications Magazine*, May, pp. 92-98.

Chen, Y., and T.D. Chiueh, (2002) "Baseband Transceiver Design of a 128 kbps Powerline Modem for Household Applications," *IEEE Trans. Power Delivery*, vol. 17, no.2, Apr. pp. 338-44.

Anatory, J., M.M. Kissaka and N.H. Mvungi, (2006) "Powerline Communications: The effects of Branches on the network performance," *IEEE-ISPLC*, Florida, USA, March. pp. 70-75

Katayama, M., T. Yamazato, and H. Okada (2006) "A Mathematical Model of Noise in Narrowband Power Line Communication Systems," *IEEE Journal on Selected Areas in Communications*, Vol. 24, No. 7, July, pp1272-1280.

Mujčić, A., N. Suljanović, M. Zajc, J. F. Tasič, (2004) "Corona noise on the 400 kV overhead power line - Measurements and Computer Modelling," *Springer Journal of Electrical Engineering*, Vol. 86, No.2, January, pp61-67.

Dlh'á'n, Farka' (2008) "Impulsive Noise Cancellation in Systems with OFDM Modulation," *Journal of Electrical Engineering*, Vol. 59, No.6, pp310-316.

Guillet, V., G. Lamarque, P. Ravier and C. Leger, (2009), "Improving the power line communication signal-to-noise ratio during a resistive load commutation," *Journal of Communications*, Vol. 4, No. 2, March, pp126-132.

Okada, M., S. Hara, and N. Morinaga, (1993) "Bit error rate performances of orthogonal multicarrier modulation radio transmission systems," in *IEICE Trans. Communications*, vol. E76-B, Feb. pp. 113–119.

Vandendorpe, L. (1993) "Multitone system in an unlimited bandwidth multipath rician fading environment," in *Proc. IEE Mobile and Personal Communications Conf.*, Dec. pp. 114–119.

Ahola J., T. Lindh, and J. Partanen, (2002)"Determination of Properties of Low Voltage Power Cables at Frequency Band 100 kHz – 30 MHz," ICEM, Bruges, Belgium, August 26-28.

Clara Lin, Joseph Curilla, (1991) "Temperature-Related Changes in Dielectric Constant and Dissipation Factor of Increase Attenuation in Data Cables Used in Building Plenums," *IEEE 16th Conference on Local Computer Networks, Minneapolis, USA, 14-17 October, pp. 74-79.*

Charles Harper, (1975), "Handbook of Plastics and Elastomers," McGraw-Hill, New York, ISBN 0-07-026681-6.

CENELEC, (1991), EN 50 065-1, Signalling on low voltage electrical installations in the frequency range 3 kHz to 148.5 kHz, CENELEC, Brussels.

Chapter Three

Modeling of Broadband Powerline Communication Channels

3.1 Introduction

Considerable efforts have been recently devoted to the determination of accurate channel models for the powerline communication environment, both for indoor and outdoor networks. Powerline communications have been used as a communication medium for many years in low bit-rate applications like automation of fault management in power distribution systems and remote meter reading [Hudson *et al.*, (1976), Lokken *et al.*, (1976)]. However, the characterization of the transfer function is a non-trivial task since PLC channel characteristics change depending on the topology, frequency of operation, and attenuation suffered in a given link. The attenuation depends more on the network topology and connected loads. The amplitude characteristic shows that, even at short distances, deep narrowband notches with attenuation occur, which can even be higher than the one of longer distances. These notches result from reflections and multipath propagation. This behavior is very similar to the one of mobile radio channels.

The conversion of networks designed to distribute electric power into communication media has been the subject of extensive research carried out over the last few years. The growing demand on information exchange calls for high rate data transmission, which will in turn requires the utilization of the power grid in the frequency range at least up to 30 MHz. Several problems are caused by the frequency dependent nature of the power grid: the presence of time varying loads, as well as by the structure of the grid itself. An aspect that may provide solutions for the many problems present today is the proper modeling of the power grid as a communication medium, and with a time-varying delay.

Several channel models from multipath propagation principles have been suggested [Philipps, (1999), Philipps, (1998)]. The work presented in Philipps, (1998) and Matov, (2004) is in fact very close to the approach introduced herein. The Philipps model was based on evolutionary strategy to get lumped circuit parameters of the SRC load, however, the model did not take the length of cable into consideration. The model proposed here is based on Monte Carlo approach to get the transmission line parameters as shown in Fig. 3.1-1, and Equations (3.1) and (3.2) below to get the SRC of the load with cable length taken into consideration.

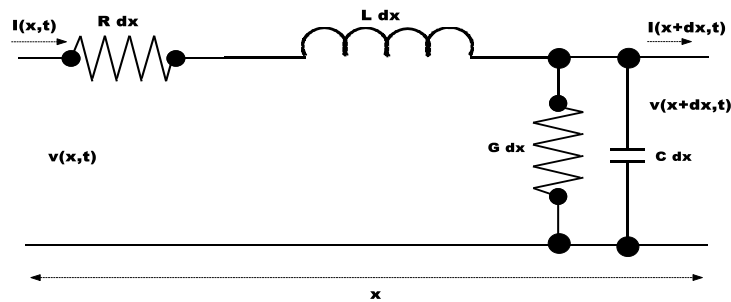


Figure 3.1-1 Two-conductor distributed transmission line.

$$\frac{\partial v(x, t)}{\partial x} + R \cdot i(x, t) + L \frac{\partial i(x, t)}{\partial t} = 0 \quad (3.1)$$

$$\frac{\partial i(x, t)}{\partial x} + G \cdot v(x, t) + C \frac{\partial v(x, t)}{\partial t} = 0 \quad (3.2)$$

In these equations x denotes the longitudinal direction of the line and R , L , G and C are the per unit length resistance (Ω/m), inductance (H/m), conductance (S/m) and capacitance (F/m) of transmission line respectively.

3.2 Transmission Line Parameters

Anatory *et al.*, (2004) have defined transmission parameters for the PLC channel system from a primary substation to the customer bracket. The separation distance D , between conductors is much greater than the radius, a of the conductors, hence the capacitance C , inductance L , and AC resistance R per loop meter are given by Equations (3.3), (3.4) and (3.5) respectively, [Hudson *et al.*, (1976), Lokken *et al.*, (1976)].

$$C = \frac{\pi \epsilon}{\cosh^{-1}(D/2a)} \quad [F/m] \quad (3.3)$$

$$L = \frac{\mu}{\pi} \cosh^{-1}(D/2a) \quad [H/m] \quad (3.4)$$

$$R = 2 \left(\frac{R_s}{2\pi a} \right) = \frac{1}{\pi a} \sqrt{\frac{\pi f \mu}{\sigma}} \quad [\Omega] \quad (3.5)$$

Here μ and σ are the permeability and conductivity of the metal conductors, respectively. The propagation coefficient γ is given by

$$\gamma = \alpha + j\beta = \sqrt{(R + j\omega L)(G + j\omega C)} \quad (3.6)$$

where α is the attenuation coefficient and β is the phase coefficient. Also the attenuation function is given by Equation (3.7), where l is the length of the cable,

$$A(f, l) = \exp(-\gamma l) \quad (3.7)$$

The characteristic impedance Z_o can be expressed as:

$$Z_o = \sqrt{\frac{R + j\omega L}{G + j\omega C}} \quad (3.8)$$

The impedance seen looking into a generalized transmission line terminated by the load Z_L is:

$$Z_{in} = Z_o \left(\frac{Z_L + Z_o \tanh(\gamma l)}{Z_o + Z_L \tanh(\gamma l)} \right) \quad (3.9)$$

and if the load terminal is short-circuited, i.e. $Z_L = 0$, (3.9) becomes,

$$Z_{in} = Z_{sc} = Z_o \tanh(\gamma l) \quad (3.10)$$

Similarly, if the load terminal is open-circuited, i.e. $Z_L \rightarrow \infty$, (3.9) becomes,

$$Z_{in} = Z_{os} = Z_o \cot h(\gamma l) \quad (3.11)$$

From (3.8) and (3.10),

$$Z_o = \sqrt{Z_{sc} \cdot Z_{os}} \quad (3.12)$$

$$\gamma = \frac{1}{l} \tanh^{-1} \sqrt{\frac{Z_{sc}}{Z_{os}}} \quad (3.13)$$

In the lossless transmission line Z_{in} can be expressed as:

$$Z_{in} = Z_o \left(\frac{Z_L + jZ_o \tan(\beta l)}{Z_o + jZ_L \tan(\beta l)} \right) \quad (3.14)$$

3.3 Transfer channel Function

The well-known transfer function $H(f)$ is the multipath model proposed by Philipps (1999) and Zimmerman *et al.*, (1999). The echo model of Philipps presents the channel impulse response as a superposition of N Dirac pulses representing the superposition of signals from N different paths as shown in Eq. (3.15).

$$H(t) = \sum_{i=1}^N |\rho_v| \cdot e^{-j\phi_v} \delta(t - \tau_v) \quad (3.15)$$

where ρ_v is a complex factor and τ_v is the delay time. Zimmerman (1999) proposed an adapted echo model that contains an additional attenuation factor. The multipath signal illustrated in Fig. 3.3-1 is investigated and analyzed simply as the link with a branch that consists of three segments (1), (2) and (3) with the lengths L_1 , L_2 and L_3 and the characteristic impedances Z_{L1} , Z_{L2} and Z_{L3} , respectively. We assume that A and C are matched, which means $Z_A = Z_{L1}$ and $Z_C = Z_{L2}$. B and D are reflection points, with reflection coefficients r_{1B} , r_{3B} , r_{3D} and the transmission coefficients are denoted as t_{1B} , t_{3B} . With these assumptions, the link can have an infinite number of propagation paths due to multiple reflections. Each path i has a weighting factor g_i , representing the product of the reflection and transmission coefficients along the path, with the standard condition:

$$|g_i| < 1 \quad (3.16)$$

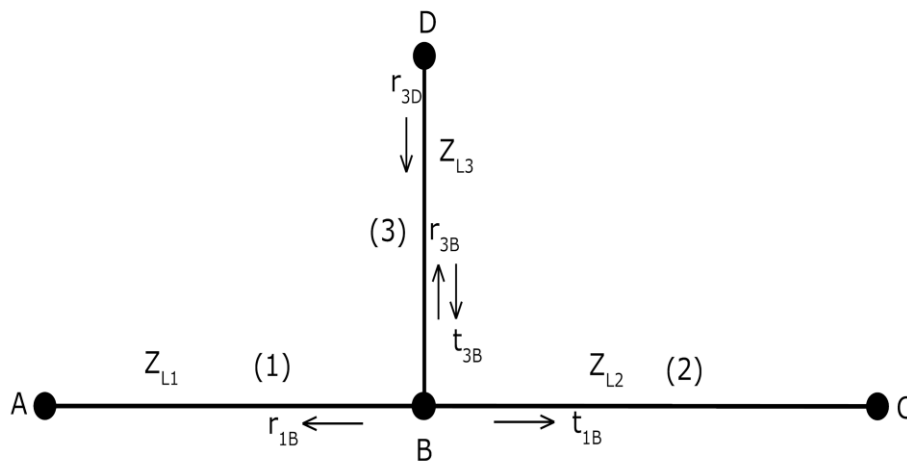


Figure 3.3-1 One tap cable multipath signal propagation

Then the transfer function $H(f)$ in the frequency range from 500 kHz to 20MHz is expressed as:

$$H(f) = \sum_{i=1}^N g_i \cdot e^{-(a_0+a_1) \cdot d_i} \cdot e^{-j2\pi f \frac{d_i}{v_p}} \quad (3.17)$$

where N is the number of paths of propagation, a_0 , a_1 and k are parameters from frequency-dependent attenuation. The relevant parameters are not derived from component properties, but from channel measurements, d_i its length and v_p is the propagation speed.

Figure 3.3-2 is an example of a PLC network with four paths, [Zimmerman *et al.*, (1999), Zimmerman *et al.*, (2002)] which considers the transfer function $H(f)$ in (3.17) and uses the data in Table 3.3-1,).

In the earlier work by Anatory *et al.*, [Anatory *et al.*, (2005), Anatory *et al.*, (2007a), Anatory *et al.*, (2007b), Anatory *et al.*, (2007c), Anatory *et al.*, (2006)], a generalized transfer function of the PLC channel is presented as:

$$H_m(f) = \prod_{d=1}^{M_T} \sum_{M=1}^L \sum_{n=1}^{N_T} T_{LM} \alpha_{mn} H_{mn}(f) \quad n \neq m \quad (3.18)$$

$$\alpha_{mn} = P_{Ln}^{M-1} \rho_{nm}^{M-1} e^{-\gamma_n(2(M-1)l_n)} \quad (3.19a)$$

$$P_{Ln} = \begin{cases} \rho_s & n = 1(\text{source}) \\ \rho_{Ln}, & \text{otherwise} \end{cases} \quad (3.19b)$$

where, N_T is the total number of branches connected at the node and terminated in any arbitrary load. This was achieved by letting n , m , M , $H_{mn}(f)$ and T_{LM} , represent any branch number, any referenced (terminated) load, number of reflections (with total L number of reflections), transfer function between line n to a referenced load m , and the transmission factor at the referenced load m , respectively.

Table 3.3-1 parameters of the multipath model [Zimmerman *et al.*, (1999), Zimmerman *et al.*, (2002)].

Path No	1	2	3	4
Delay in μs	1.0	1.25	1.76	2.64
Equivalent length in m	150	188	264	397
Weighting factor g_i	0.4	-0.4	-0.8	-1.5
$K=0.5$	$a_0 = 0$		$a_1 = 0$	

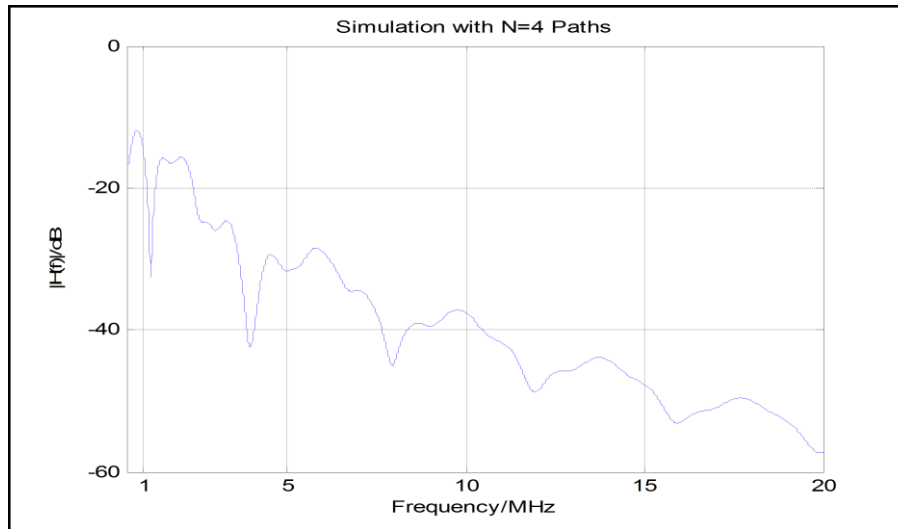


Figure 3.3-2 Multipath model from [Zimmerman *et al.*, (2002)]

They also proposed the signal contribution factor α_{mn} given by (3.19a), where ρ_{mn} is the reflection factor at node B , [Anatory *et al.*, (2005)], between line n to the referenced load m . γ_n is the propagation constant of line n that has line length l_n . All terminal reflection factors P_{Ln} in general are given by (3.19b), except at source where $\rho_{LI} = \rho_s$ is the source reflection factor.

Philipps' measurements indicate that the impedance of the electrical loads can be described by one or few resonant circuits (SRC) that consist of resistance R , capacitance C and inductance L as shown in Fig. 3.3-3. The impedance Z_s of the resonant circuit is frequency-dependent and can be described by:

$$Z_s(f) = R + j2\pi fL + \frac{1}{j2\pi fC} \quad (3.20)$$

At resonance frequency the f_m given by:

$$f_m = \frac{1}{2\pi\sqrt{LC}} \quad (3.21)$$

The impedance is minimal with an imaginary part of the impedance equal to zero and a real part equal to R . The transfer function $H(f)$ is:

$$H(f) = \frac{1}{1 + \frac{Z_0}{Z_s(f)}} \quad (3.22)$$

where, Z_0 is the characteristic impedance of the line.

And the quality factor of the resonance circuit is defined by:

$$Q = \frac{1}{R} \sqrt{\frac{L}{C}} \quad (3.23)$$

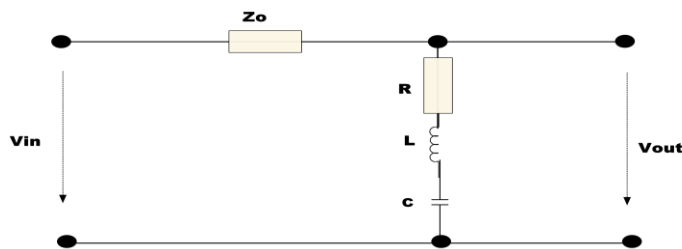


Figure 3.3-3 Series resonant circuit

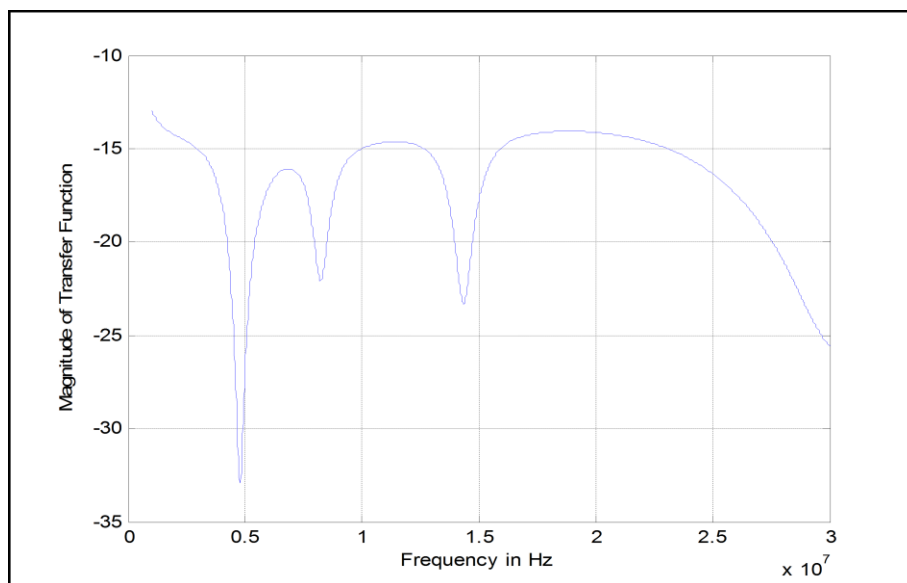


Figure 3.3-4 Transfer function of the series resonance model

where Q is a function of the width of the notch: the higher the Q , the narrower the notch.

Philipps [Philipps, (1999)] describes the transfer function $H(f)$ as the overall function of each resonant circuit transfer function $H_i(f)$, expressed as:

$$H(f) = \prod_{i=1}^N H_i(f) \quad (3.24)$$

Each resonant circuit is described by three parameters: resistance R , inductance L and capacitance C . In addition, the characteristic impedance Z has to be defined in this case, and it corresponds to the measurement in [Philipps, (1999)], where Z is 90 *Ohm*. Also in order to fit a model with N resonant circuits to a measured transfer function, $3 \times N$ parameters have to be optimized. The author carried out the optimization by means of an evolutionary strategy. Table 3.3-2 summarizes the values of the parameters and the resulting resonance frequencies and Q factor by means of an evolutionary strategy. Fig. 3.3-4 shows the simulation of the Philipps model.

Table 3.3-2 Set of parameters of series resonance circuits model

No	R in Ohm	L in μH	C in nF	f_{res} in MHz	Q
1	21.4	0.137	10.8908	4.122	0.165
2	12.1	8.264	0.1334	4.793	20.640
3	67.9	18.919	0.0197	8.238	14.431
4	46.4	11.948	0.0103	14.324	23.183
5	19.6	1.008	0.0273	30.357	9.799

Table 3.3-3 Set of parameters of proposed model

Branch	Length in m	L_m in $\mu\text{H}/\text{m}$	C_m in nF/m	f_m in MHz	Q	R
AB	70	20.692	2.635	0.596	3.6725	0.0080
BC	10	2.668	0.4171	4.77	2.0403	0.0013
BD	12	3.201	0.501	4.77	1.2242	0.0016
BF	10	2.667	0.418	4.77	3.6725	0.0013
BE	3	0.8803	0.1376	14.37	9.7673	0.00043

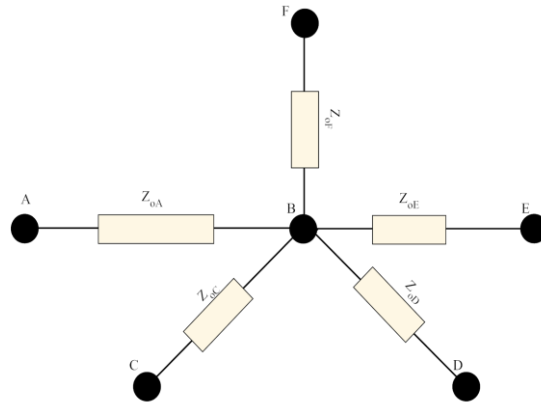


Figure 3.3-5 Simulation network model

3.4 Proposed Transfer Function

The Philipps model was based on evolutionary strategy to get lumped circuit parameters of the SRC load, however, the model did not take the length of cable in consideration.

The model we are proposing is based on Monte Carlo approach to get transmission line parameters as shown Fig. 3.1-1, to get the SRC of the load, and with cable length taking in consideration. Once we have all parameters of the branch, we use equations (3.20) and (3.22) to generate the transfer function of the transmission line using MATLAB tool. Here we consider multiple branches at a single node as

shown in Fig. 3.3-5, AB is the distributed branch from the distribution transformer to the customer's pole.

Here, we refer to BC , BD , BE and BF as end user branches (receivers) and the AB branch is from the distribution transformer (transmitter). Z_{oA} , Z_{oC} , Z_{oD} , Z_{oE} and Z_{oF} represent characteristic impedances of each one of the branches and all of them are terminated by load, R_C , R_D , R_E , and R_F . AB link is the customer pole with 70 m , radius r_m of conductor is 7 mm and the spacing between the conductors d_m is 18 mm . The end user branches are $BD = 12\text{ m}$; $BF = 10\text{ m}$; $BC = 10\text{ m}$; $BE = 3\text{ m}$, radius r of conductor is 6.5 mm , and the space between conductors D is 17 mm . Based on Equations (3.3), (3.4) and (3.5) and the network parameters, we carry out the lump circuit parameters as at the customers end, with $L = 26.677\text{ }\mu\text{H/m}$, $C = 16.683\text{ nF/m}$ and R is given for different frequencies as summarized in the Table 3.3-3. As R is small compared to the resistive load terminated by each branch, we neglected it.

We consider the network as shown in Fig. 3.3-5 from the first configuration, and Table 3.3-3. We observe that by varying the length of the branch, we change the position of the resonance frequency of the transfer function, meaning the position of the notch. The lower the length of the line, the higher is the resonance frequency as shown in Fig. 3.4-1 and 3.4-2. To fit our model into the existing one, we fixed the loads as follows: $R_{AB} = 95\text{ }\Omega$ at distance of 35 m , $R_{BC} = 20\text{ }\Omega$ at distance of 10 m , $R_{BD} = 75\text{ }\Omega$ at distance of 10 m , $R_{BE} = 25\text{ }\Omega$ at distance of 3.32 m and $R_{BF} = 8.4\text{ }\Omega$ at distance of 10 m .

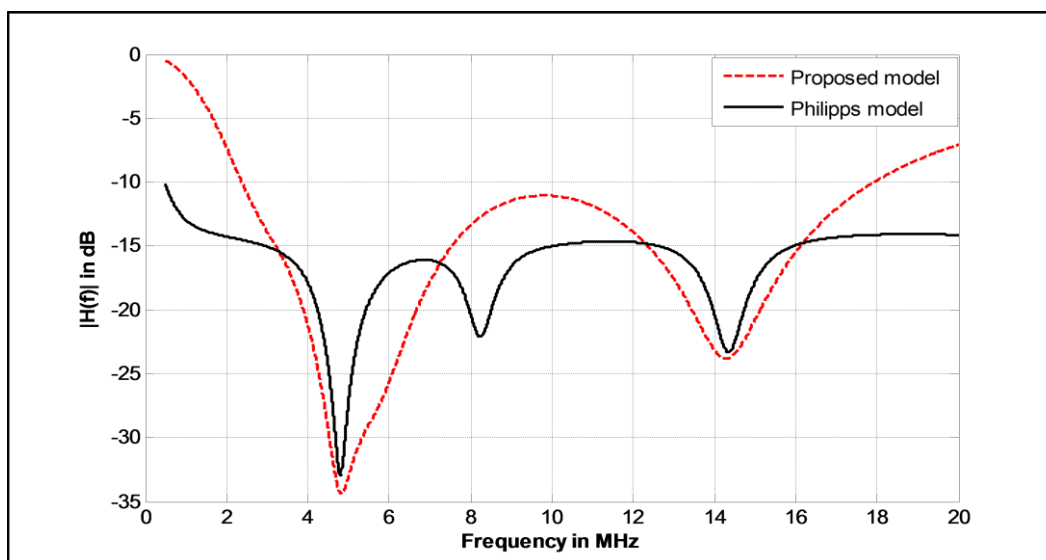


Figure 3 4-1 Transfer function model

However there are some differences between the proposed model and Philipp's model transfer characteristics. This is due to the fact that the proposed model peaks for the parallel resonance occur at different frequencies compared to Philipps model. For example, the peaks for the proposed model occur at the following frequencies: 0.5, 10 and 20 MHz and for Philipps model the peaks occur at the following frequencies: 7, 11 and 18 MHz.

By setting the number of degrees of freedom at 42, the proposed model leads to an average root-mean-square error (*RMSE*) test statistic value of approximately 3.3 dB.

$$RMSE = \sqrt{\frac{1}{n} \sum_{i=1}^n (x_i - x'_n)^2} \quad (3.25)$$

while chi-square (χ^2) statistic test is given by:

$$\chi^2 = \sum_{i=1}^n \frac{(x_i - x'_n)^2}{x'_n} \quad (3.26)$$

where $\{x_1, x_2, x_3, \dots, x_n\}$ is experiment data set; $\{x'_1, x'_2, x'_3, \dots, x'_n\}$ is theoretical model data set. And, $df = n - 1$ where df is the number of degrees of freedom. The significance level used in this work is 1%. In our case, $n = 42$, $df = 41$, then $\chi^2 = 71.63$ and χ^2 statistic threshold = 74.75.

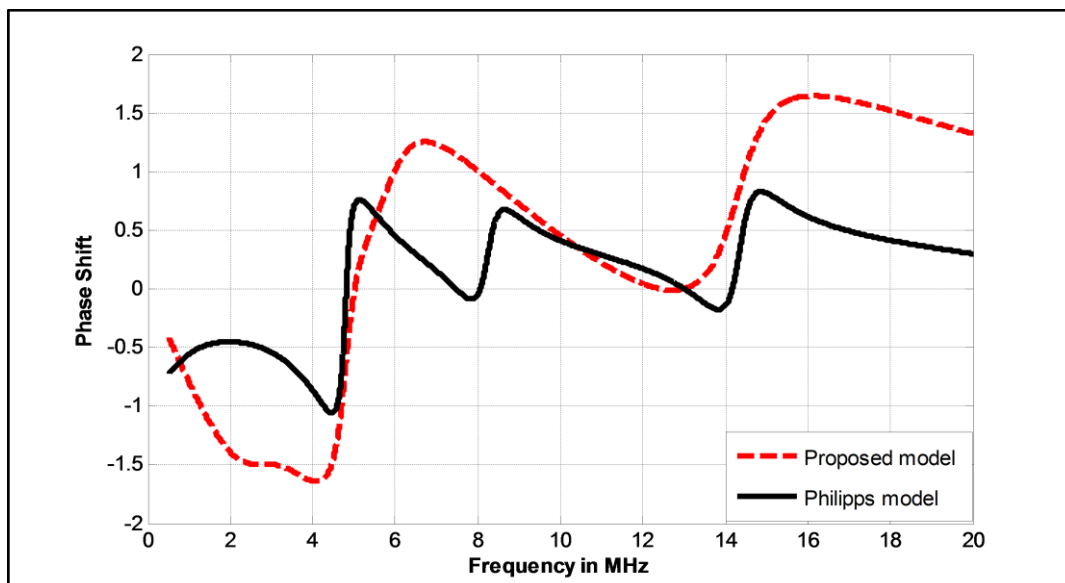


Figure 3.4-2 Phase response of the transmission Line

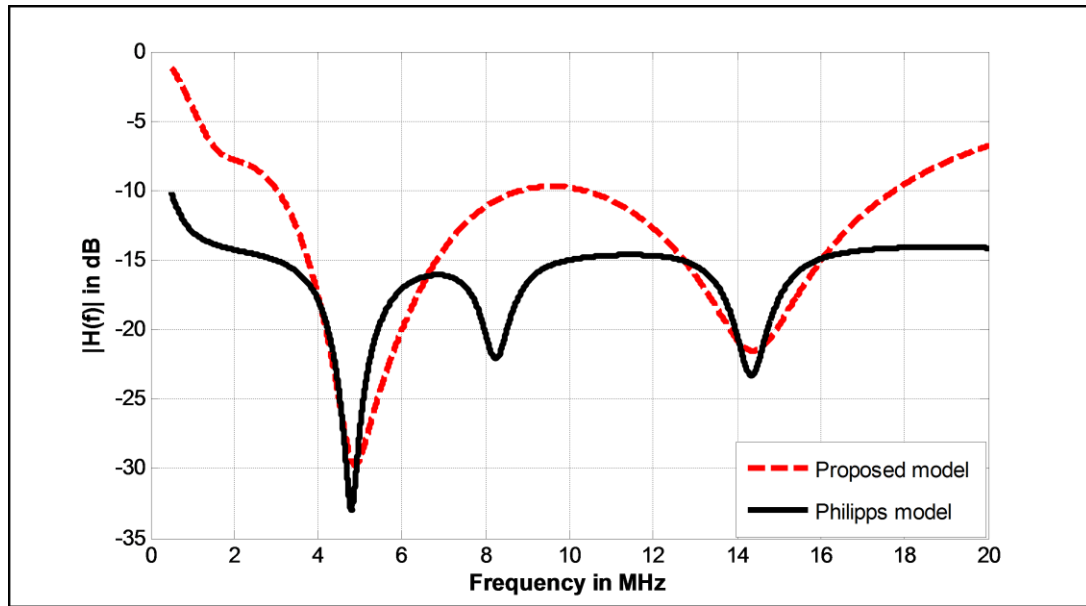


Figure 3.4-3 Amplitude response with a and D varying

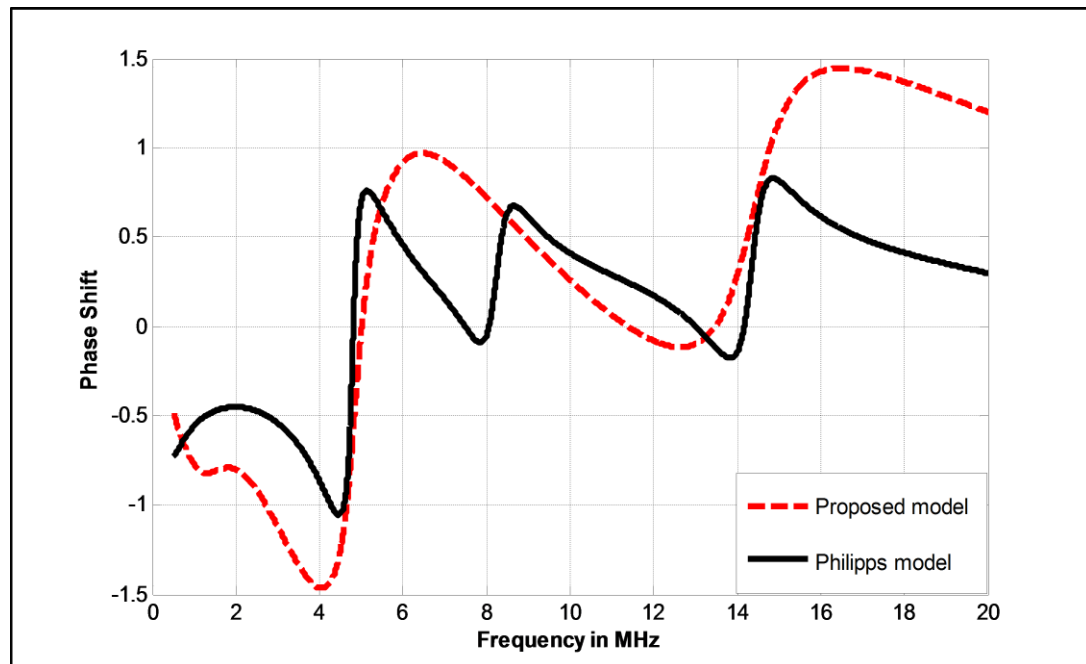


Figure 3.4-4 Phase response with r and D varying

The second configuration consists of changing the radius r_m of the main cable, the space between conductors D and radius r at the customer end. It is observed that notches become narrow. This implies that the quality factor Q is lower at resonance frequencies such as at 0.5, 4.77 and 14.6 MHz as the loads are higher according to Equation (3.21).

We vary the radius r_m of the main cable, from 7 mm to 9 mm and the space between conductors D from 18 mm to 20 mm, at the user customer end; and radius r from 6.5 mm to 7 mm and the space between conductors D from 17 mm to 19 mm. Figures 3.4-3 and 3.4-4 show that the amplitude of the

notches increase, which implies that the transfer function also depends on these two parameters.

For the third configuration, we vary the loads only. First of all, we increase all five resistive loads as follows: $R_{AB} = 350 \Omega$, $R_{BC} = 65\Omega$, $R_{BD} = 80\Omega$, $R_{BE} = 12 \Omega$ and $R_{BF} = 30 \Omega$. It is observed that the sharpness of the curve tends to be flat as indicated in Figures 3.4-5 and 3.4-6, meaning the quality factor Q decreases when resistive load connected is increased. Also, the notches move backward compared to Philipps model.

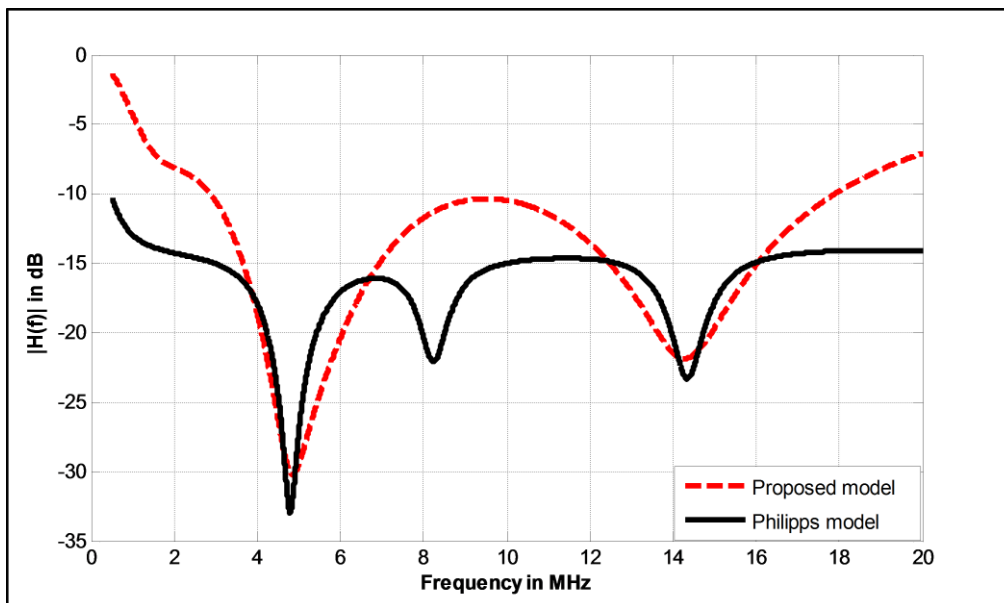


Figure 3.4-5 Amplitude response with resistance loads increased

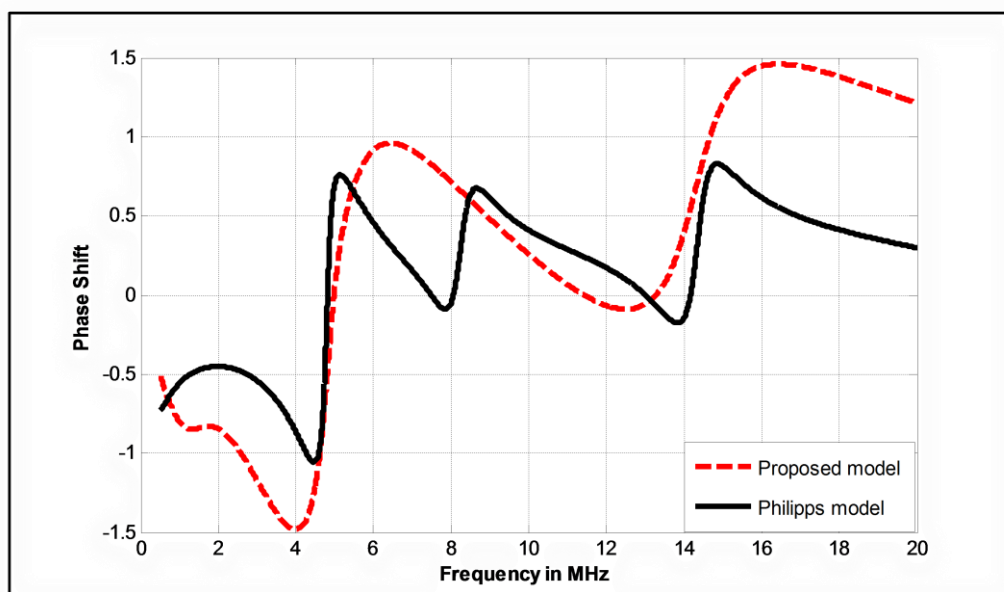


Figure 3.4-6 Phase response with resistance loads increased.

3.5 Chapter Conclusion

Currently there is no universal model for the transfer function of the powerline as there are many parameters that need to be known or measured before determining the transfer function. The model suggested here using transmission line parameters is comparable to the *SRC* model of Philipps, which is based on the evolutionary strategy with the root mean square error of 1.62 dB. In addition, the model is dynamic with lengths of branches and load. The Philipps model does not give enough information about the influence of length on the transfer function. By setting the number of degrees of freedom to 42, the proposed model leads to an average RMS value of approximately 5.2 dB. With the same conditions, the Philipps model leads to an average RMS value of approximately 1.62 dB. In the next chapter, we consider the line as one single element, and its length is divided into a grid of small areas or scattering points with dimensions ranging from 0.5 to 3 mm. The relationship between the specific attenuation versus the number of branching nodes and specific attenuation versus frequency power laws are then determined.

3.6 References

Hudson, A. G., D. R. Beuerle and H. J. Fiedler, (1976), "SSB Carrier for utility control and communication," *Proc. of IEEE National Telecommunication Conf.*, pp. 2.1.1-2.17.

Lokken, G., N. R. Jagoda and J. D'Auteuil, (1976). "The Proposed Wisconsin Electric Power Company Load Management System Using Power Line Over Distribution Lines," *Proc. of IEEE National Telecommunication Conf.*, pp. 2.2.1-2.2.3.

Philipps, H., (1999), "Modelling of Powerline Communication Channels," in *Proc. ISPLC*, pp. 14-21.

Philipps, H., (1998), "Performance Measurements of Powerline Channels at High Frequencies," *Proceeding of the 1998 International Symposium on Powerline Communications and its Applications (ISPLCA '98)*, Tokyo, Japan, March, p. 229-237.

Zimmermann, M., and K. Dostert, (1999). "A Multi-Path Propagation Model for the Power-Line channel in the High Frequency Range," in *Proc. ISPLC*, pp. 45-61.

Matov, A. (2001). "A Planning Tool for High Bit Rate Transmission over Power Line Communication Channels *Proceeding of ISPLC channel*, pp. 15-20. Malmö, Sweden, April.

Zimmermann, M., and K. Dostert, (2002). "A Multi-Path Model for the Powerline Channel," *IEEE Transactions on communications*, vol. 50, No. 4, April, pp. 553-539.

Anatory, J., Theethayi, N., Thottappillil, R., Kissaka M. M., Mvungi, N. H., (2005). "The effects of Interconnections and Branched Network in the Broadband Power line Communications," *International Gathering of Radio Science*, India, 23rd–29th October.

Anatory, J., Kissaka, M. M., Mvungi, N. H., (2007a). "Channel Model for Broadband Power line Communication," *IEEE Trans. On Power Delivery*, January, No. 1, pp. 135-141.

Anatory, J., Theethayi, N., Thottappillil, R., Kissaka M. M., Mvungi, N. H., (2007b). "The Effects of Load Impedance, Line Length and Branches in the BPLC- Transmission Lines Analysis: A Case of Indoor Voltage Channel," *IEEE Trans. On Power Delivery*, October, Vol. 22, No. 4, pp. 2150-2155.

Anatory, J., Theethayi, N., Thottappillil, R., Kissaka M.M., Mvungi, N.H., (2007c). "Broadband Power line Communications: Factors Influencing the Signal propagations in the Medium Voltage Lines," *IEEE ISPLC2007*, Pisa, Italy, 26-28, March.

Anatory, J., Kissaka, M.M., Mvungi, N.H., (2006). "Power line Communications: The effects of Branches on the network performance," *IEEE-ISPLC*, Florida, USA, March.

Chapter Four

Semi-empirical Model for Indoor Broadband Powerline Communication Channels

4.1 Introduction

In this chapter we investigate the effect of the number of branching nodes in the PLC network and derive a scattering distribution model for PLC channels. The model is based on the assumption of a randomly spread multitude of scatterers in the vicinity of the channel that only requires a sufficient number of impedance discontinuity points [Sabih Güzelgöz, (2011)]. We considered the line as one single element, and its length is divided into a grid of small areas or scattering points with dimensions ranging from 0.5 to 3 mm. The relationship between the specific attenuation versus number of branching nodes and specific attenuation versus frequency power laws are then determined.

4.2 Scattering Points Size Distribution for Indoor Broadband PLC Channels

The multipath propagation of the powerline communication channel (PLC) arises from the presence of several branches and impedance mismatches that cause multiple reflections. Each path comprises of scattering points that reflect the signal a specific number of times at specific points of discontinuity along its routes. In Papaleonidopoulos (2002), scattering points' spatial allocation, by which path amplitude distributions and path arrival time distributions are obtained, they are shown to follow the lognormal distribution for different number of branches. Borrowing from those findings, in this chapter, a model based on the validation of the assumption of a randomly spread multitude of scatterers in the vicinity of the channel that only require a sufficient number of impedance discontinuity points is proposed [Sabih Güzelgöz, (2011)]. We considered the line as one single element, and its length is divided into a grid of small areas with dimensions ranging from 0.5 to 3 mm.

However, the power cable structure of an electric power network is designed and optimized primarily for 50 or 60 Hz, and not as a communication medium at high frequency (HF). Furthermore, its transfer properties display considerable variation across the HF band [Papaleonidopoulos (2002), Malack (1976)]. First, wave propagation techniques through the use of distributed-element transmission line models are required in order to explain HF signal propagation over powerlines, as corresponding wavelengths are comparable to distances usually found within indoor grids [Malack (1976)]. Secondly, due to the variation of the loads, indoor electric power networks show certain time-variance, which is well dominated by wave propagation principles rather than those of classical circuit types [Papaleonidopoulos (2002)].

Several reflections are caused by the joints of the network's cables, connection boxes, serial connections of cables with different characteristic impedances, and in general, points of discontinuity, due to impedance mismatches that occur [Zimmermann (1999), [Philips (1999)], and these can be generally referred to as "scatterers". Multipath propagation constitutes the principal broadband signal transfer mechanism over electric power network, by virtue of which the PLC channel links are characterized as strongly fading channels [Zimmermann (1999)]. Therefore, each path comprises of signals that are reflected at specific number of times at specific scattering points of discontinuity along its routes.

4.2.1 Multipath Propagation Model

Papaleonidopoulos (2002)' proposed assumptions based on indoor electric network's topology are adopted with regard to scattering points' special allocation, by which path amplitudes are demonstrated to follow the lognormal distribution. Verification of the statistical modeling is established, involving path inventory through simulations.

The path amplitude distribution within a group k is given as the function of the random variable τ_k that displays the normal distribution according to Papaleonidopoulos (2002), and forming the arrival-time sequence set $(\tau = \tau_1, \tau_2, \dots, \tau_{N_g})$, of the channel considered. The channel response is given by:

$$H_k(f) = |g_k| \cdot e^{-ac \cdot \tau_k} \quad (4.1)$$

where $|g_k|$ is a constant. As the path amplitude of each group is exponentially dependent on a normally distributed random variable, it therefore follows the Log-normal distribution, having the mean parameter equal to $(\mu_k + \ln|g_k|)$, and the variance equal to σ_k^2 . The corresponding probability density function (PDF) is given by:

$$P_k(x) = \frac{1}{\sigma\sqrt{2\pi}} \exp \frac{-(\ln x - (\mu_k + \ln|g_k|))^2}{2\sigma_k^2} \quad (4.2)$$

And forming the amplitude sequence set of the channel, as considered in Papaleonidopoulos (2002), given by:

$$H(F) = |H_1(f)|, |H_2(f)|, \dots, |H_{N_g}(f)| \quad (4.3)$$

The transmission of an impulse $\delta(t)$ through a multipath environment with L paths results in a train of delayed impulses [Papaleonidopoulos *et al.*, (2003)] given by:

$$H(\tau_d, t) = \sum_{i=1}^L r_i e^{j\theta_i} \cdot e^{-\alpha l_i} \cdot \delta(t - \tau_{di}) \quad (4.4)$$

where,

$$\tau_{di} = \frac{l_i}{v} = \frac{l_i}{\omega/\beta} \quad (4.5)$$

$(r_i e^{j\theta_i})$ is reflection factor of the i th path, given by:

$$r_i e^{j\theta_i} = \prod_{k=1}^{M_1} T_{ik} \prod_{n=1}^{M_2} \Gamma_{in} \quad (4.6)$$

where M and k present the number of reflection and transmission coefficients included in path, l_i is the path's length and v is the group velocity of propagation, T and Γ represent transmission and reflection coefficients, respectively. With this observation, the transmission characterization along the direct path ($i = 0$) is essential for understanding the first arrival path.

We note here that the reflection factor of the first arrival path is composed of only the transmission coefficients experienced along the direct path stemming from the impedance discontinuities at the branching nodes. So, calculating it is sufficient in order to characterize the reflection factor of the first arrival path.

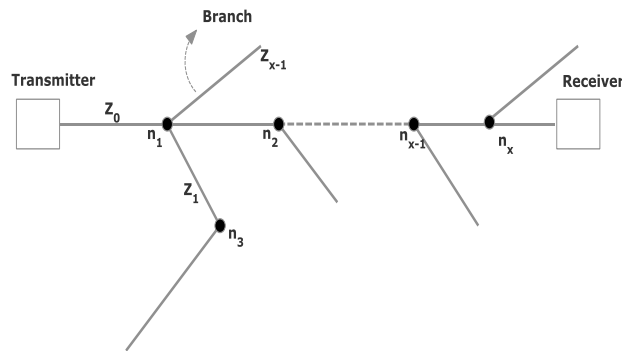


Figure 4.2-1 PLC channel network analysis

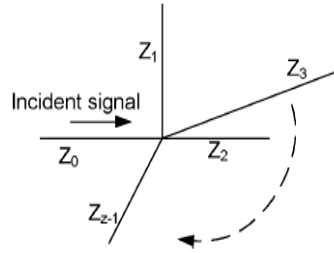


Figure 4.2-2 Reflection and transmission at a branching node.

Also, we can have it in equivalent frequency response, [Papaleonidopoulos *et al.*, (2003)], expressed as:

$$\begin{aligned}
 H(f) &= \sum_{i=1}^L r_i e^{j\theta_i} \cdot e^{-\alpha l_i} \cdot e^{-j\omega\tau_{di}} \\
 &= \sum_{i=1}^L r_i e^{j\theta_i} \cdot e^{-\gamma l_i}
 \end{aligned} \tag{4.7}$$

where, γ is the propagation coefficient.

Figure 4.2-1, shows the direct propagation path between the transmitter and the receiver operating on a PLC channel system that consists of several branching nodes denoted by n_i . These branches extending from each branching node may be terminated by an electrical load or lead to another branching node depending upon the network structure.

In transmission line theory, reflection and transmission coefficients at a branching node are expressed by considering parallel connections of extended branches as follows [Lindell, (2001)]:

$$\Gamma = \frac{(Z_1 // Z_2 \dots // Z_z) - Z_0}{(Z_1 // Z_2 \dots // Z_z) + Z_0}; \quad T = \Gamma + 1 \tag{4.8}$$

where Z_0 is characteristic impedance of the incident signal and Z_z is characteristic impedance of branching node. If all branches are equal to each other (Z_0), Eq. 4.8 can be expressed as:

$$\Gamma = \frac{2 - z}{z}; T = \frac{2}{z} \tag{4.9}$$

where z refers to the total number of branches extending from a particular branching node as shown in Fig. 4.2-2. Referring to Fig. 4.2-1, and assuming that the transmitter and the receiver are matched to

the impedance of the corresponding characteristic impedance of the cable for the sake of simplicity, $r_0 e^{j\theta_0}$ is composed of multiplication of x transmission coefficients as follows:

$$r_0 e^{j\theta_0} = \frac{2}{n_1} \frac{2}{n_2} \dots \frac{2}{n_x} = \frac{2^x}{n_1 * n_2 * \dots * n_x} \quad (4.10)$$

where $n_i (i = 1, 2, \dots, x)$ is the number of paths extending from a branching node, including the path on which the incident signal propagates. Note that the phase term θ of the reflection factor is 0 for this particular case since n_i cannot be a complex number ($r_0 e^{j\theta_0} = r_0$).

Equation (4.10) can be expressed as:

$$Y = \ln(|r_0|) = x \ln 2 - \sum_{i=1}^x \ln n_i \quad (4.11a)$$

where Y is an RV with the following mean, μ and variance, σ^2 :

$$\mu = x \ln 2 - \sum_{i=1}^x [\ln(n_i)] \text{ and } \sigma^2 = \sum_{i=1}^x \text{Var}[\ln(n_i)] \quad (4.11b)$$

where n is used to refer to both the branching node itself and the number of the branches extending from it. The mean and variance as shown in Fig. 4.2-2 are related to the number of branching nodes with the following two equations:

$$\mu = -0.822x - 9.23 \times 10^{-5} \quad (4.12a)$$

$$\sigma^2 = 0.086x - 0.00237 \quad (4.12b)$$

To confirm that a branching occurs at the nodes, a and b must be greater than or equal to three (3).

Putting this statement into consideration, we arrive at the conclusion that, [Güzelgöz *et al.*, (2011)]:

$$\mu = \frac{-x}{b-a+1} \ln \frac{b!}{(a-1)!} + x \ln 2 \quad (4.13)$$

Having a homogeneous PLC channel medium is physically very difficult even though the same type of cable is used throughout the network due to the variety of factors that affect the characteristic impedance.

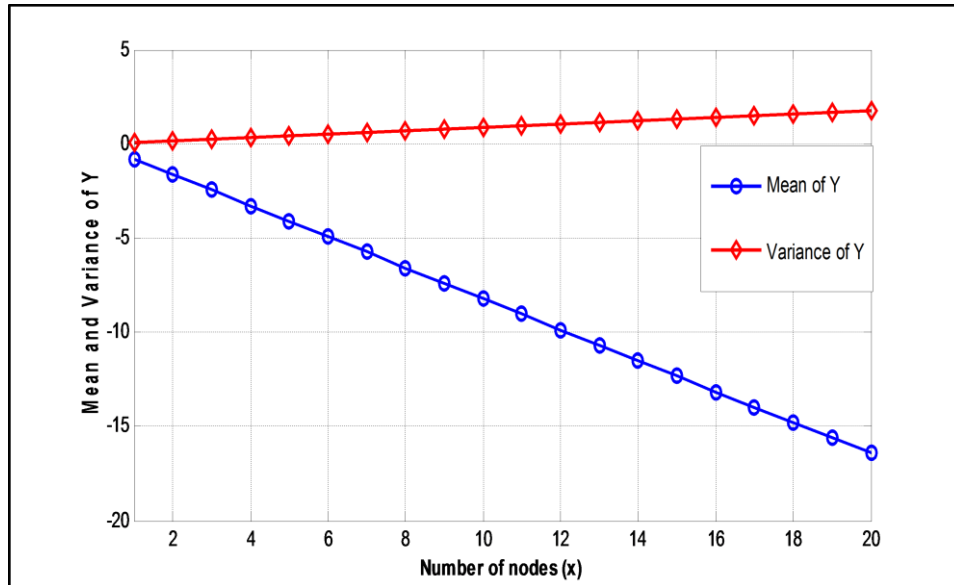


Figure 4.2-3 Variance and mean of Y with $Z_o = 50\Omega$ and $d_e = U[-25\Omega, 25\Omega]$

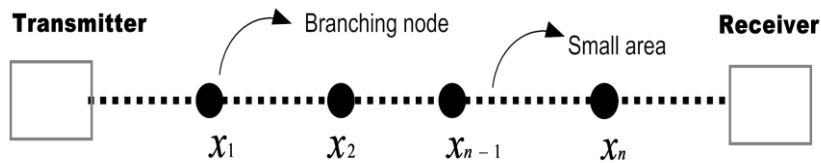


Figure 4.2-4 Indoor PLC channel model

In this chapter, we consider the line as one single element, and its length is divided into a grid of small areas with dimensions range from 0.5 to 3 mm as in Figure 4.2-3. Thus, each small area transmits an echo and the forward scattered response gets to the receiver. With this approach, specific attenuation can be determined using Olsen’s model for specific attenuation. In this case, the number of branching nodes is considered like rain rate and raindrops are presented by small areas. This analogy is presented in Figure 4.2-3 below.

4.2.2 Scattering Points Approximation Model

In this section, we propose the lognormal distribution model for scattering points that involve nodes and number of the branching nodes in the channel of the transmission line that we will later use in the next section, with the Mie scattering theory in order to determine the specific signal attenuation in the network.

The efficiencies Q_i for the interaction of radiation with a sphere of radius a are cross sections σ_i normalized to the geometrical particle cross section, $\sigma_g = \pi a^2$ where i stands for extinction ($i = ext$), absorption ($i = abs$), and scattering ($i = sca$). Energy conservation requires that [Mulangu, (2009), Mätzler, (2002b), Bohren, (2004)]:

$$Q_{ext} = Q_{sca} + Q_{abs}, \text{ or } \sigma_{ext} = \sigma_{sca} + \sigma_{abs} \quad (4.16)$$

where,

$$Q_{sca} = \frac{2}{x} \sum_{n=1}^{\infty} (2n+1)(|a_n|^2 + |b_n|^2); \quad (4.17)$$

$$Q_{ext} = \frac{2}{x} \sum_{n=1}^{\infty} (2n+1)Re(a_n + b_n); \quad (4.18)$$

The key parameters for Mie calculations are the Mie Coefficients a_n and b_n required to compute the amplitudes of the scattered field. The index n runs from 1 to ∞ , but the infinite series occurring in Mie formulas can be truncated at a maximum n_{max} , given in Bohren, (2004):

$$n_{max} = x + 4x^{1/3} + 2 \quad (4.19)$$

This value is used in this computation. The size parameter is given by $x = ka$.

In [Papaleonidopoulos (2002), Sabih Güzelgöz (2011)], the estimation of the path amplitude distribution is done using Log-normal distribution with two parameters, μ and σ . In our current model, we included a third parameter N_t as in equation below:

$$N(D_i) = \frac{N_t}{\sigma\sqrt{2\pi}} \exp\left\{-\frac{(\ln(D_i) - \mu_i)^2}{2\sigma_i^2}\right\} \quad (4.20)$$

where N_t is the number of impedance discontinuity points. The independent input, D_i is the mean diameter of the small area. The input parameters N_t, μ , and σ are obtained by using Monte Carlo simulations with corresponding branching nodes (K) to yield the following set of expressions:

$$N_t = a_o x^{b_o} \quad (4.21a)$$

$$\mu = A_\mu + B_\mu \ln(K) \quad (4.21b)$$

$$\sigma^2 = A_\sigma + B_\sigma \ln(K) \tag{4.21c}$$

where $a_o, b_o, A_\mu, B_\mu, A_\sigma$ and B_σ all represent the regression coefficients of input parameters corresponding to the Log-normal model. Table 4.2-1 shows the applied regression fittings for the proposed lognormal model, according to the input parameters for the number of branching nodes as described in (4.21). We note that the fitted results of the values N_t show dependency to the number of branching nodes (K). Figures 4.2-5 to 4.2-9 show the small areas scattering distribution models developed for PLC channel for different number of branching nodes (x): $x = 4, 10, 15$ and 20 .

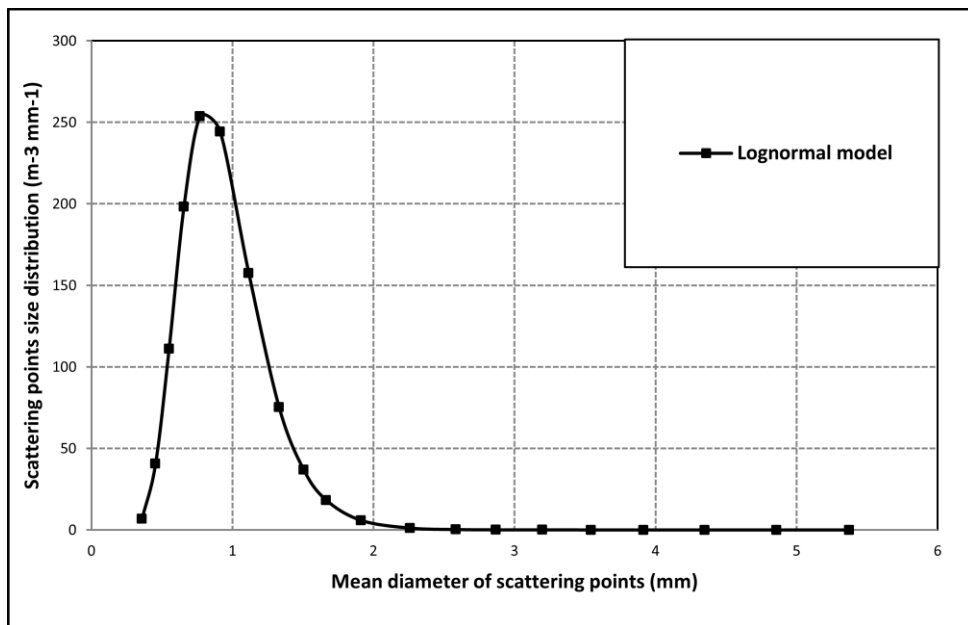


Figure 4.2-5 Scattering point size distribution for PLC channel with twenty branching nodes

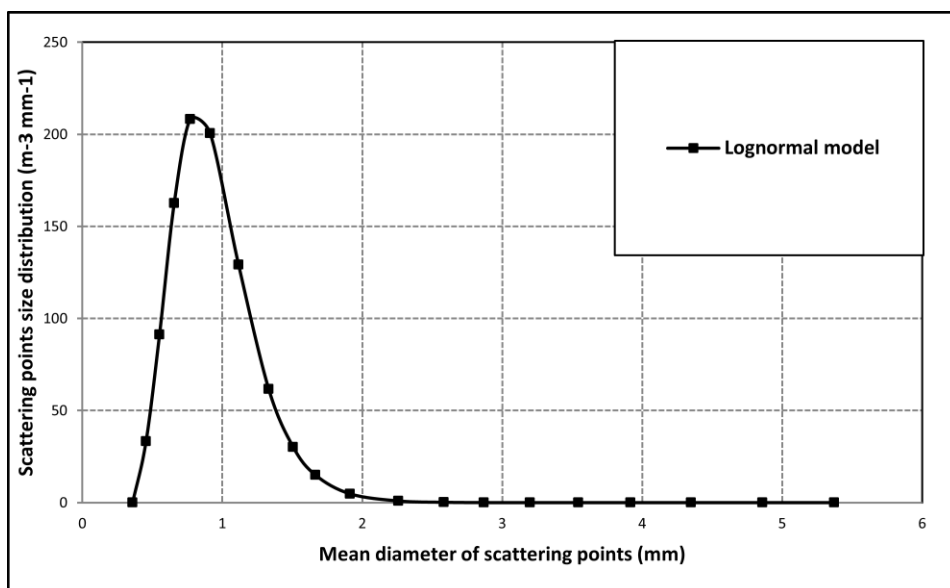


Figure 4.2-6 Scattering point size distribution for PLC channel with ten branching nodes

The small areas scattering distribution and probability density distribution in the indoor single-phase networks show that there are more scattering points at lower diameter sizes where the mean peak diameter is about 0.8 mm. This implies more signal reflections in this range of diameters. This would imply that in this range of diameters more signal attenuation will occur. The results show that the distributions do not depend on indoor network topology. Also, the results obtained will be used together with Mie scattering to determine the attenuation constant for the PLC channels.

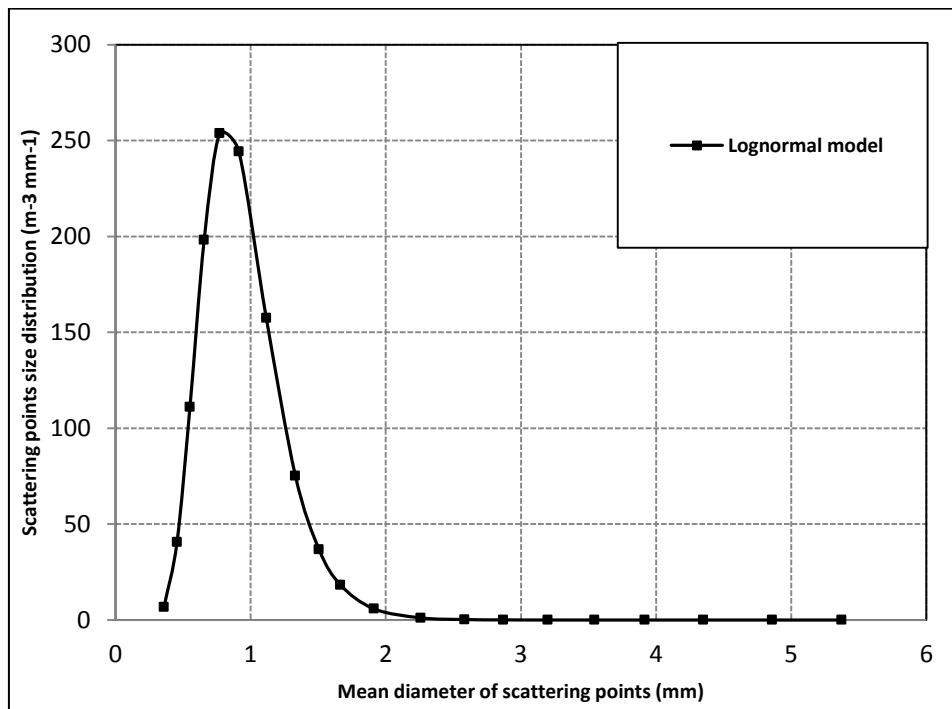


Figure 4.2-7 Scattering point size distribution for PLC channel with fifteen branching nodes

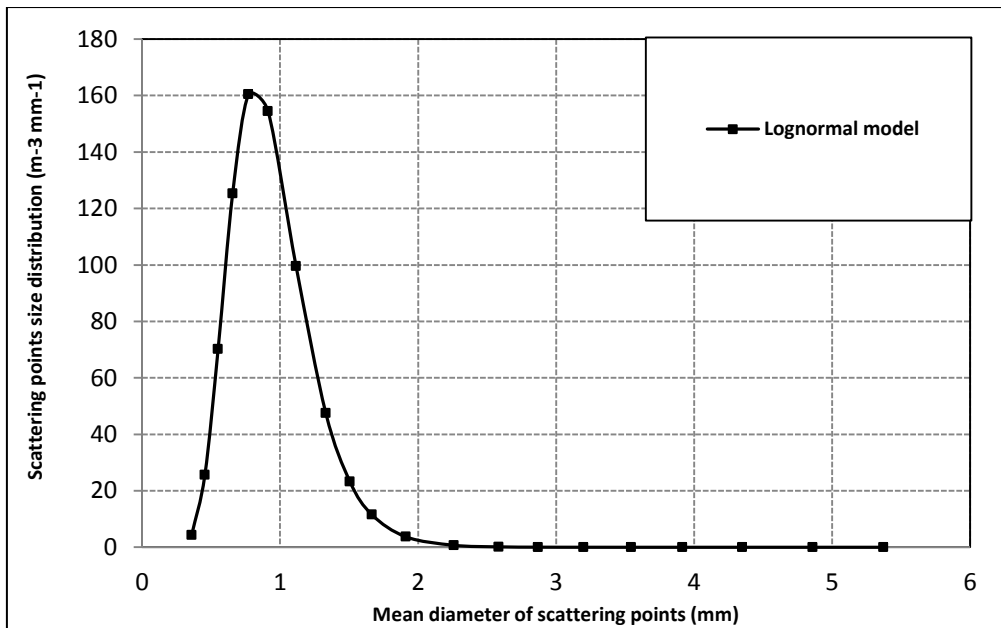


Figure 4.2-8 Scattering point size distribution for PLC channel with four branching nodes

Table 4.2-1 Model parameters

a_o	b_o	A_μ	B_μ	A_σ	B_σ
73.1	0.285	-0.479	0.003	0.072	0

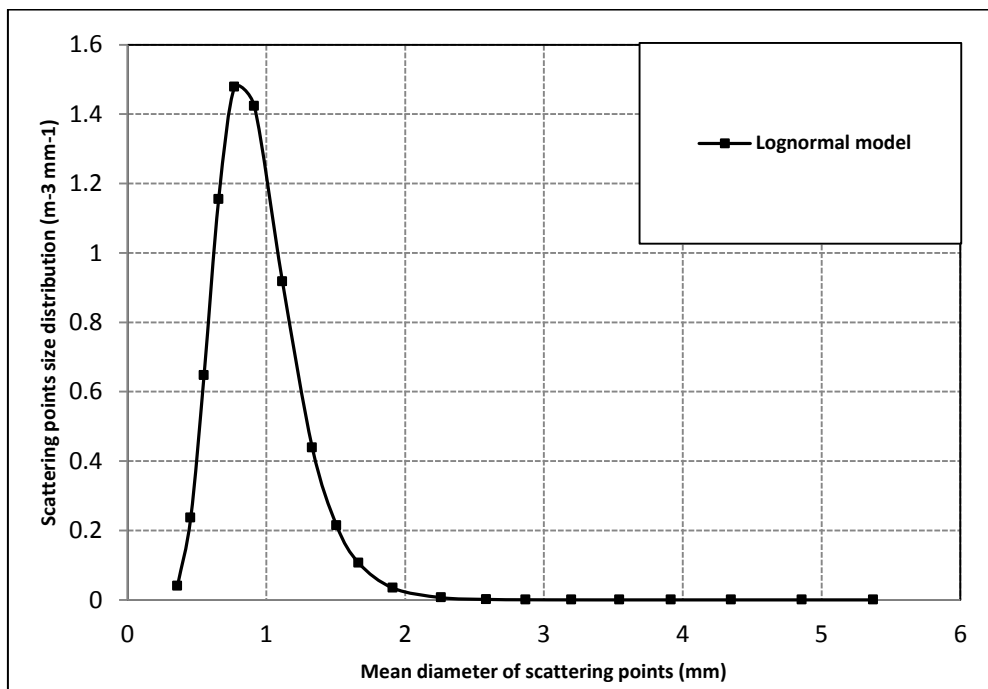


Figure 4.2-9 Probability density function of scattering points for PLC channel

4.3 Estimation of Specific Attenuation due to Scattering Points for Broadband PLC Channels

In Subsection 4.2.2, we have studied Mie scattering theories as applicable to branching nodes in order to determine the attenuation in PLC channels and a power law model is proposed where only the number of branching nodes is needed to estimate the specific attenuation.

The low voltage (LV) power network is a new option for providing access for high-speed communications. This option supports the concept of broadband powerline communications (PLC). With this system, it is possible to build an in-house communication network or access the internet in a very cost-effective way.

In this section, we investigate the effect of the number of branches and the numbers of reflections that occur at each node. The Mie scattering theory is then applied to the nodes in the network to determine the resulting specific signal attenuation in the network. The frequency of interest ranges between 10 MHz and 100 MHz.

4.3.1 Specific Attenuation Model and Optimization

The amplitude of an electromagnetic wave travelling through a volume, containing N identical scattering particles with diameter D , at any distance l , decreases by the factor of $e^{-\gamma l}$. The attenuation coefficient γ is given by:

$$\gamma = NQ_{ext}(D) \quad (4.22)$$

The attenuation of the wave is then given in dB as follows:

$$A_{dB} = 10 \log \frac{1}{e^{-\gamma l}} = 4.343\gamma l \quad (4.23)$$

and the specific attenuation in dB/km is given by:

$$A_s = 4.343\gamma \quad (4.24)$$

$$A_s [dB/km] = 4.343 \times 10^3 \int_0^{\infty} N(D)Q_{ext}(D)dD \quad (4.25)$$

From Mätzler (2002b) and Mulangu *et al.*, (2009) the expression in (4.25) is given as:

$$A_s[\text{dB}/\text{km}] = 0.25\pi \int_0^{\infty} D^2 N(D) Q_{ext}(D) dD \quad (4.26)$$

4.3.1.1 Optimization of the Estimated Model

The specific powerline attenuation model is formulated based on the Log-normal distribution model discussed in Subsection 4.2.2 of this work. Ahola *et al.*, (2002) and Ahola, (2003) presented a formula for the specific attenuation as a function of frequency using the power curve fitting algorithm.

Figures 4.3-1 and 4.3-2 below show the specific powerline attenuation models calculated from theoretical model, Ahola model and the scattering model. In Fig. 4.3-1 and 4.3-2 where there is no branching node, at 10 MHz, the theoretical model gives the highest attenuation values for frequencies up to 88 MHz. The scattering model is seen to give lower attenuation at lower frequencies, but increases rapidly at frequencies above 88 MHz. This behavior is due to the fact that Mie scattering is not accurate at lower frequencies.

4.3.1.2 Power Law Model for Specific Powerline Attenuation

Figure 4.3-3 below shows the specific powerline attenuation models calculated from theoretical model with 4 mm diameter and optimized model. The estimated model is given by:

$$67 \times 10^{-4} \times f^{0.9601} \quad (4.27)$$

where f is the frequency in MHz.

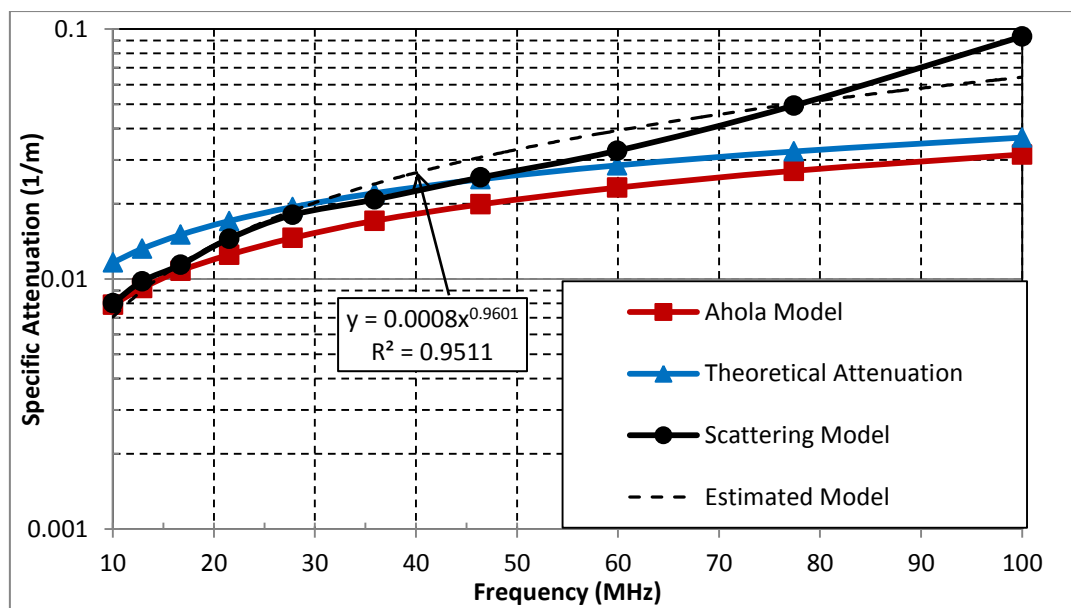


Figure 4.3-1 Comparison of estimated specific attenuation model for PLC channel

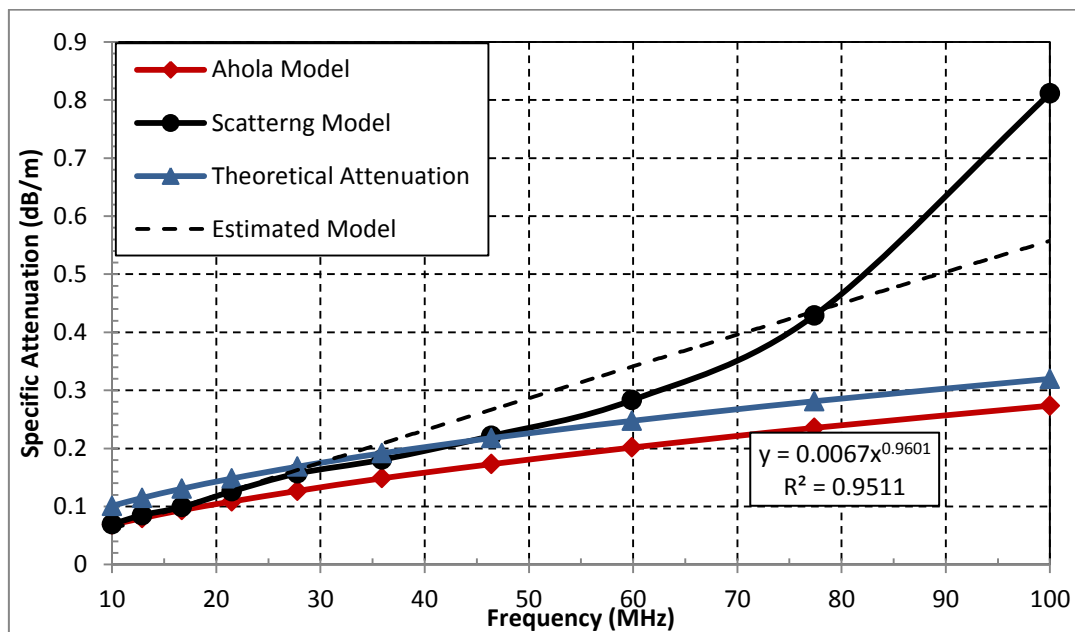


Figure 4.3-2 Regression fitting for specific attenuation in dB.

The root-mean-square error (*RMSE*) test and the chi-square χ^2 statistic test are used to optimize the proposed model. The expressions for the two are given in Equations (3.25) and (3.26) respectively.

In the case of χ^2 , ($N-1$) degrees of freedom are applied to determine the significance level of the preferred model. The significance level used in this work is 1%. The *RMSE* indicates the deviation of the proposed specific attenuation model from theoretical model. Therefore, the model with the least error is fitted. On the other hand, χ^2 indicates the closeness of the proposed specific attenuation model with the theoretical model.

In this work, as shown in Fig. 4.3-5 and Fig. 4.3-6, with 30 degrees of freedom, the χ^2 equals 1.77 with the threshold value given as 37.566 at 1% significance level. With the same degrees of freedom, the RMSE is 0.078 dB/m.

From Fig. 4.3-4 and 4.3-7 and Table 4.4-1, the specific attenuation is reported for different number of branching nodes. However, the specific attenuation is not linear due to the fact that the dielectric characteristics and the skin effect decrease at frequencies above 1 MHz. Conductance of the cable is also nonlinear as it is directly affected by both the dielectric characteristics and the skin effect. The nonlinearity of resistance and conductance of the cable cause the specific attenuation to be nonlinear as a function of frequency.

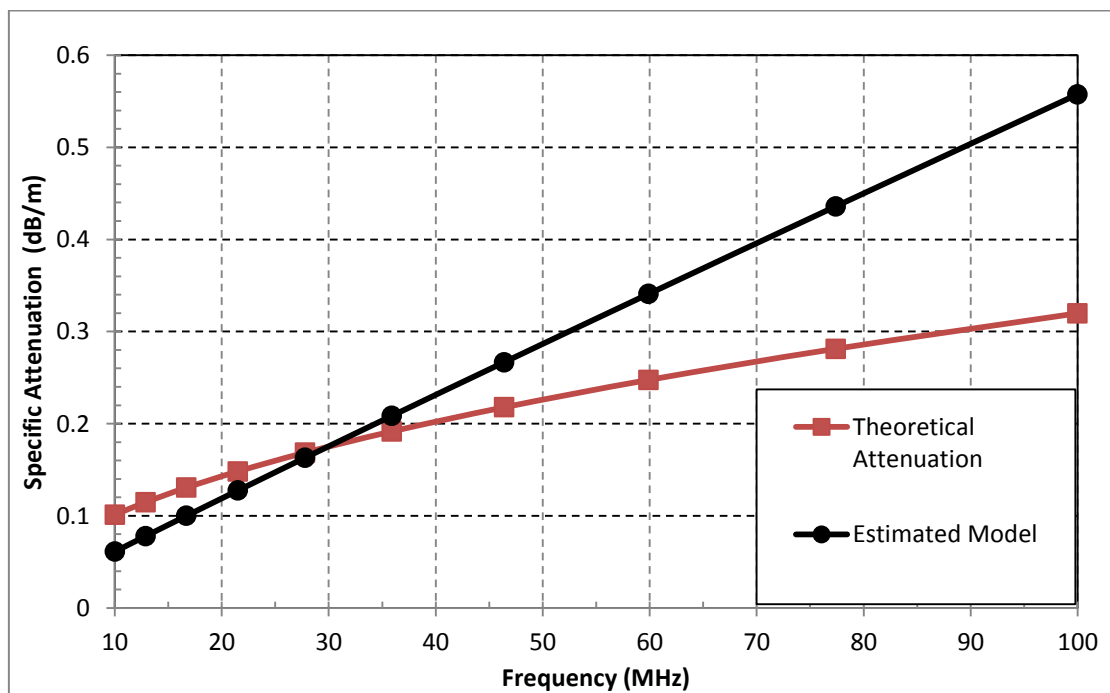


Figure 4.3-3 Optimized model for specific powerline attenuation.

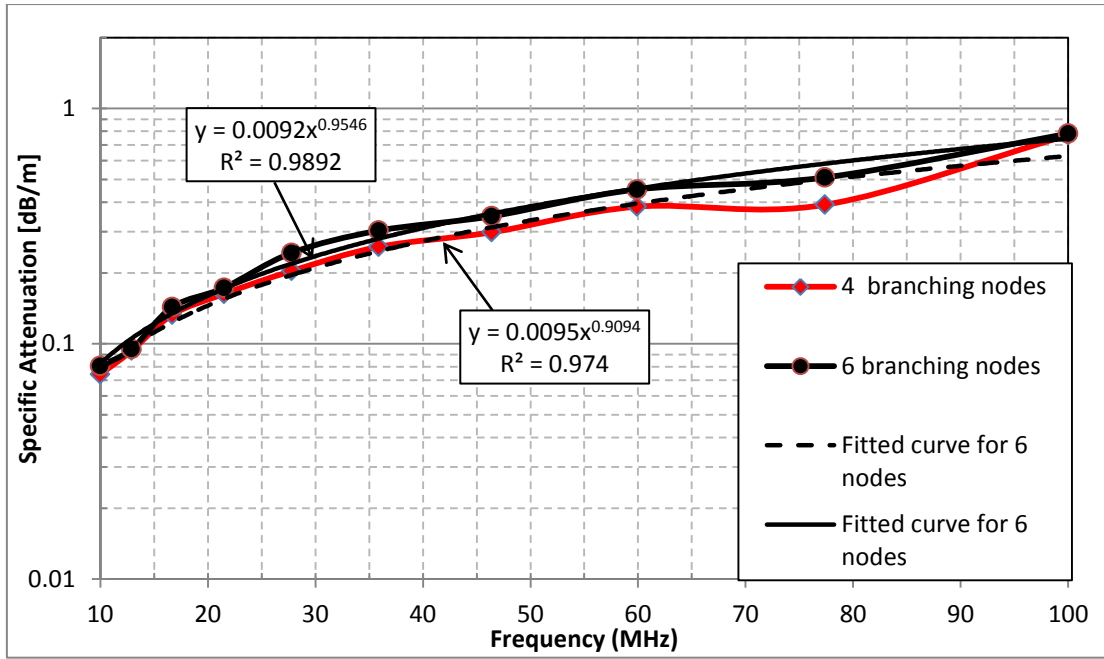


Figure 4.3-4: Model for 4 and 6 branching nodes at 10-100 MHz.

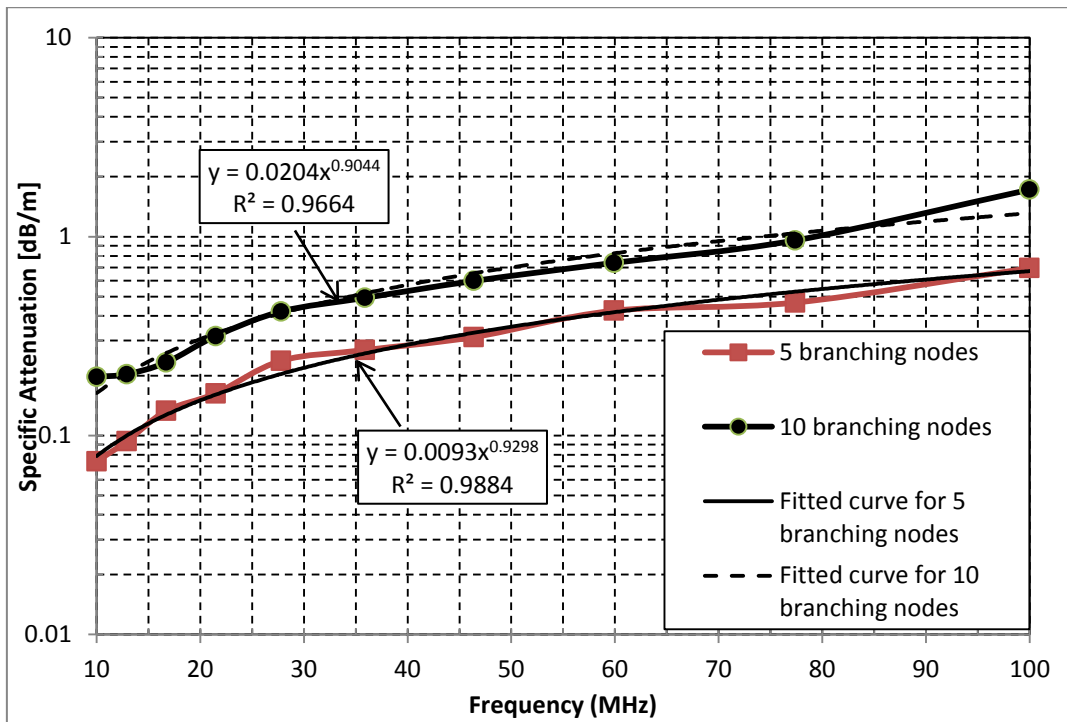


Figure 4.3-5: Models for 5 and 10 branching nodes at 10-100 MHz.

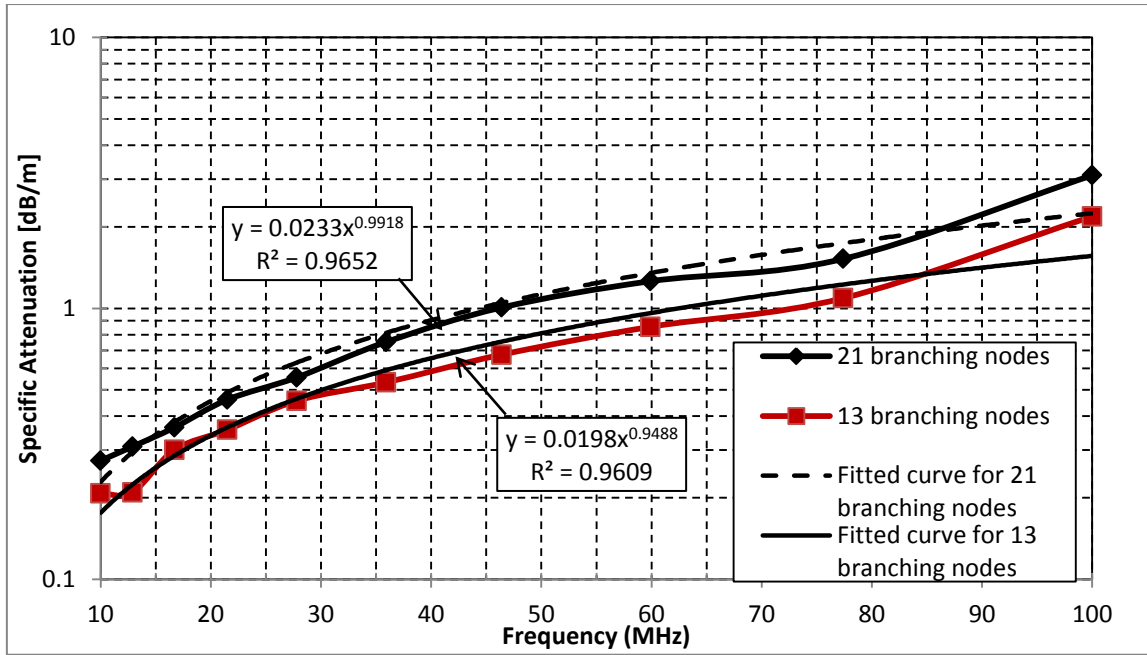


Figure 4.3-6: Models for 13 and 21 branching nodes at 10-100 MHz.

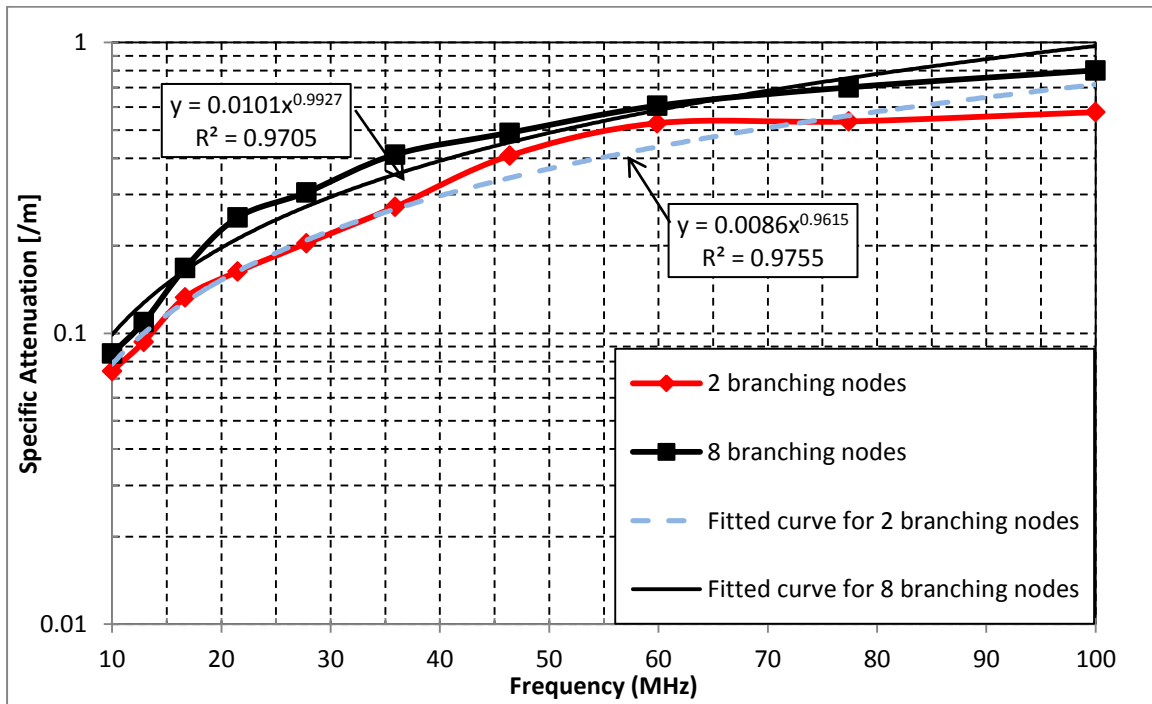


Figure 4.3-7: Models for 4 and 8 branching nodes at 10-100 MHz.

The specific power attenuation can also be represented in power law form as is the case with rain attenuation in Olsen *et al.*, (1978):

$$A_s = \rho K^\xi \tag{4.28}$$

where ρ and ξ are coefficients to be determined and K is the numbers of the branching nodes. Figures 4.3-8 to 4.3-10 below show the specific powerline attenuation models calculated from scattering models using a different set of frequencies. In Figure 4.3-8 where the frequencies used are 10, 16.7 and 21.7 MHz, respectively, the number of the branching nodes K is employed in the estimation of α and ξ through a regression fitting procedure. It is observed that the fitted model has a high coefficient of goodness ($R^2 = 0.98$) indicating a good fit to proposed model. We found $\rho = 0.0023$ and $\xi = 0.9689$ for 10 MHz; $\rho = 0.0074$ and $\xi = 0.9765$ for 16.7 MHz; $\rho = 0.0133$ and $\xi = 0.9781$ for 21.7 MHz. Table 4.3-2 summarises the results of the regression coefficients.

Table 4.3-1 Attenuation parameters for different number of branching nodes at 10 – 100 MHz.

Number of the Branching nodes	Model	Parameters	Coeff. of goodness R^2
2	a_1	86×10^{-4}	0.974
	k	0.9615	
4	a_1	95×10^{-4}	0.974
	k	0.9094	
5	a_1	93×10^{-4}	0.9884
	k	0.9298	
6	a_1	92×10^{-4}	0.9892
	k	0.9546	
8	a_1	101×10^{-4}	0.9705
	k	0.9927	
10	a_1	204×10^{-4}	0.9664
	k	0.9044	
13	a_1	198×10^{-4}	0.9609
	k	0.9609	
21	a_1	233×10^{-4}	0.9652
	k	0.9918	

Table 4.3-2 Power law attenuation parameters for different frequencies.

Freq(MHz)	10	16.7	21.5	27.8	35.9	46.4	59.9	77.4	100
α	0.0023	0.0074	0.0133	0.0237	0.0385	0.0768	0.1398	0.2582	0.491
ξ	0.9689	0.9765	0.9781	0.9877	0.0403	1.013	1.0322	1.0559	1.0762
R^2	0.9859	0.9863	0.9867	0.9871	0.9847	0.988	0.9887	0.9891	0.9888

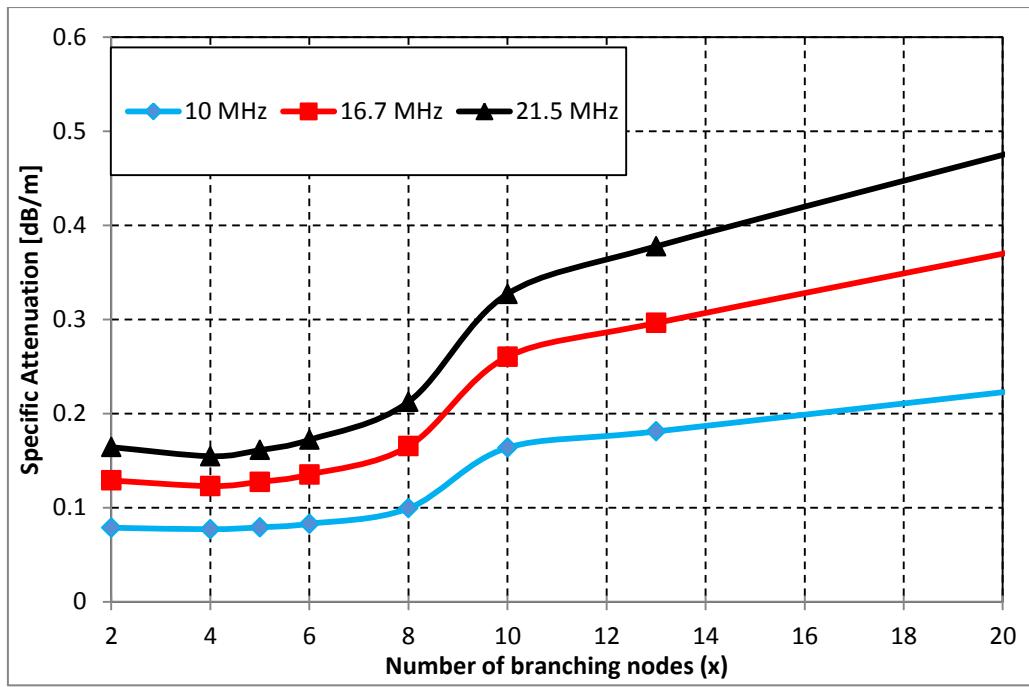


Figure 4.3-8 Specific attenuation at 10, 16.7 and 21.5 MHz with number of branching nodes

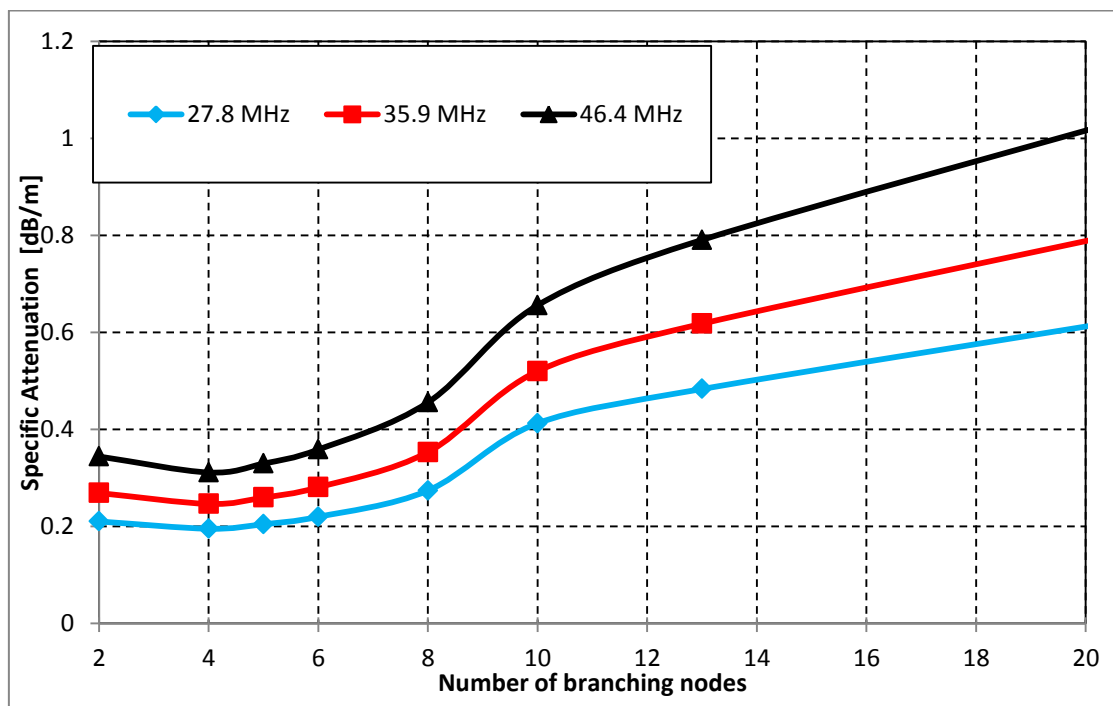


Figure 4.3-9 Specific attenuation at 27.8, 35.9 and 46.4 MHz with number of branching nodes

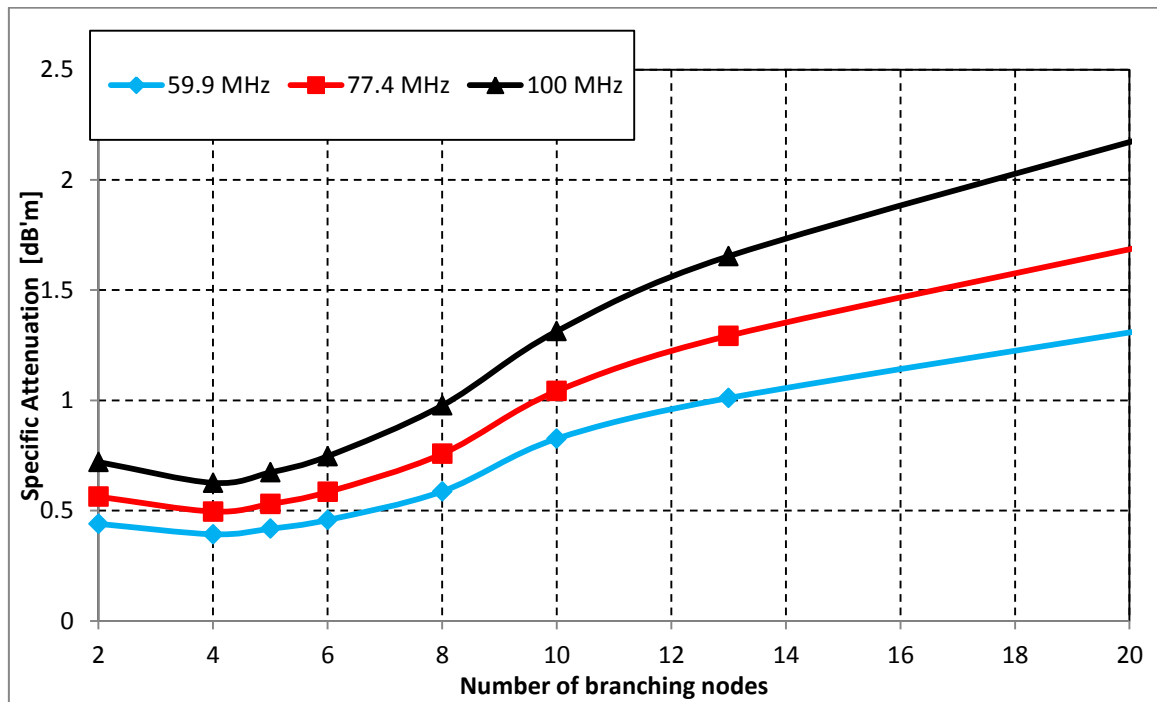


Figure 4.3-10 Specific attenuation at 59.9, 77.4 and 100 MHz with number of branching nodes

4.4 Phase shift Due to Number of Branching Nodes in the PLC Channels

The phase shift model is formulated based on the propagation constant discussed in Section 2.4 of this work. The propagation constant as given in Equation (2.10) can also be expressed as:

$$\gamma = \alpha + j\beta = \sqrt{(R + j\omega L)(G + j\omega C)} \quad (4.29)$$

Branching nodes induce phase shift (deg/m) in the channel. Oguchi (1966) earlier proposed that the expression for the propagation constant can also be modeled using Mie scattering as given in Equation (4.30):

$$\gamma = \frac{2\pi}{k_0} \int_0^{\infty} f(0)N(D)dD \quad (4.30)$$

where, $f(0)$ is the scattering amplitude function of a scatterer with diameter D in the forward directions and k_0 is the free space wave number. And later on, Oguchi (1981) derived the attenuation, α in dB and phase shift, β in degrees as:

$$\alpha = 8.686 \text{ Re}(\gamma L) \quad (4.31)$$

$$\beta = \frac{180}{\pi} \text{Im}(\gamma L) \quad (4.32)$$

where L is the propagation path length.

In practical applications, it is necessary to express attenuation and phase shift by an approximate power law or linear law in the frequency range. This is given as:

$$\alpha = \alpha_0 + \alpha_1 f^k; \quad \beta = j\beta_0 + \beta_1 f^\varepsilon \quad (4.33)$$

where $\alpha_0, \alpha_1, k, \beta_0, \beta_1$ and ε are parameters that depend on scattering point distribution, the reflective index of wire and temperature. The parameters $\alpha_0, \alpha_1, k, \beta_0, \beta_1$ and ε in Equation (4.33) were determined using power regression between the specific attenuation, specific phase shift and frequency at a fixed number of branching nodes, as shown in Fig. 4.4-2 to 4.4-6, where ε is zero in the frequency range of 10 to 100 MHz. Table 4.4-1 summarizes the phase shift parameters for different number of branching nodes.

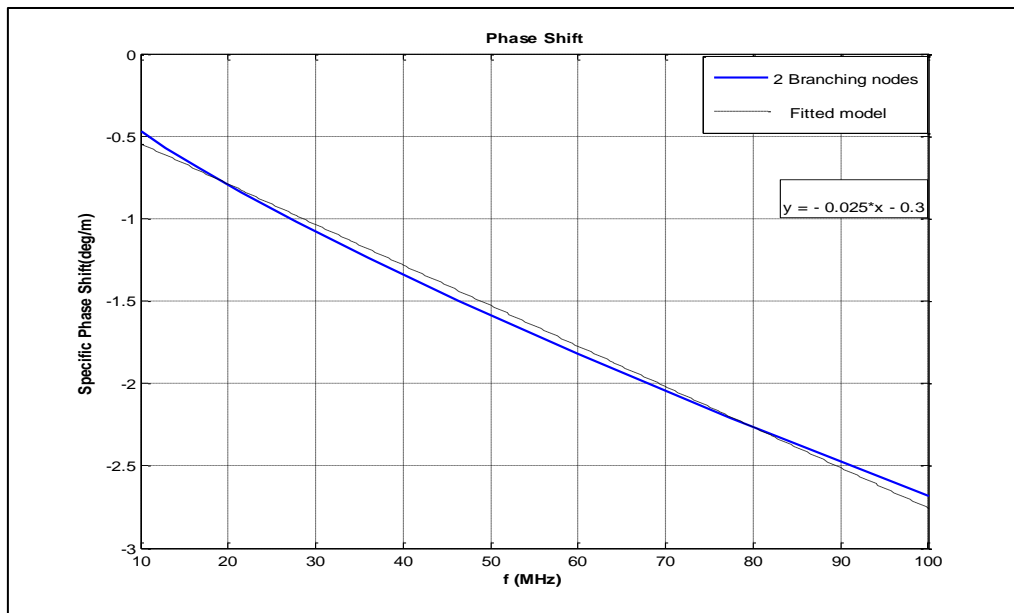


Figure 4.4-1 Specific Phase shift for scattering points (2 branching nodes) using lognormal distribution.

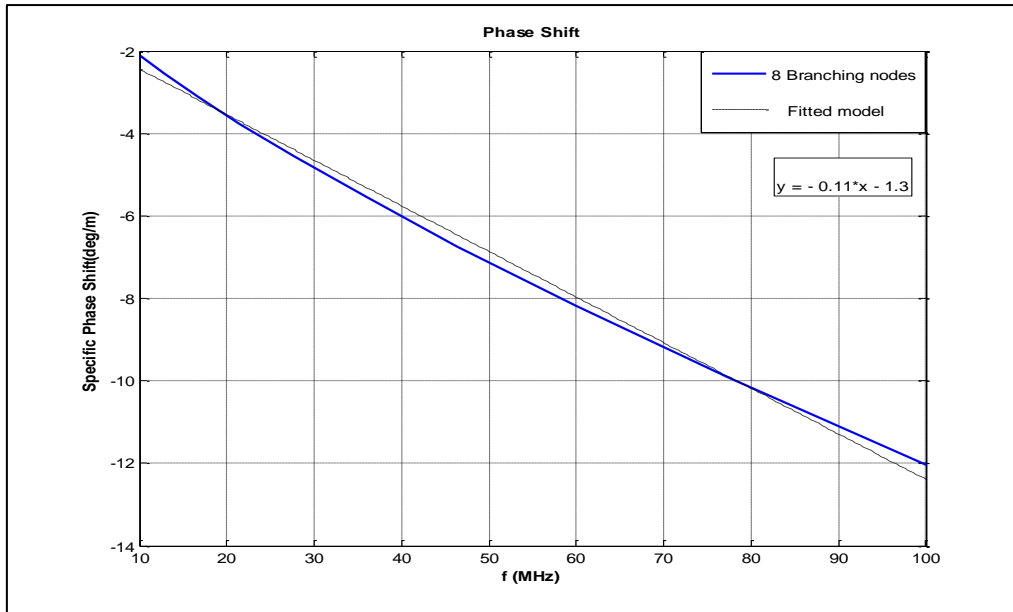


Figure 4.4-2 Specific Phase shift for scattering points (8 branching nodes) using lognormal distribution

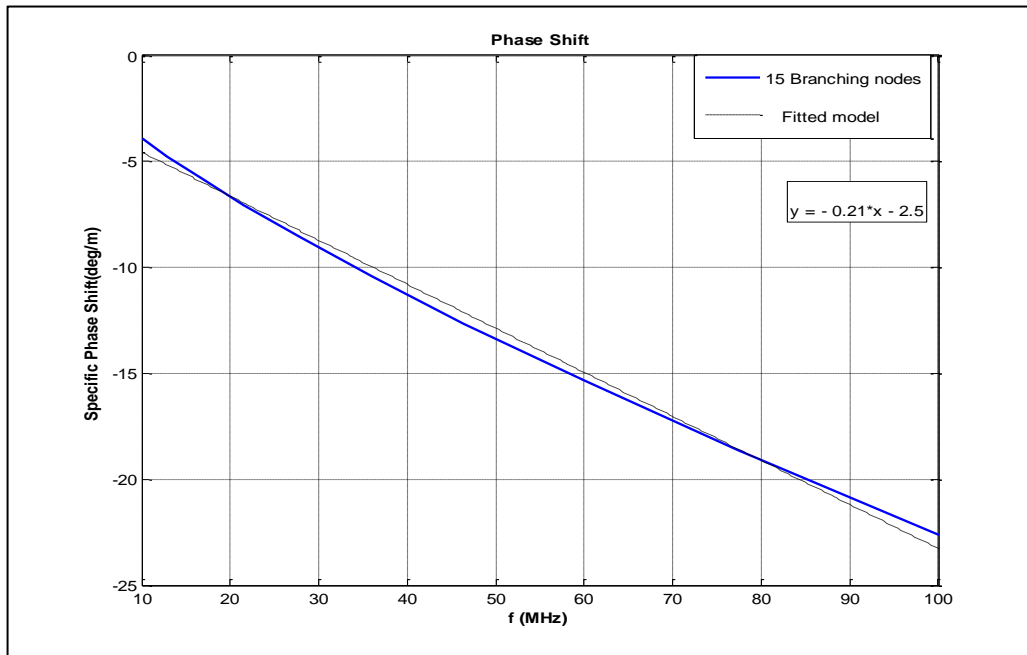


Figure 4.4-3 Specific Phase shift for scattering points (15 branching nodes) using lognormal distribution

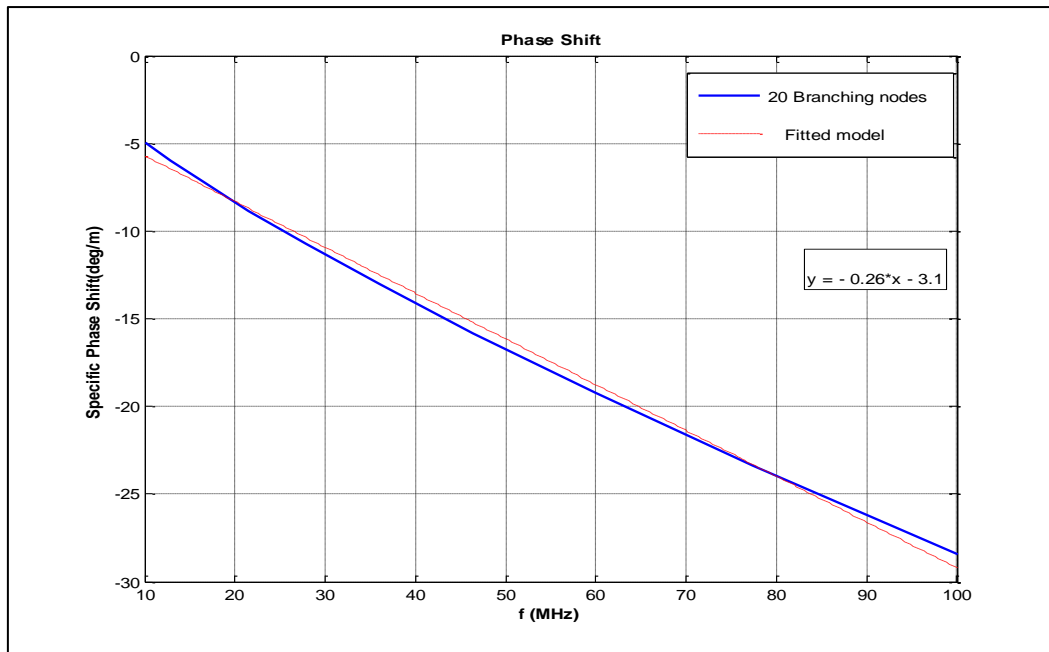


Figure 4.4-4 Specific Phase shift for scattering points (20 branching nodes) using lognormal distribution

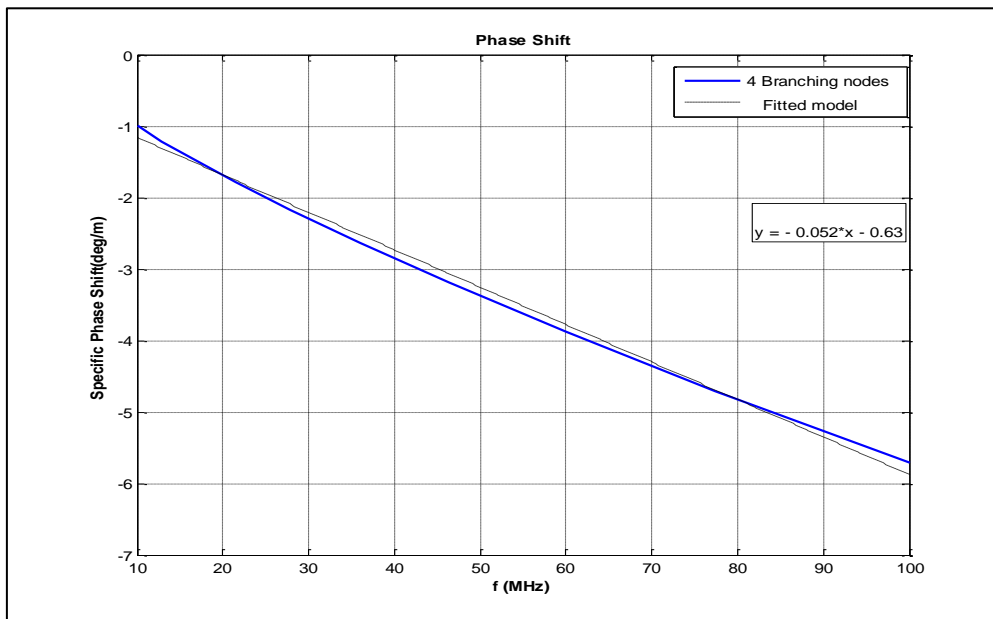


Figure 4.4-5 Specific Phase shift for scattering points (8 branching nodes) using lognormal distribution

Fig. 4.4-6 shows specific phase shift as function of branching nodes. The phase shift decrease as branching nodes increase.

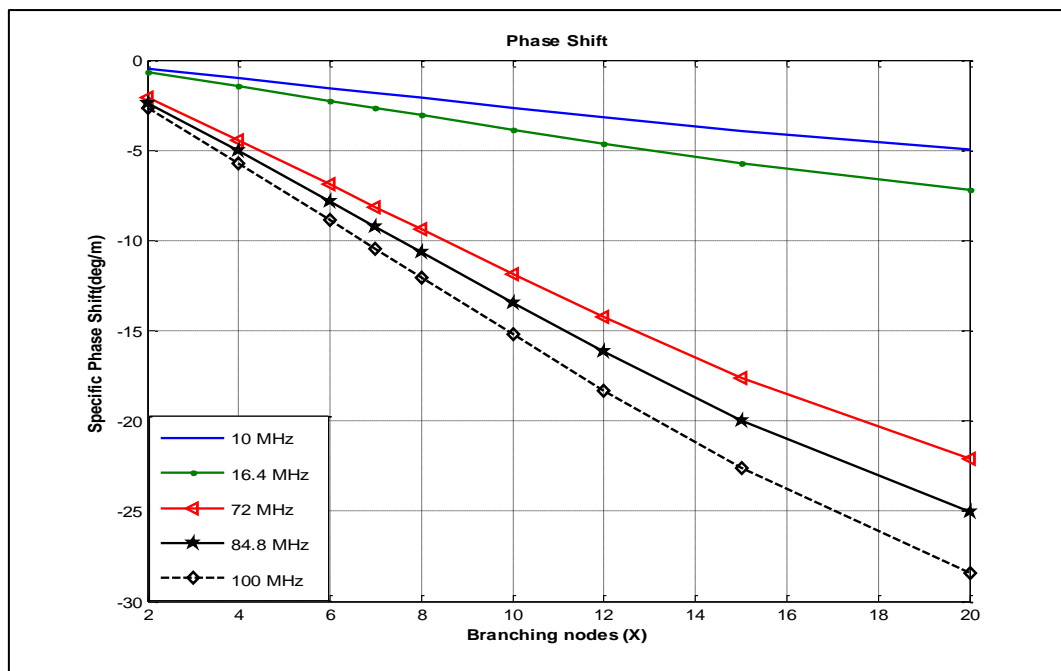


Figure 4.4-6 Phase shift for scattering points using lognormal distribution

Table 4.4-1 Phase Shift parameters for frequency range of 10-100 MHz

Number of the Branching nodes	Model Parameters		Coeff. of goodness R^2
	β_0	β_1	
2	β_0	-0.025	1
	ε	0	
	β_1	-0.3	
4	β_0	-0.52	1
	ε	2.7	
	β_1	-0.63	
5	β_0	-0.4	0.99
	ε	0	
	a1	-0.219	
8	β_0	-0.11	0.98
	ε	0	
	β_1	-1.3	
15	β_0	-0.21	0.99
	ε	0	
	β_1	2.5	
20	β_0	-0.25	0.99
	ε	0	
	β_1	-3.1	

4.5 Frequency Response for PLC Channel

4.5.1.1 ABCD Parameters of the Network

The two-wire transmission line can be modeled as two-port network using ABCD parameters as shown in Fig. 4.5-1, [Starr *et al.*, (1999)]. The ABCD parameters can be expressed in the following matrix relation in order to satisfy the port voltage and current dependency on the source and load impedances, as:

$$\begin{bmatrix} V_1 \\ I_1 \end{bmatrix} = \begin{bmatrix} A & B \\ C & D \end{bmatrix} \cdot \begin{bmatrix} V_2 \\ I_2 \end{bmatrix} \quad (4.34)$$

In the case of a cascade of two-port networks, as shown in Fig. 4.5-2 below, the ABCD parameters of this network will be the matrix multiplication of ABCD matrices for each individual two-port network as expressed in Equation (4.35) below:

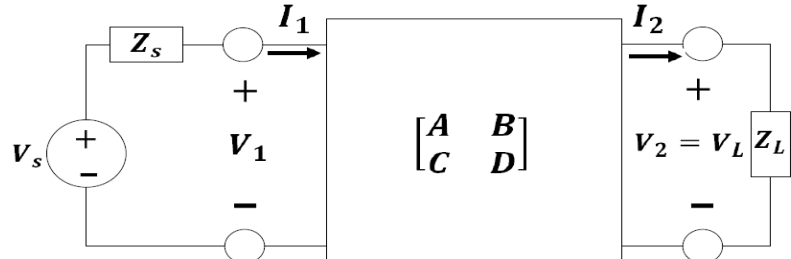
$$\begin{bmatrix} A & B \\ C & D \end{bmatrix} = \begin{bmatrix} A_1 & B_1 \\ C_1 & D_1 \end{bmatrix} \begin{bmatrix} A_2 & B_2 \\ C_2 & D_2 \end{bmatrix} \quad (4.35)$$


Figure 4.5-1: Two-port network model of two-wire transmission line

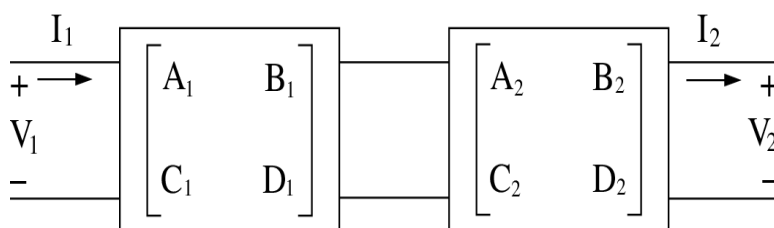


Figure 4.5-2: A Cascade two-port networks model of two-wire transmission line

The transfer function of the network in Fig. 4.5-1 and Fig. 4.5-2 using the ABCD model can be calculated by $H = V_L/V_s$. The fact that $I_2 = V_2/Z_L$ as in Fig. 4.5-1, means that the transfer function can be expressed as:

$$H = \frac{V_L}{V_s} = \frac{Z_L}{AZ_L + B + CZ_L Z_s + DZ_s} \quad (4.36)$$

The ABCD matrix for a transmission line with characteristic impedance of Z_o and propagation constant of γ and a length of l can be expressed as:

$$\begin{bmatrix} A & B \\ C & D \end{bmatrix} = \begin{bmatrix} \cosh(\gamma l) & Z_o \sinh(\gamma l) \\ Z_o^{-1} \sinh(\gamma l) & \cosh(\gamma l) \end{bmatrix} \quad (4.37)$$

4.5.1.2 Simulation of a Segmented Transmission Line

The chain matrix theory was used to compute the transfer function of transmission lines since the analytical models of attenuation constant and phase constant were derived from Sections 4.3 and 4.4. The transmission line channel with two branching points as shown in Fig. 4.5-3, and the segmented piece of the cable is modelled as a four terminal network represented by an ABCD matrix as shown in Fig. 4.5-4 and Fig. 4.5-5. The parameters $A_i, B_i, C_i,$ and D_i in Fig. 4.5-5 corresponding to the transmission line segments (1),(3), and (5) are the four terminal constants of the transmission matrix expressed as:

$$\begin{bmatrix} A_i & B_i \\ C_i & D_i \end{bmatrix} = \begin{bmatrix} \cosh \gamma l_i & Z_o \sinh \gamma l_i \\ Z_o^{-1} & \cosh \gamma l_i \end{bmatrix} \quad (4.38)$$

where, γ is the propagation constant, l_i is the length of the i -th cable, and Z_o is the characteristic impedance. The transmission matrix of the branch cables (2) and (4) is given as:

$$\begin{bmatrix} 1 & 0 \\ 1/Z_1 & 1 \end{bmatrix} \quad (4.39)$$

Where Z_1 is the equivalent impedance of the bridge tap, given by:

$$Z_1 = Z_o \left(\frac{Z_L + Z_o \tanh(\gamma l)}{Z_o + Z_L \tanh(\gamma l)} \right) \quad (4.40)$$

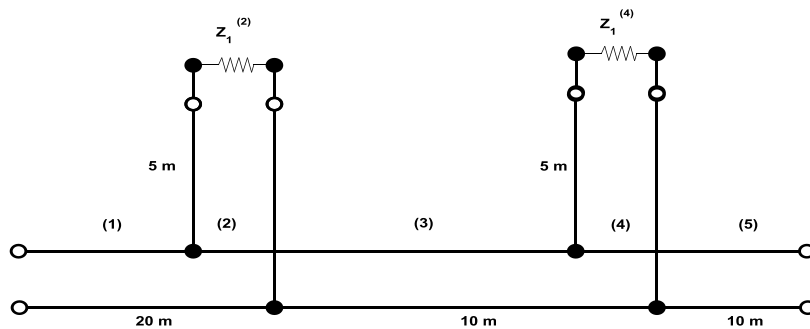


Figure 4.5-3: Network configuration for two-wire transmission line

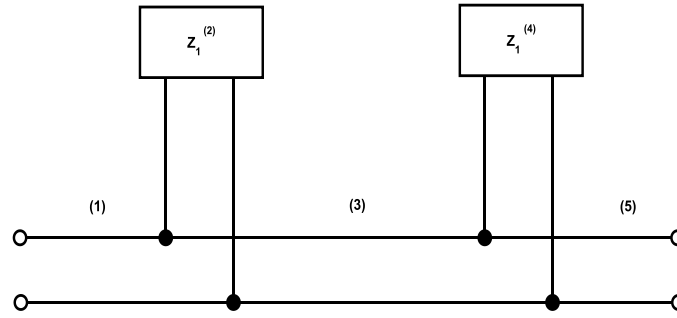


Figure 4.5-4: Network configuration for two-wire transmission line equivalent

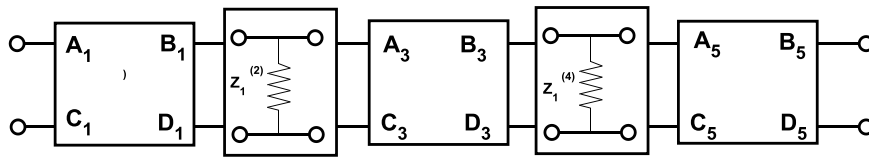


Figure 4.5-5: Network configuration for two-wire transmission line as ABCD matrix

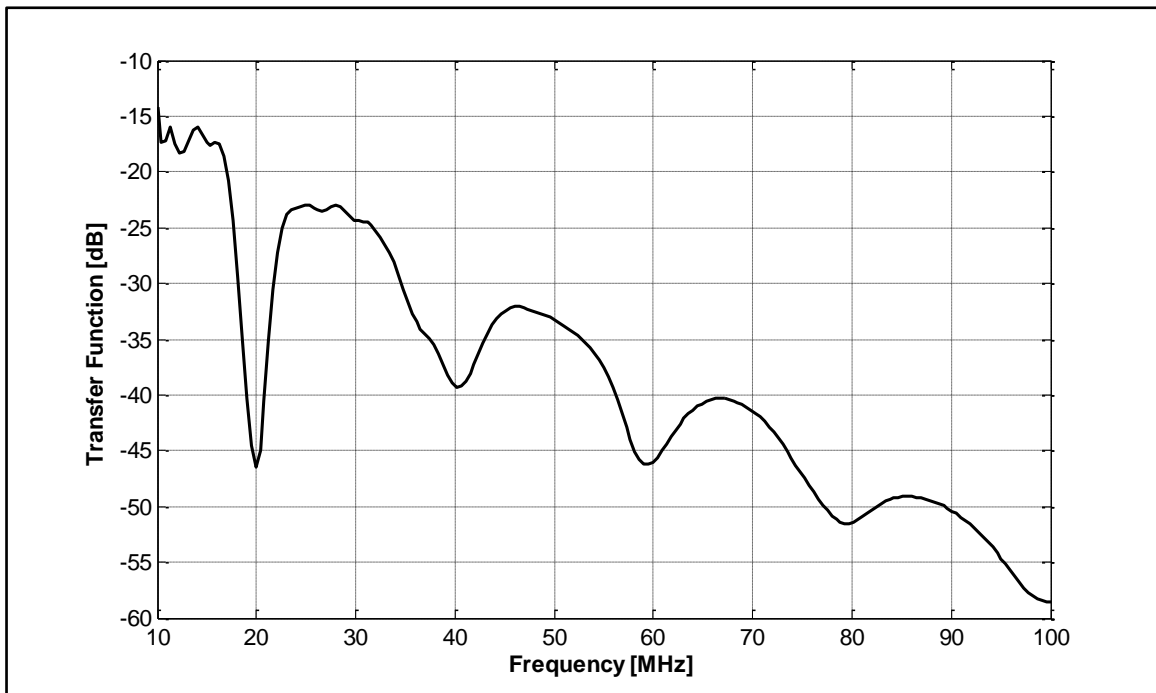


Figure 4.5-6: The frequency response of a 40 m two-wire transmission with two-branch of length 5 m each terminated by a load of 50Ω .

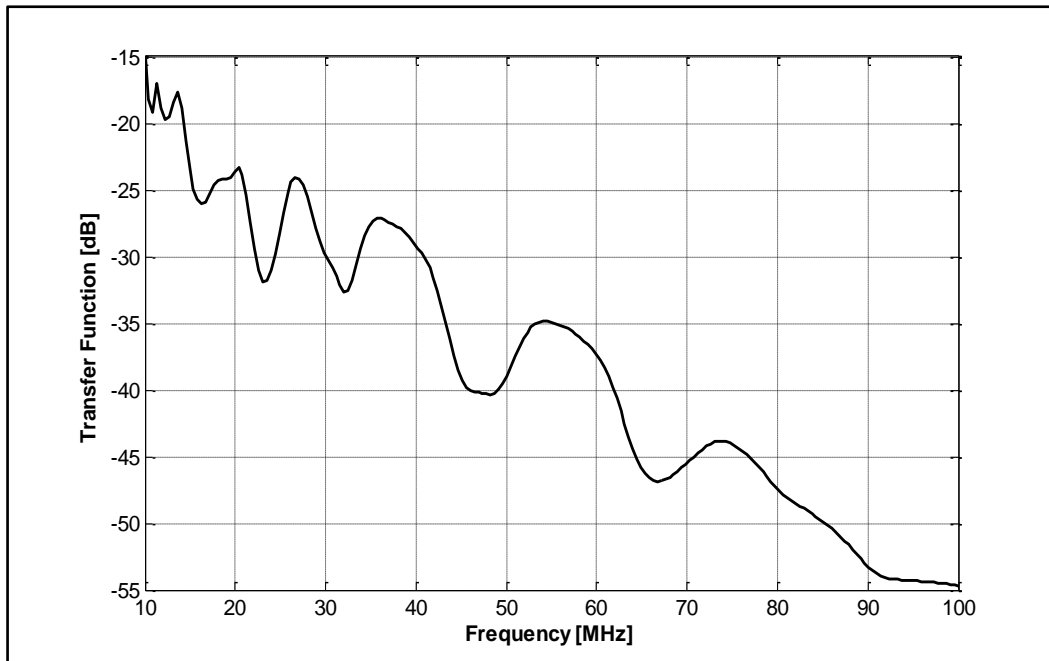


Figure 4.5-7: The frequency response of a 40 m two-wire transmission with two open-circuited branches of length 5 m each.

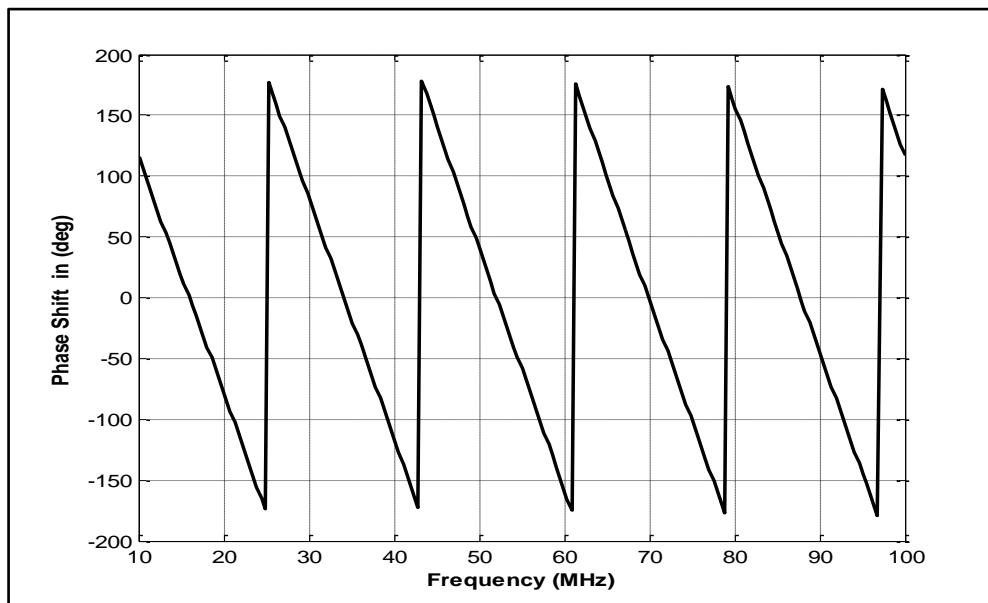


Figure 4.5-8: The phase shift of a two-wire transmission with two open-circuited branches of length 5 m each.

Therefore, the ABCD matrix of the network denoted by $[T]$, is given as

$$[T] = \begin{bmatrix} A_1 & B_1 \\ C_1 & D_1 \end{bmatrix} \begin{bmatrix} 1 & 0 \\ 1/Z_1^{(2)} & 1 \end{bmatrix} \begin{bmatrix} A_3 & B_3 \\ D_3 & C_3 \end{bmatrix} \times \begin{bmatrix} 1 & 0 \\ Z_1^{(4)} & 1 \end{bmatrix} \begin{bmatrix} A_5 & B_5 \\ C_5 & D_5 \end{bmatrix} \quad (4.41)$$

And the equivalent to the transfer function of the network is the reciprocal of A in $[T]$, [Tsuzuki *et al.*, (2002)]. Fig. 4.5-6, 4.5-7 and Fig. 4.5-8 show the simulation of transfer function and phase shift of two-wire transmission line with segments (2) and (4) terminated by 50Ω each by the using two-port

network modeling in MATLAB. The input parameters in Fig. 4.5-6, Fig. 4.5-7 and Fig. 4.5-8 are the characteristic impedance Z_o and the propagation constant γ which are used to describe a transmission line. The analytical models of the attenuation constant α and the phase constant β are derived in Sections 4.3 and 4.4 while Z_o is derived in Section 3.2. For the topology in Figure 4.5-3, which has two branching points or taps, the following parameters were used:

$$\alpha = 86 \times 10^{-4} \times f^{0.9615} \text{ and } \beta = -j0.025 - 0.386. \quad (4.42)$$

4.6 Chapter Conclusion

There are a lot of factors that influence the reliable communication of high-speed data in single-phase LV networks. Among these factors, the distribution of scattering points that lead signal attenuation is the main one, which must be studied extensively.

In Section 4.2, an analytical model of scattering size distribution and probability density distribution in broadband PLC channels is presented. The analysis performed show that there are more scattering points at lower diameter sizes of branches in indoor networks where the peak is reached at a mean diameter of 0.8 mm, which implies more reflections of the signal. In fact, there is extensive coupling and uncoupling of appliances connecting to the branches of this mean diameter in indoor single-phase networks. But on the high diameter range (above 2 mm), scattering points are smaller and the reflection is less. Also, the results show the independency of the distributions towards the indoor network topology.

In Section 4.3, a specific attenuation model of a powerline network using Mie scattering theory was developed at the nodes where mismatch occurs. The proposed model was estimated for different number of branching nodes. By using the frequency range of 10 MHz to 100 MHz, we compared the proposed model with the theoretical attenuation. The results showed that the proposed model underestimates the attenuation at the frequencies below 20 MHz and overestimates the attenuation value at the frequencies above 50 MHz compared to the theoretical attenuation. Also, we developed a power law model that relies on the knowledge of the number of branching nodes in the network and thus, the attenuation can be predicted from this model. We also investigated the phase shift that occurs in the PLC channel due to a varying number of branches. Finally, the analytical models of the attenuation constant α and the phase constant β are derived in Sections 4.3 and 4.4 and Z_o derived in Section 3.2, were used in the two-port model in order to simulate the channel frequency response. In Chapter five, channel measurements are done to ascertain the accuracy of the models developed.

4.7 References

Papaleonidopoulos, I.C., C.N. Capsalis, C.G. Karagiannopoulos and N.J. Theodorou, (2003), "Statistical Analysis and Simulation of Indoor Single-Phase Low Voltage Powerline Communication Channels on the basis of Multipath Propagation," *IEEE Trans. Consumer Electronics*, Vol.49, No. 1, pp. 89-99, February.

Papaleonidopoulos, I.C., C.G. Karagiannopoulos, N.J. Theodorou, C.E. Anagnostopoulos and I.E. Anagnostopoulos, (2002), "Modelling of Indoor Low-Voltage Cables in the High Frequency range," in *Proc. ISPLC'97*, pp. 267-271.

Malack, J.A. and J.R. Engstrom, (1976) "RF Impedance of United States and European Power Lines," *IEEE Trans. Electromagnetic Compatibility*, vol. EMC-18, pp. 36-38, February.

Zimmermann, M. and K. Dostert, (1999) "A multi-path signal propagation model for the powerline channel in the high frequency range," *ISPLC'1999*, pp.45-51, Lancaster U.K.

Philips, H. (1999), "Modelling of Powerline Communication Channels," in *Proc. ISPLC'99*, pp. 14-21.

Güzelgöz, S., H. B. Çelebi, and H. Arslan, (2011), "Statistical Characterization of the Paths in Multipath PLC channel Channels," *IEEE Trans. On Power Delivery*, vol.26, No.1, January.

Papaleonidopoulos, I. C., C. G. Karagiannopoulos, N. J. Theodorou, C. E. Anagnostopoulos and I. E. Anagnostopoulos, (2002), "Modelling of Indoor Low-Voltage Cables in the High Frequency range," in *Proc. ISPLC'97*, pp. 267-271.

Pahlavan, K. and A.H. Levesque, (1995), *Wireless Information Networks*, John Wiley & Sons, Inc.: New York, pp. 37-142.

Papaleonidopoulos, I. C., C. N. Capsalis, C. G. Karagiannopoulos and N. J. Theodorou, (2003) "Statistical Analysis and Simulation of Indoor Single-Phase Low Voltage Powerline Communication Channels on the basis of Multipath Propagation," *IEEE Trans. Consumer Electronics*, Vol.49, No. 1, pp. 89-99, February.

Zimmermann, M. and K. Dostert, (1999), "A multi-path signal propagation model for the powerline channel in the high frequency range," *ISPLC'1999*, pp.45-51, Lancaster U.K.

Philips, H., (1999), "Modelling of Powerline Communication Channels," in *Proc. ISPLC*, pp. 14-21.

Oguchi, T., (1966), "Scattering and absorption of a millimeter wave due to rain and melting hailstones," *J. Radio Res Laboratories*, 13: 141-172.

Oguchi, T., (1981), "Summary studies on scattering of centimeter and millimeter waves due to rain and hail," *Ann. Telecommun.*, 36: 383-399.

C. T. Mulangu, T. J. O. Afullo and N. M. Ijumba, (2012) "Scattering Points Size Distribution for Indoor Broadband PLC Channels," *PIERS, Malaysia, March*, ISSN: 1559-9450.

Tsuzuki, S., T. Takamatsu, H. Nishio and Y. Yamada, (2002) "An estimation method of the transfer function of indoor powerline channels for Japanese houses," in *Proc. Int. Symp. Power-lines Comm.*, Athens, Greece, pp.55-99.

Feynman, R. P., R. B. Leighton and M. Sands, (1964), "The Feynman Lectures on Physics," *Vol. No.2*, Addison-Wesley.

Mulangu, C.T and T. J. Afullo, (2009) "Variability of the Propagation Coefficients Due to Rain for Microwave Links in Southern Africa," *Radio Sci.*, Vol. 44.

Mätzler, C. (2002b), MATLAB Functions for Mie Scattering and Absorption, Version 2, *IAP Res. Rep. No. 2002-08*, University of Bern, Switzerland, June.

Bohren, C.F and D. R. Huffman, (2004) "Absorption and scattering of light particles," Wienheim, John Wiley.

Olsen, R. L., D. V. Rogers and D. B. Hodge, (1978), "The aR^b Relation in the Calculation of Rain Attenuation," *IEEE Trans. Antennas Propagat.*, AP-26(2), pp. 318-329.

Brown, P. A., (1995) "High frequency conditioned power networks," in *UTC Annu. Conf. Proc.*, July/Aug.

Lindell, G., (2001), "On Coding and Modulation for the PowerlineCommunication Channel", *Proceeding of ISPLC channel 2001*, Sep., pp. 14-17.

Sebeck, M., and G. Bumiller, (2000) "A Network Management System for Powerline Communication and its Verification by Simulation," *Proceeding of ISPLC channel 2000, Limerick, Ireland*, April, pp.225-232.

Dostert, K., (1997) "Telecommunications over power distribution grid: Possibilities and limitations," *ISPLC'1997*, Essen Germany.

Esmailian, T., P.G. Gulak, and F.R. Kschischang, (2000)"A discrete multitone power line communications system," *Proc. of ICASSP*, vol. 5, pp. 2953-2956, Jun.

Liu, E., Y. Gao, G. Samdani, Omar Mukhtar, and T. Korhonen, (2005) "Broadband powerline channel and capacity analysis," *ISPLC channel 2005*, pp.7-11, April.

Zimmermann, M., and K. Dostert, (2002) "A Multipath Model for the Power Line Channel," *IEEE Trans. Commun.*, vol. 50, no. 4, pp.553-559, April.

Mulangu, C.T, T. J. Afullo and N. M. Ijumba, (2012a) "Scattering points Size Distribution for Indoor Broadband PLC channel Channels," *PIERS Progress In Electromagnetics Research Symposium. PIERS 2012*, ISSN: 1559-9450, Kuala Lumpur, Malaysia, March.

Mulangu, C.T, T. J. Afullo and N. M. Ijumba, (2012b) "Estimation of Specific Attenuation due to Scattering Points for Broadband PLC channel Channels, " *PIERS Progress In Electromagnetics Research Symposium. PIERS 2012*, , ISSN: 1559-9450, Kuala Lumpur, Malaysia, March.

T. Starr, J.M. Cioffi and P.J. Silverman, "Understanding Digital Subscriber Line Technology," New York, Prentice Hall.

S. Tsuzuki, T. Takamatsu, H. Nishio, Y. Yamada, "An Estimation Method of the Transfer Function of Indoor Power-line Channels for Japanese Houses," *Proc. of the 6th ISPLC*, 27-29 March **2002**, Athens.

Ahola J., T. Lindh, and J. Partanen, (2002) "Determination of Properties of Low Voltage Power Cables at Frequency Band 100 kHz – 30 MHz," ICEM, Bruges, Belgium, August 26-28, 2002.

Ahola Jero, (2003), "Applicability of Powerline Communications to Data Transfer of Online Condition Monitoring of Electrical Drives," PhD thesis, Lappeenranta University of Technology, Aug.

Chapter Five

Channel Model Validation Using Measurements

5.1 Introduction

The measurements were carried out with an oscilloscope, vector analyzer and a function generator. To protect the sensitive equipment from the damaging 220 V / 50 Hz signal used for power distribution, passive coupling circuits were used. A schematic of the setup is shown in Figure 5.1-1.

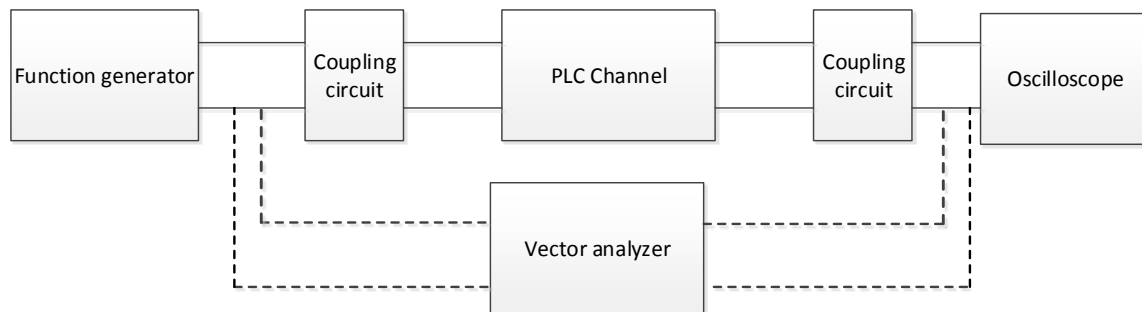


Figure 5.1-1 Schematic diagram for measurements.

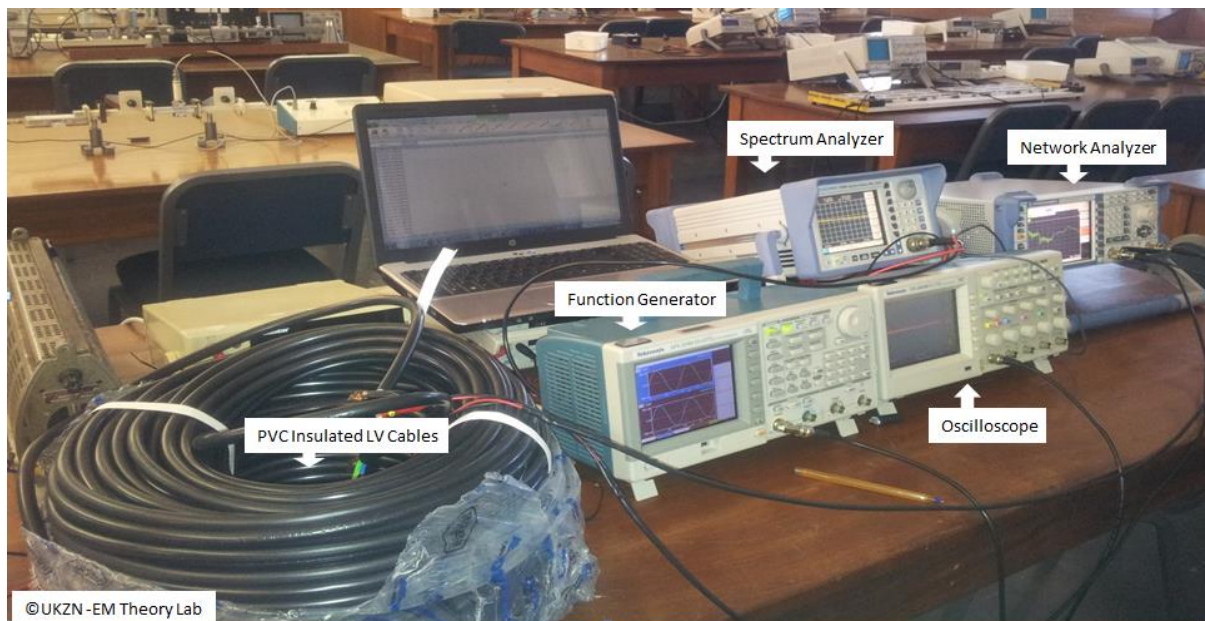


Figure 5.1-2 System setup for measurements

5.2 Measurement Devices

5.2.1 Network Analyzer

This piece of equipment is needed to analyze open, short-circuit and load impedances at different frequencies while connected at selected powerline network configurations. The Rohde & Schwarz

ZVL13 Network Analyzer was used. This is a general-purpose network analyzer with comprehensive functionality to support network and impedance measurements for electronic devices from LF to RF, with the following characteristics:

- Frequency range of 9 kHz to 13.6 GHz
- 50 ohm S-parameter test set
- Output Power: -27 dBm / 20 V DC

5.2.2 Oscilloscope

This scope enables us to analyze the signal and noise in the time domain as a time series. The oscilloscope used was the Tektronix TDS2024B Oscilloscope with the following characteristics;

- 200 MHz, 4 channels
- 2GS/s Real time
- 2.5K Record Length
- Color or Monochrome LCD Display
- Removable Data Storage using the Front-panel USB Port
- Seamless PC Connectivity through the USB Device Port, with Open Choice[®] and NI Signal Express[®] PC Software
- Advanced Triggers including Pulse Width Trigger and Line-selectable Video Trigger
- FFT Standard on All Models
- 12 Automatic Measurements

5.2.3 Signal Generator

The signal generator was used as our signal source during testing. The TEKTRONIX - AFG3102 - FUNCTION GENERATOR, ARBITRARY was used. This signal generator has the following characteristics:

- FUNCTION GENERATOR, ARBITRARY
- Signal Generator Type: Arbitrary, Function
- Bandwidth: 100MHz
- Modulation Type: AM, FM, FSK, PM, PWM
- Supply Voltage Range: 100V to 240V
- External Height: 156.3mm
- External Width: 329.6mm
- External Depth: 168mm

- Plug Type: Euro, UK
- Series: AFG3000
- Sweep Rate Range: 1Hz to 50MHz lin/log

5.3 Measurement Techniques

A series of input impedance measurements was carried out for two PVC flexible low voltage power cables. The type of cable under consideration is generally used in building wiring in South Africa as shown in Fig. 5.3-1. The measured cables type was CABTYRE CABLE- FLEXIBLE WIRING CABLE (300/500 V) and the dimensions of the cables are: $3 \times 4 + 100 \text{ m}$ and $3 \times 2.5 + 100 \text{ m}$. The longest cable was 100 m and its diameter was 3.0 mm, and the shortest cable was 50 m and diameter was 2.0 mm. In order to determine the characteristic impedance of transmission line cable from measured data, the input impedance was measured when the cable end was opened-circuited and then when it was short-circuited.



Figure 5.3-1: PVC insulated flexible cable.

5.3.1 Input Impedance Measurements

The characteristic impedance of a transmission line is determined by performing two input impedance measurements. The input impedance has to be measured when the cable end is open and short-circuited. When the cable end is short-circuited, the voltage at the end is zero and when the cable end is open, the current at the end is zero. The network analyzer used can only measure the scattering parameters (S) that are then converted to impedance parameters (Z). The measurement scheme is shown in Fig.5.3-2.

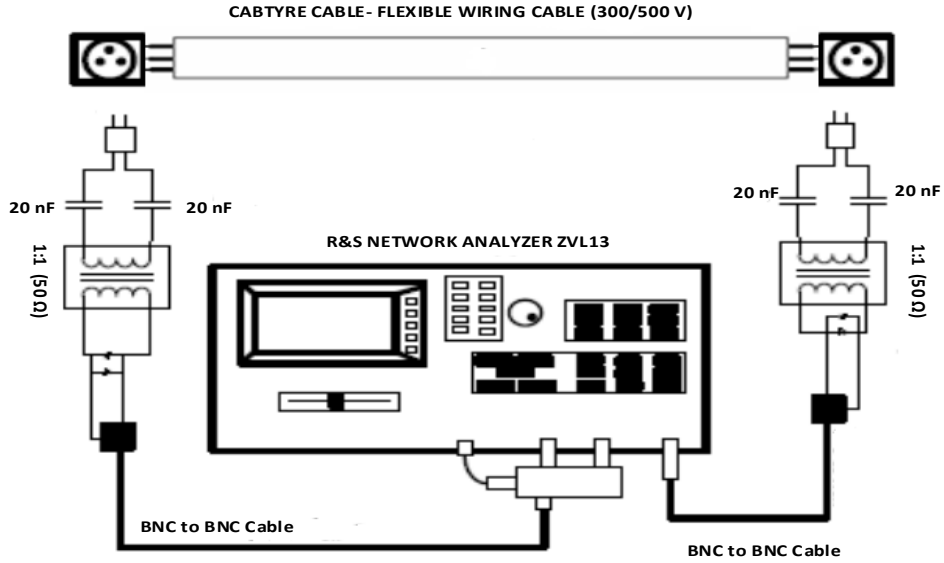


Figure 5.3-2: Measurements setup using network analyzer.

The voltage ratio V_2 (A port of the network analyzer) to V_1 (Reference port) is given as:

$$\frac{V_2}{V_1} = \frac{2 \frac{Z_{11open} Z_R}{Z_{11open} + Z_R}}{Z_R \frac{Z_{11open} Z_R}{Z_{11open} + Z_R}} = S_{21} \quad (5.1)$$

Since Z_R is the output and input impedance of the network analyzer, $Z_R = 50 \Omega$. Then Z_{11open} is given by:

$$Z_{11open} = \frac{25S_{21}}{1 - S_{21}} \quad (5.2)$$

If $Z_L = Z_o$, then Γ_L is zero and so $a_2 = \Gamma_L b_2 = 0$

So

$$S_{11} = \left. \frac{b_1}{a_1} \right|_{Z_L=Z_o} \quad (5.3)$$

So when $Z_L = Z_R$ then input impedance $Z_{in}|_{Z_L=Z_R} = Z_{11short}$, therefore:

$$S_{11} = \frac{Z_{11} - Z_R}{Z_{11} + Z_R} = \Gamma_{in} \quad (5.4)$$

Which implies that:

$$Z_{11short} = Z_R \left(\frac{1 + S_{11}}{1 - S_{11}} \right) \quad (5.5)$$

Table 5.3-1 shows the sample of the measurement parameters. We measured the magnitude and angle of S_{11} for open and short circuit, both in dB and linear. We also measured the imaginary and real parts of the same.

Table 5.3-1: Measured S_{11} data

Freq [MHz]	S11[SCLin]	S11[SC°]	S11[OCRe]	S11[OCIm]	S11[OC°]	S11[OC Lin]
10	0.230767	-7.99596	0.133493	-0.17636	-52.6315	0.221684
10.45	0.250235	-17.8383	-0.08895	-0.13262	-123.684	0.160586
15.4	0.291987	-32.6099	-0.07213	0.01488	170.0826	0.074046
19.45	0.320258	-51.7511	-0.02053	-0.04353	-117.996	0.048313
23.05	0.354855	-58.8807	-0.05027	-0.00473	-175.582	0.050496
26.65	0.397986	-76.1365	-0.02213	0.0305	126.9319	0.041109
33.4	0.513416	-120.282	0.025434	-0.0041	4.317777	0.018785
40.15	0.476296	-152.948	0.006563	-0.00129	-18.3872	0.008526
50.05	0.573068	151.2981	-0.00479	-0.00906	-107.718	0.010949
60.4	0.607185	94.37352	-0.01316	0.008199	152.8286	0.017771
70.3	0.66437	44.60826	0.007233	0.00182	8.467035	0.008014
80.2	0.651217	-8.22218	-0.00121	0.002935	151.5859	0.001023
90.1	0.714541	-45.9243	0.072786	-0.06753	-37.535	0.086602
100	0.773982	-98.3332	-0.0071	0.00282	178.9864	0.006776

In Figure 5.3-3, we consider the 100 m of cable lengths with cross-section of 4 mm² and without branching nodes. We first measured the propagation speed in the transmission line terminated by equivalent impedance to characteristic impedance, ($Z = Z_0 = 50 \Omega$) at 100 MHz as shown in Fig. 5.3-2 below. The measured time difference t_d between the sending end and the receiving end of the sine wave signal was 750 nS. The snapshot in Figure 5.3-3 below shows the sending end and the receiving end of the signal. The trigger holdoff was set at 500 nS. The corresponding propagation velocity is given by:

$$v_p = \frac{l}{t_d} = \frac{100m}{750 \times 10^{-9} S} = 0.13 \times 10^9 \frac{m}{S} \quad (5.6)$$

where, l is the length of the transmission line cable. The propagation velocity can be also written as function of the speed of light c_0 as $0.44c_0$

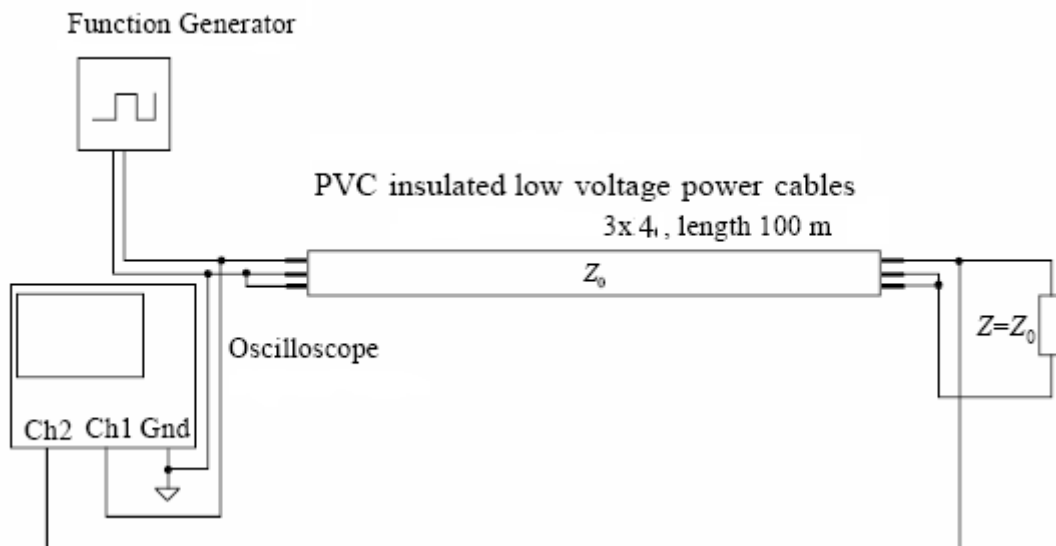


Figure 5.3-3: Measurement set up of the propagation speed of transmission line

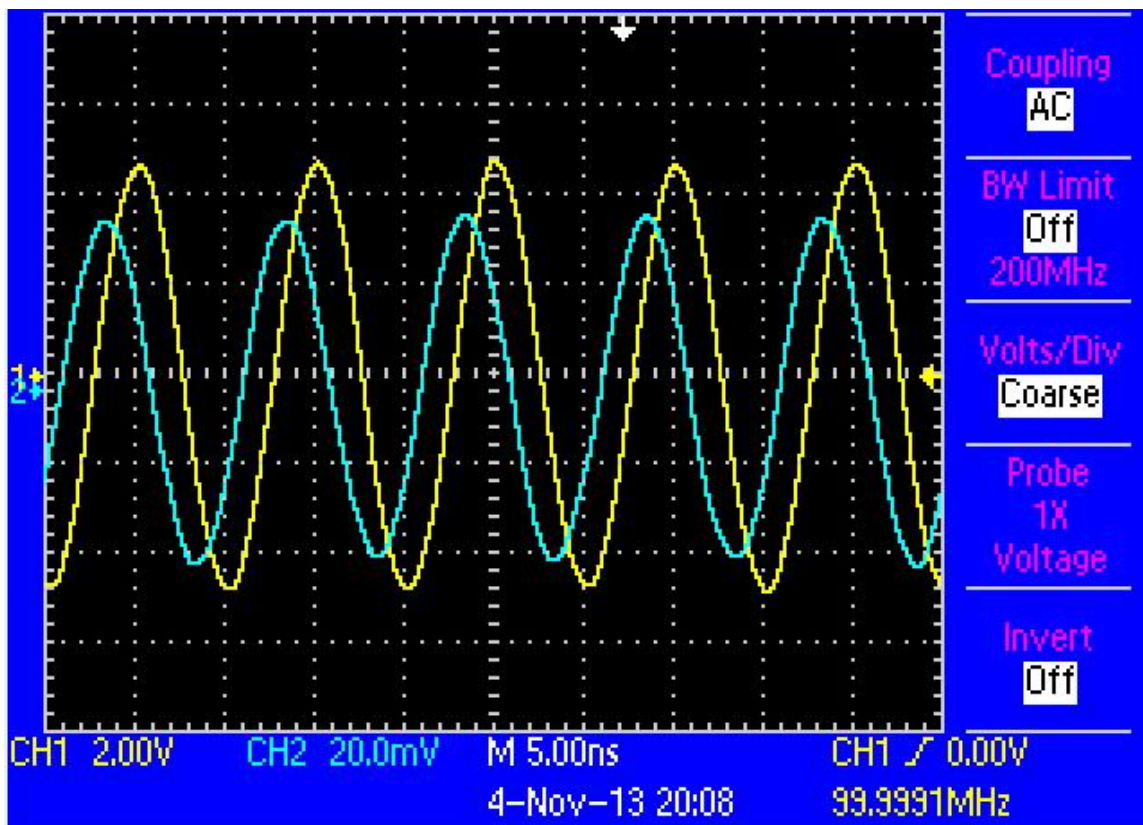


Figure 5.3-4: Snap shot of the sending end (yellow) and receiving end (blue) of the signal in a 100 m long transmission line

The complex input impedance $Z_{11\ open}$ for the cable with length L , is given by:

$$Z_{11\ open} = Z_o \coth(\gamma L) \quad (5.7)$$

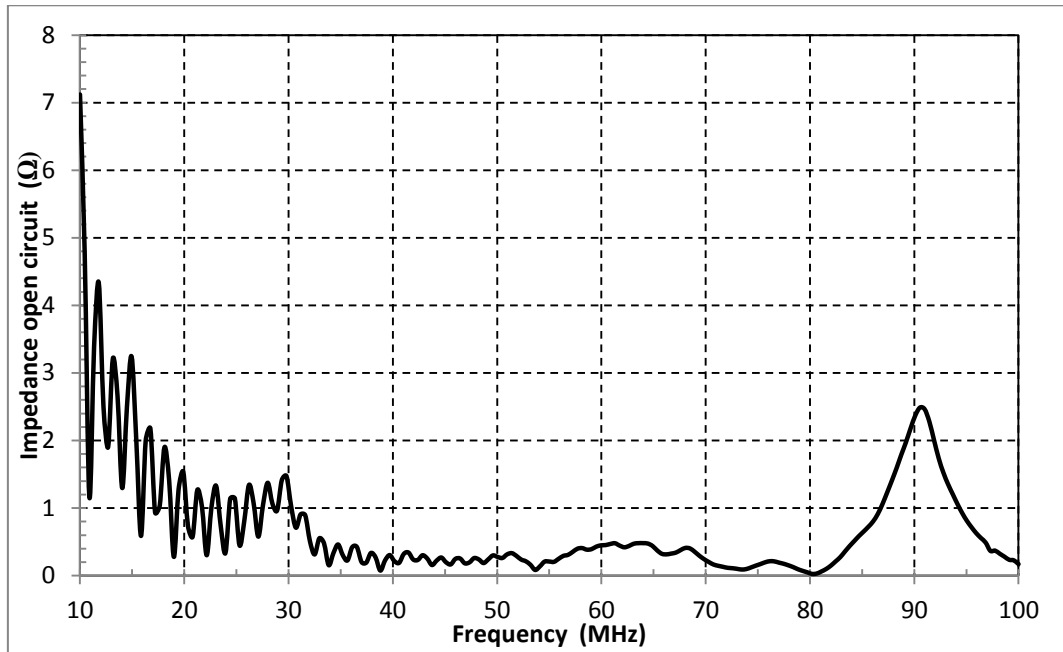


Figure 5.3-5: Net input impedance measured when the cable end is open-circuited as a function of frequency in the range of 10 – 100 MHz.

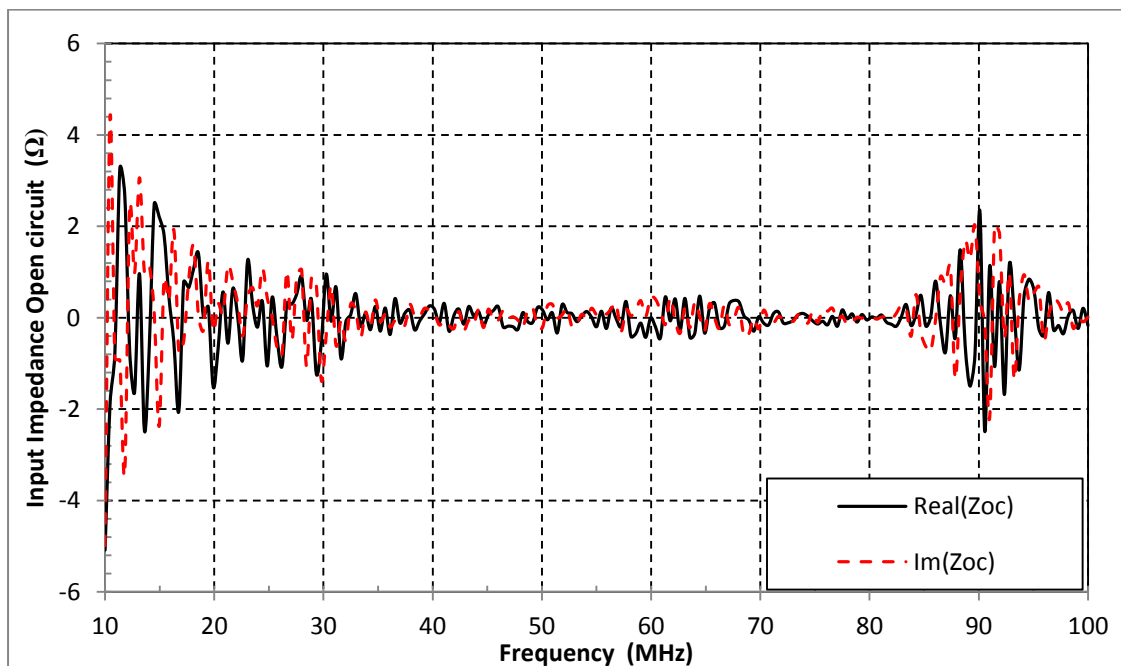


Figure 5.3-6: Complex input impedance measured when the cable end is open as a function of frequency in the range of 10 – 100 MHz.

Similarly, when the end of the cable is short-circuited, which means, $Z_L = 0$, the equation for the input impedance $Z_{11short}$ is given by:

$$Z_{11short} = Z_o \tanh(\gamma L) \tag{5.8}$$

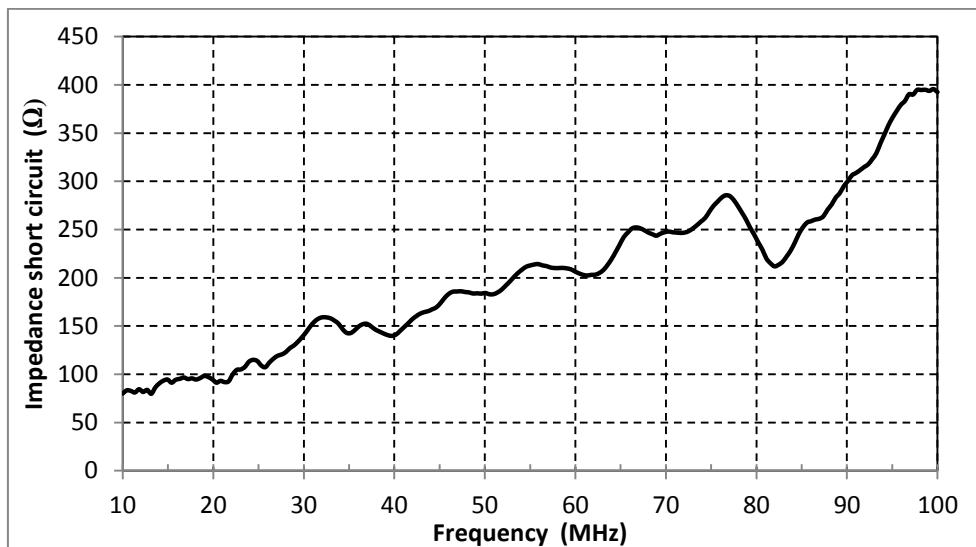


Figure 5.3-7: Input impedance measured when the cable end is short-circuited as a function of frequency in the range of 10 – 100 MHz. the length of the cable is 100 m.

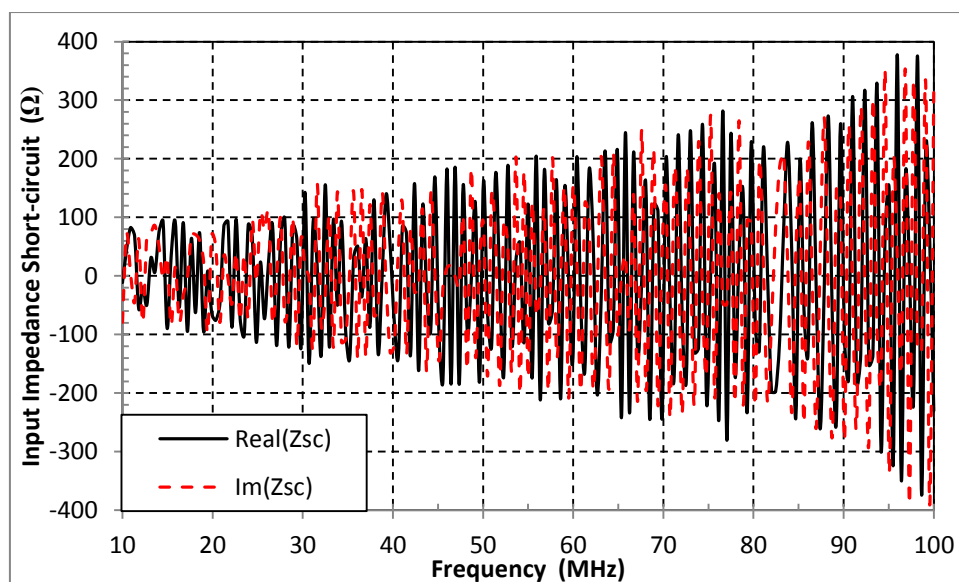


Figure 5.3-8: The real (continuous) and imaginary (dashed) of input impedance measured when the cable end is short-circuited as a function of frequency in the range of 10 – 100 MHz; the length of the cable is 100 m.

The equation for the characteristic impedance is combining Equations 5.7 and 5.8:

$$Z_o = \sqrt{Z_{11\ open} Z_{11\ short}} \quad (5.9)$$

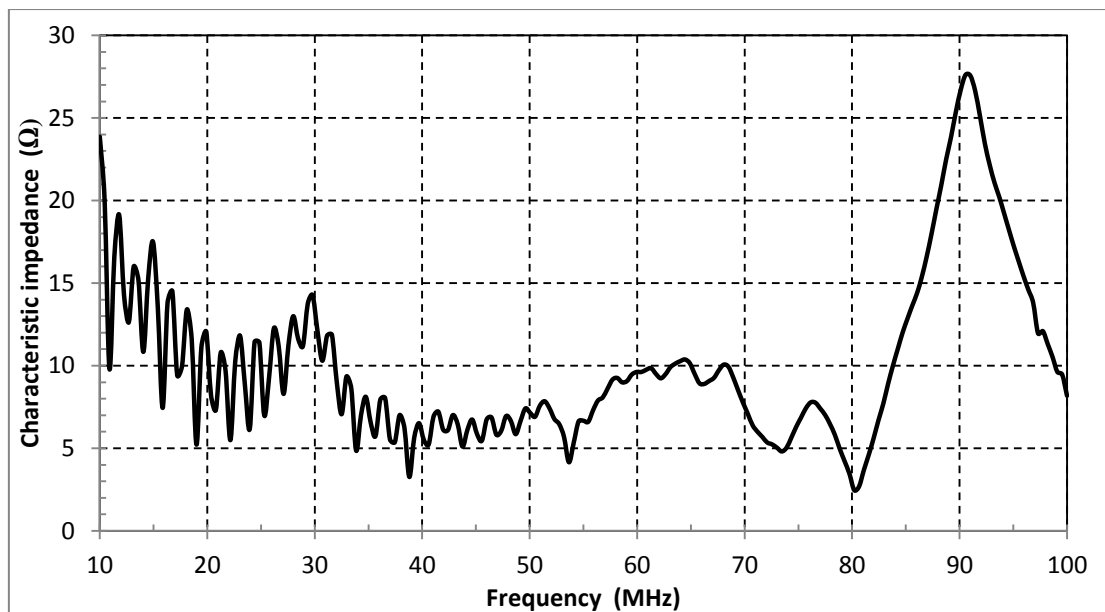


Figure 5.3-9: Characteristic impedance of the cable as a function of frequency in the range of 10 – 100 MHz; the length of the cable is 100 m.

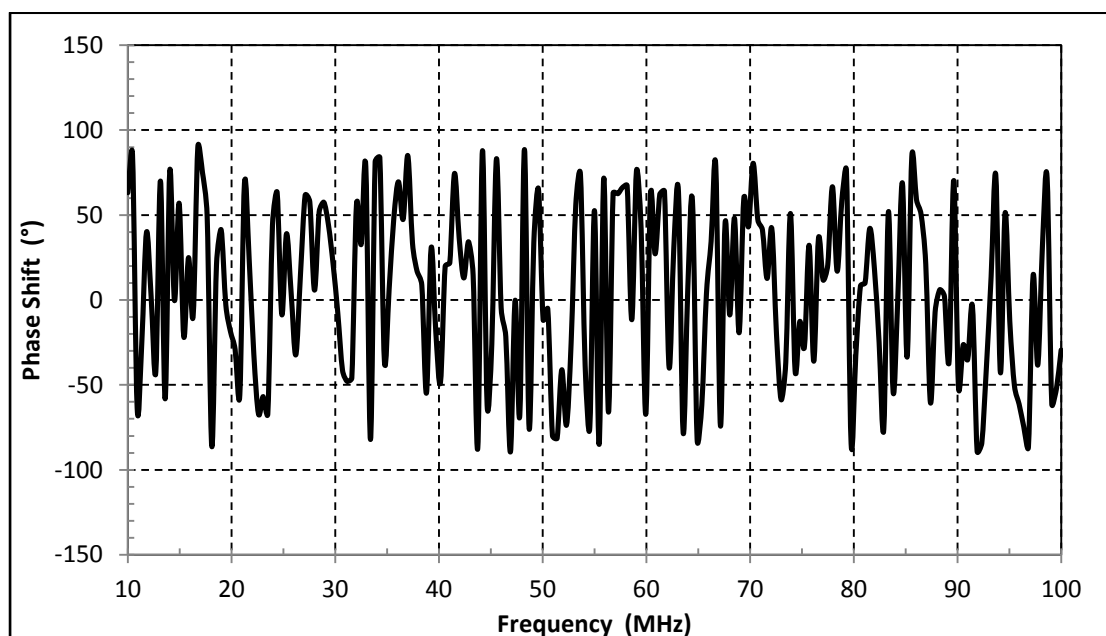


Figure 5.3-10: Phase of the characteristic impedance of the cable as a function of frequency in the range of 10 – 100 MHz; the length of the cable is 100 m.

From Figures 5.3-3 to 5.3-5, we observe that at the cable end there is impedance mismatch. In these figures, there are repeated notches at lower frequencies up to about 55 MHz. In Figure 5.3-3, we observed local peaks along all of frequency range of interest. The maximum impedance value is 14 Ω at 10 MHz while the minimum value is 0 Ω at 80 MHz in Fig. 5.3-5. In Figure 5.3-7, the impedance increases with frequency, it gets the maximum of 399 Ω and the minimum of 70 Ω . In Fig. 5.3-5, the effects of the impedance mismatch, which causes multiple reflections in the cable, can be seen. In the characteristic impedance graph, there are recurring notches and peaks. At the impedance peak, the

cable behaves like a parallel resonance circuit and at the impedance minimum, it behaves like a serial resonance circuit. For a lossless cable, there is infinite input impedance when the cable is in parallel resonance and zero when the cable is in serial resonance. The input impedance phase at resonant frequency is always zero while it is hundreds of ohms in parallel resonance, when the signal frequency is low. The peaks get less pronounced as the signal frequency increases up to 80 MHz then increases sharply up to the maximum of 38Ω at 92 MHz. This implies that as the frequency is increased, the cable losses increase proportionately. If the cable was infinitely long, at high frequencies, the signal would be reflected back and attenuated completely due to impedance mismatch in the cable end before reaching the sending point again.

Figure 5.3-11 shows a 40 m transmission line with diameter of 2.0 mm, with two 5 m branches. During the measurement, the cable was matched with a characteristic impedance $Z_L = 50 \Omega$.

When the load, Z_L is not connected and the end of the cable is opened, $Z_{11 \text{ open}}$ can be written using Equation (5.1). Fig.5.3-12 below shows the relationship between $Z_{11 \text{ open}}$ and the frequency. The maximum value of the open circuit impedance is 11Ω at 10 MHz while the minimum value is 0Ω at 80 MHz. Fig. 5.3-13 shows the real and imaginary parts of the input impedance. At lower frequencies, both component of impedance are highly varying but stabilizes at 40 MHz and beyond.

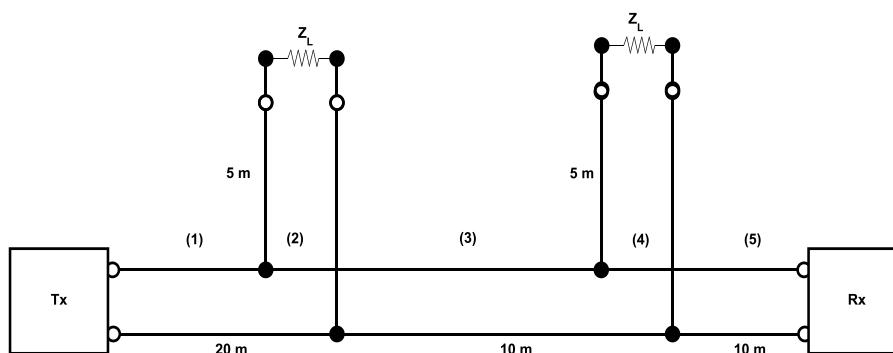


Figure 5.3-11: Network configuration

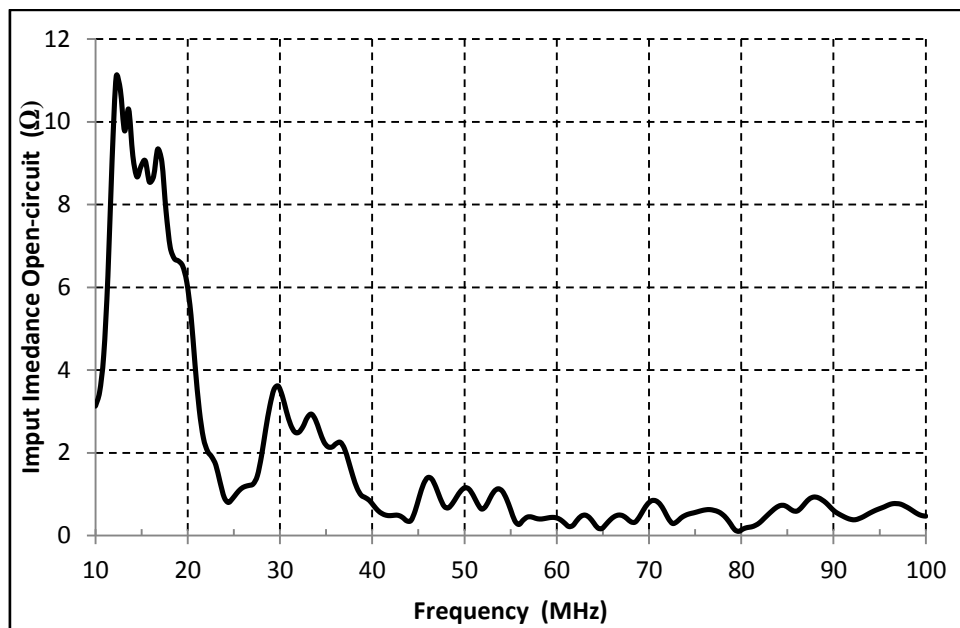


Figure 5.3-12: Input impedance measured when the cable end is open as function of frequency in the range of 10 – 100 MHz; the length of the cable is 40 m with bridge taped with 5 m branch each.

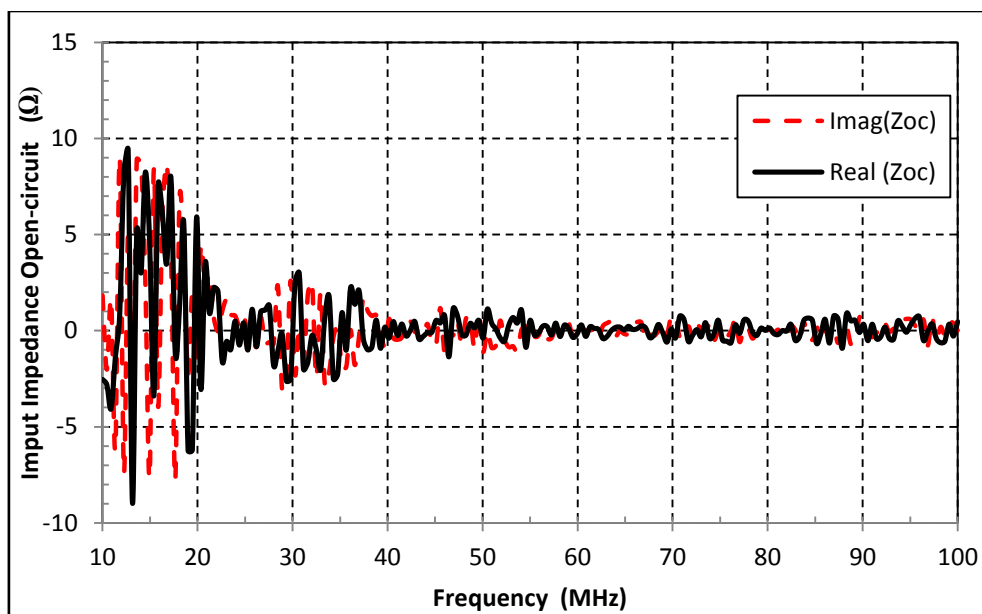


Figure 5.3-13: Input impedance measured when the cable end is open as function of frequency in the range of 10 – 100 MHz; the length of the cable is 40 m with bridge taped with 5 m branch each.

Similarly, when the end of the cable is short-circuited, this means, $Z_L = 0$, the equation for the input impedance $Z_{11short}$ given in Equation (5.2) above. Figure 5.3-14 below shows the relationship between $Z_{11short}$ and the frequency. The input impedance short-circuited is 280 Ω at the maximum at 73 MHz and 60 Ω as the minimum at 10 MHz. Figure 5.3-15, shows the complex input impedance where repeating notches and peaks are observed over the frequency range of interest.

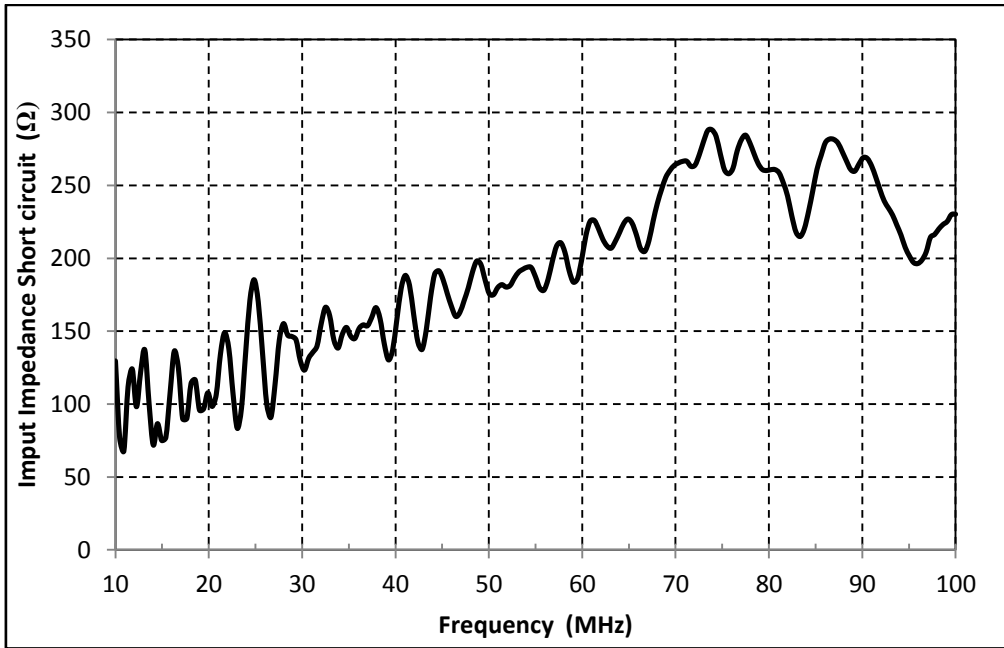


Figure 5.3-14: Input impedance measured when the cable end is short-circuited as a function of frequency in the range of 10 – 100 MHz; the length of the cable is 40 m with bridge taped with 5 m branch each.

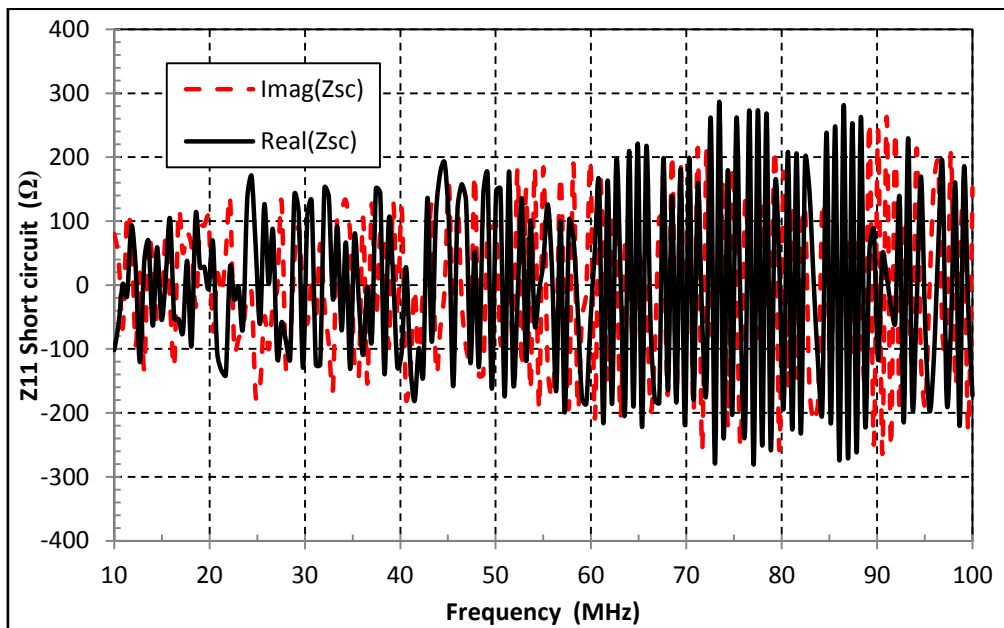


Figure 5.3-15: The real (continuous) and image (dashed) of input impedance measured when the cable end is short-circuited as function of frequency in the range of 10 – 100 MHz; the length of the cable is 40 m with bridge taped with 5 m branch each.

Then Z_o is determined by using the expression in Equation 5.3 and Figure 5.3-16 below shows the relationship between Z_o and the frequency. In the characteristic impedance graph, the peaks get less pronounced as the signal frequency increases, the maximum of 40 Ω in the range of 12 to 15 MHz

and the minimum of 6Ω at 80 MHz. This implies that as the frequency is increased, the cable losses increase proportionately. The input impedance phase at resonant frequency is always zero as seen Fig. 5.3-17. The peaks get less pronounced as the signal frequency increases throughout the frequency range of interest.

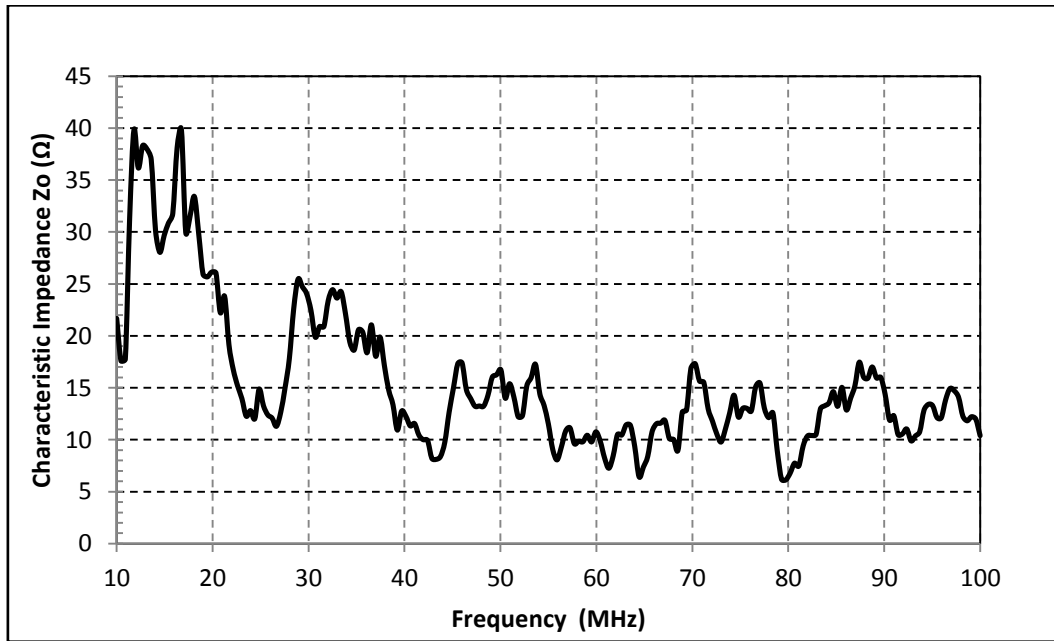


Figure 5.3-16: Characteristic impedance of the cable as function of frequency in the range of 10 – 50 MHz; the length of the cable is 40 m with bridge taped with 5 m branch each.

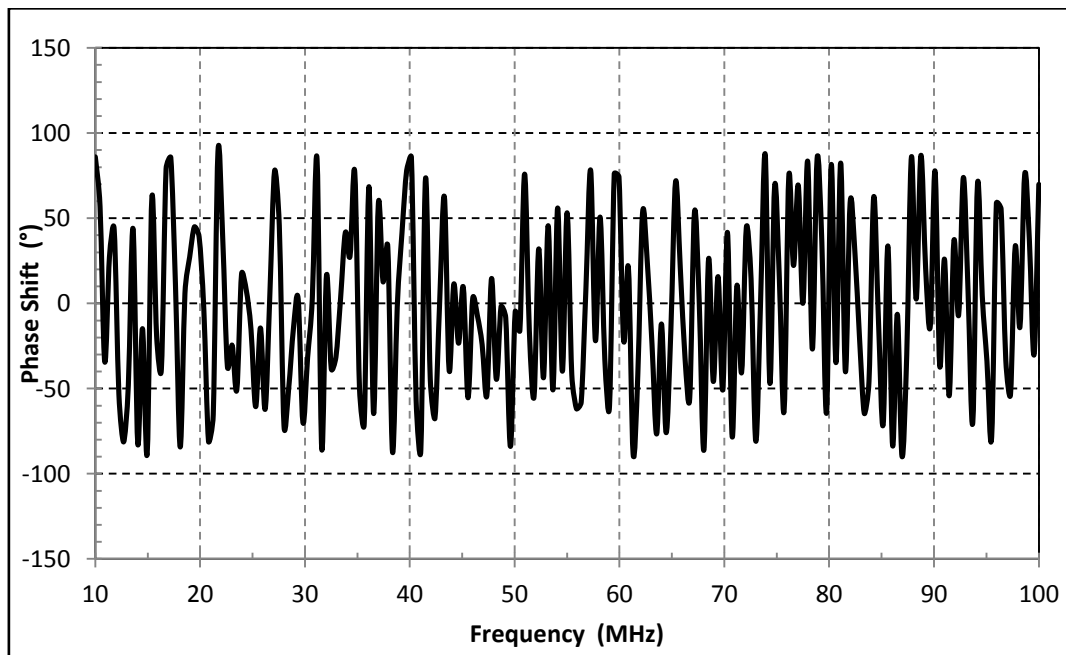


Figure 5.3-17: Phase of the characteristic impedance of the cable as function of frequency in the range of 10 – 100 MHz; the length of the cable is 40 m with bridge taped with 5 m branch each.

The characteristic impedances of the power cables used for measurements are low compared to those of conventional cables used for data transfer, and this is due to the dimensions of the conductor when compared to its layer of insulation. This arises from the design perspective of low voltage power cables, which is to carry low voltages and heavy currents. Generally, the characteristic impedances range between 5 to 50 ohms, and they are dependent on the type of the cable and the type of the signal coupling used. These results are in line with observations made by Aloha *et al.*, (2002) and Aloha *et al.*, (2003).

5.3.2 Attenuation Measurements

The attenuation has been calculated from the input impedance measured data using the propagation constant, Equation (5.10), below and the attenuation is the real part of it.

$$\gamma = \frac{1}{L} \operatorname{arctanh} \sqrt{\frac{Z_{11\text{short}}}{Z_{11\text{open}}}} \quad (5.10)$$

The experimental attenuation of PVC insulated low voltage power cables increases as a function of frequency, even though the relationship of frequency and the attenuation coefficient is not linear. The reasons for the nonlinear behavior of the attenuation coefficient are the dielectric characteristics of the PVC insulation material and skin effect. According to Ahola (2003), both the dielectric constant and the dissipation factor of PVC decrease as a function of frequency at frequencies higher than 1 MHz. Figure 5.3-18 shows the experimental powerline attenuation for the two configurations.

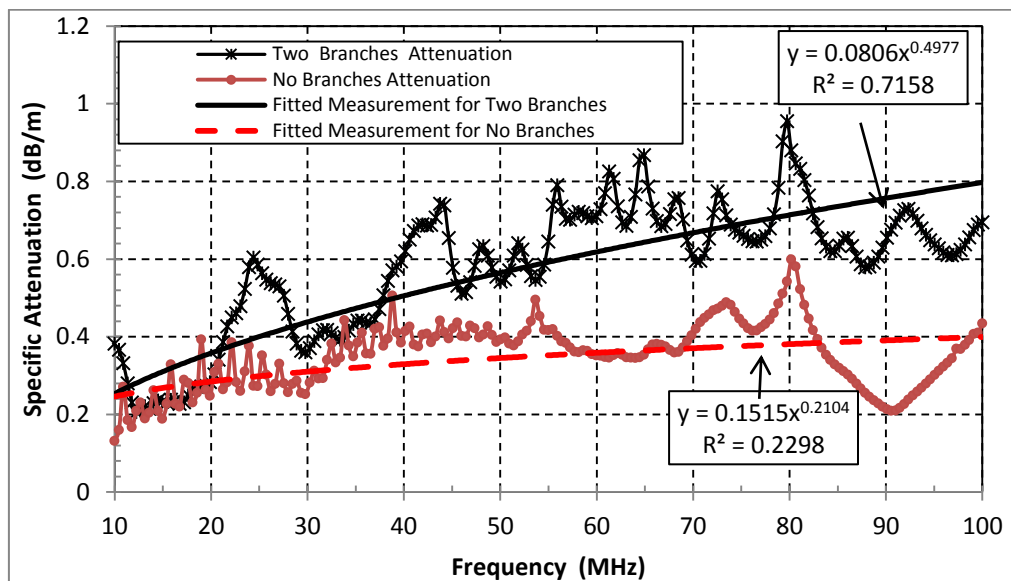


Figure 5.3-18: The specific attenuation of two configuration transmission line.

The frequency in these configurations ranging from 10 MHz to 100 MHz resulted in attenuation range of 0.2 dB/m and 95 dB/m along the two branches transmission line and 0.15 dB/m and 0.6 dB/m along the path for a transmission line without branching. It is observed from these curves that each configuration has its own attenuation values despite the fact that it may be of the same frequency values. In addition, the two-branching configuration experiences comparatively higher attenuation as expected. Again, it can be seen from the measurements that the signal attenuation is directly proportional to the number of branches, and this is the ascertainment made by many previous researchers.

The power-law model was found to result in the best fit for the measured data. Consequently, for the two branches transmission line, with f denoting the frequency in MHz, the fitted model for the specific attenuation, α (dB/m) may be expressed as:

$$\alpha = 807 \times 10^{-4} \times f^{0.4977} \quad (5.11)$$

And for no branches transmission line, the fitted model can be expressed as:

$$\alpha = 1515 \times 10^{-4} \times f^{0.214} \quad (5.12)$$

5.4 Analysis of Powerline Attenuation Models

Figures 5.4-1 to 5.4-2 below show the specific attenuation plots for two network configurations of transmission lines along with Ahola model and our analytical model. Figure 5.4-1 shows, the first configuration, the experimental powerline attenuation, with no branching nodes. The estimated model shown in Equation (4.26) may also be reproduced here as:

$$\alpha = 67 \times 10^{-4} \times f^{0.9601} \quad (5.13)$$

The analytical model RMSE is 0.11 dB while the Ahola model has RMSE is 0.16 dB.

Figure 5.4-1 shows the fitted specific attenuation of two branching nodes of transmission line of 2.5 mm² compared with the Ahola model and the analytical model which is summarized in Table 4.3-1, using Equation (5.14), as:

$$\alpha = 84 \times 10^{-4} \times f^{0.9615} \quad (5.14)$$

Based on RMSE, the analytical model shows the least error with 0.10 dB/m while Ahola model depicts an RMSE error of 0.40 dB/m. The higher attenuation in transmission line can be attributed to dielectric loss as it is shown in Chapter 2 that at higher frequencies, the attenuation due to PVC insulation increases.

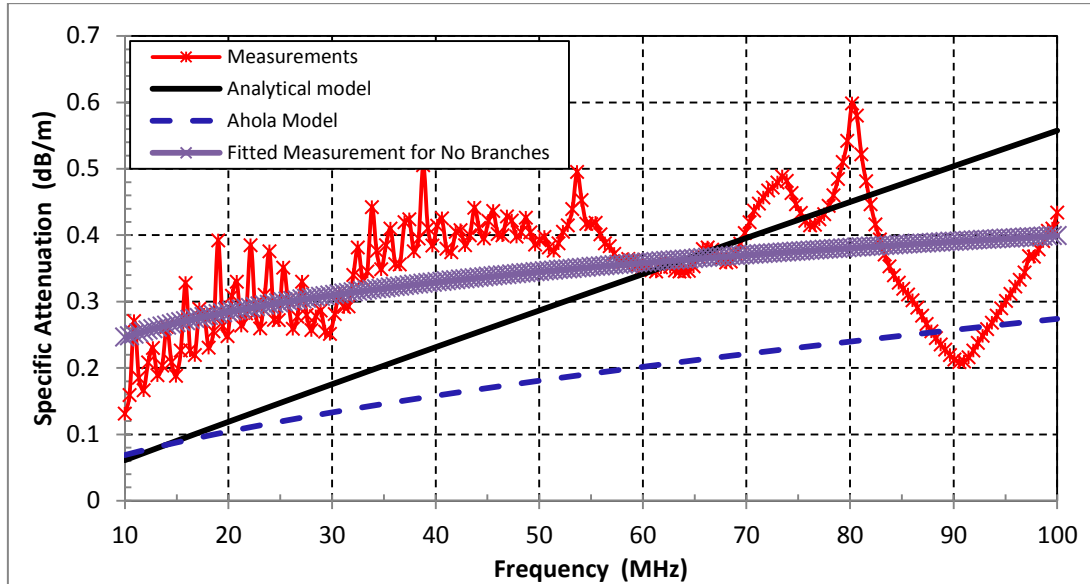


Figure 5.4-1: The specific attenuation of a transmission line without branches, calculated from measured data and estimated model derived from scattering model.

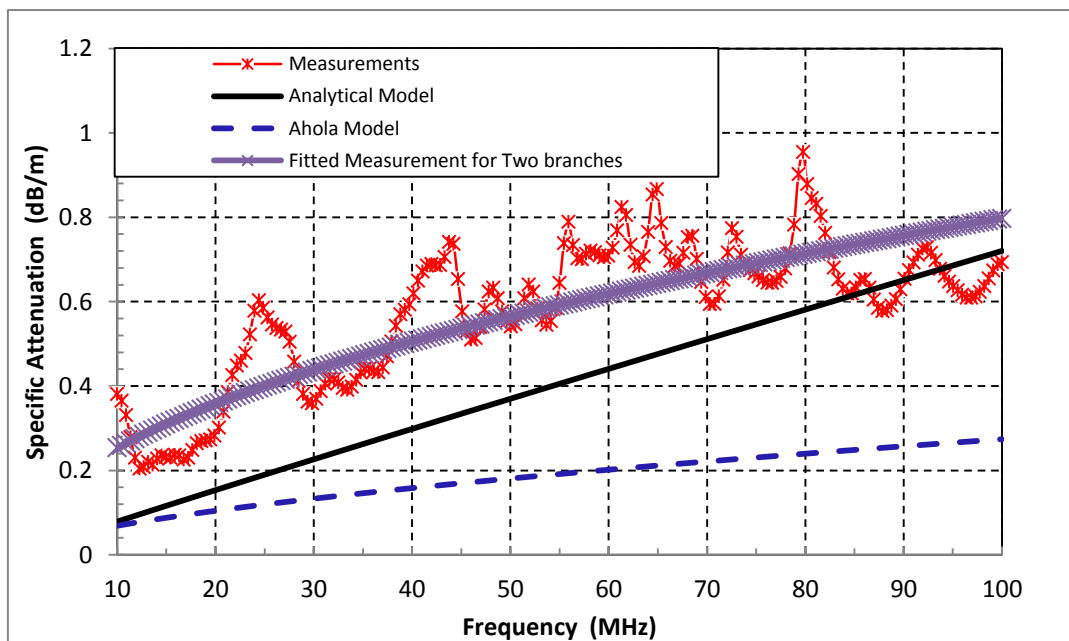


Figure 5.4-2: The specific attenuation of a transmission line with two branching points, calculated from measured data and estimated model derived from scattering model. The length of the cable is 40 m with bridge taped with 5 m branch each.

5.5 PLC Channel Network Measurements

Figure 5.3-11 shows the network topology where the length of the cable is 40 m with bridge taped with 5 m branch each and the channel frequency and phase response were measured using the network analyzer. The simulation and measurement of channel transfer responses of the two branching point transmission line are shown in Figure 5.5-1 Figure 5.5-2 below. In addition, Figure 5.5-2 shows the simulation and measurement of phase shifts of the two branching points transmission line with no load at the branches end.

The simulated and measured frequency responses shown in Fig. 5.5-1 were very close throughout the observation frequency of interest ranging up to 80 MHz. However, at higher signal frequencies for the two-port network, slightly larger differences between simulation and the measurement results were observed. Based on RMSE, the analytical model shows an error of 2.01 dB as compared to the measured model. These results are in line with observations made by Ahola *et al.*, (2002) and Ahola *et al.*, (2003).

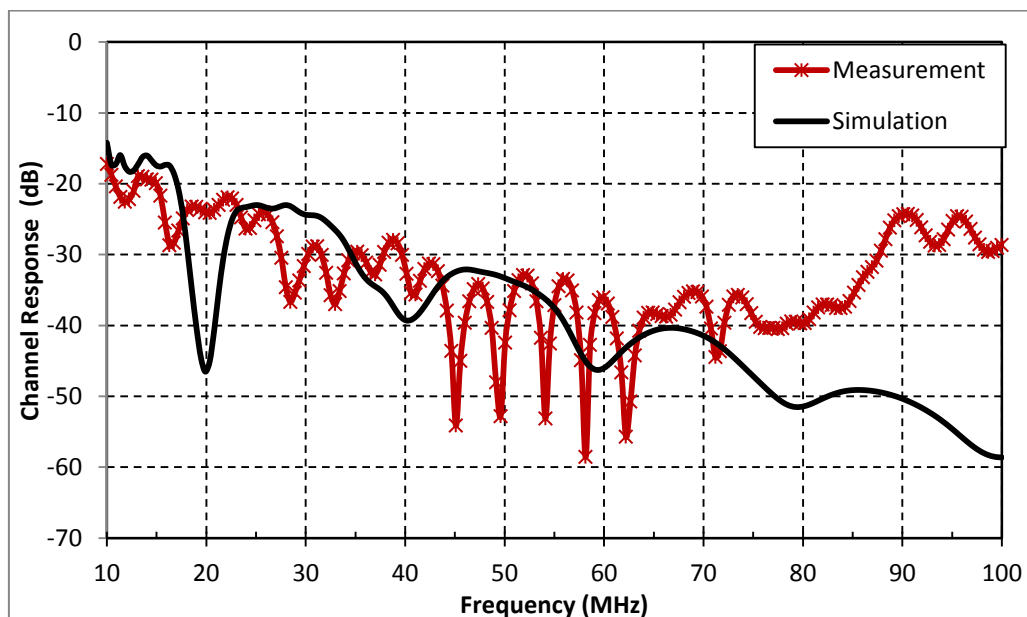


Figure 5.5-1: Channel transfer response with 50Ω load at the branches end.

A comparison between the measured values and the simulation results in Figure 5.5-2 shows a very good agreement up to 70 MHz. The agreement demonstrates applicability of the models in a practical environment. The frequency response periodic ripples are caused by reflections in an open branch. A small frequency response ripple is due to unmatched impedance between the transmitter and receiver. Thus we conclude that the models developed do not require knowledge either of the link topology or

the cable models but requires an extensive measurement campaign. Based on RMSE, the analytical model shows an error of 2.1 dB as compared to the measured model.

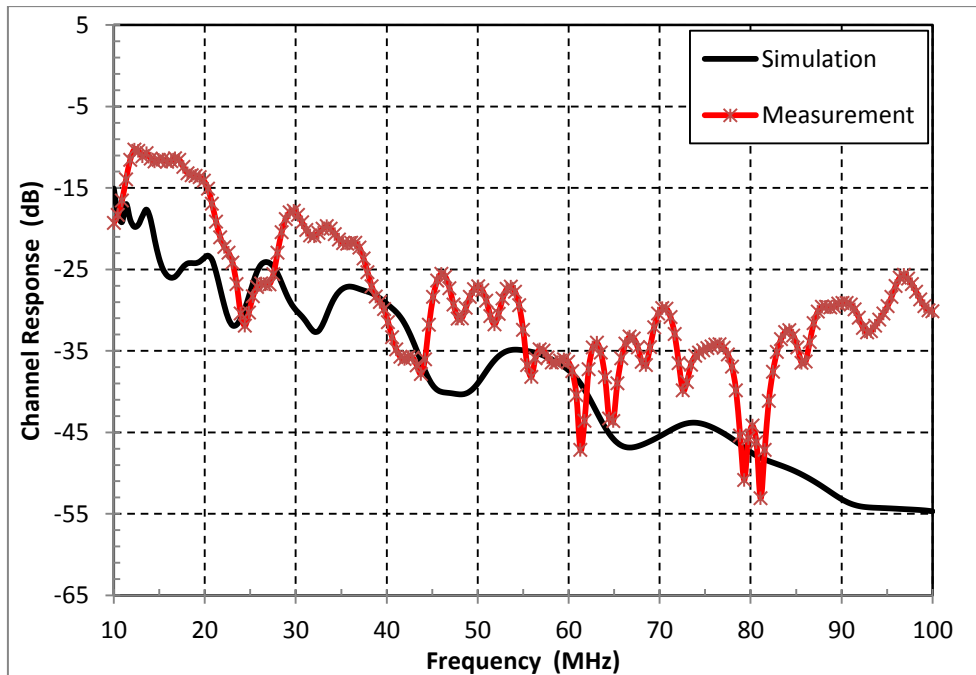


Figure 5.5-2: Channel transfer response with the branches open-circuited.

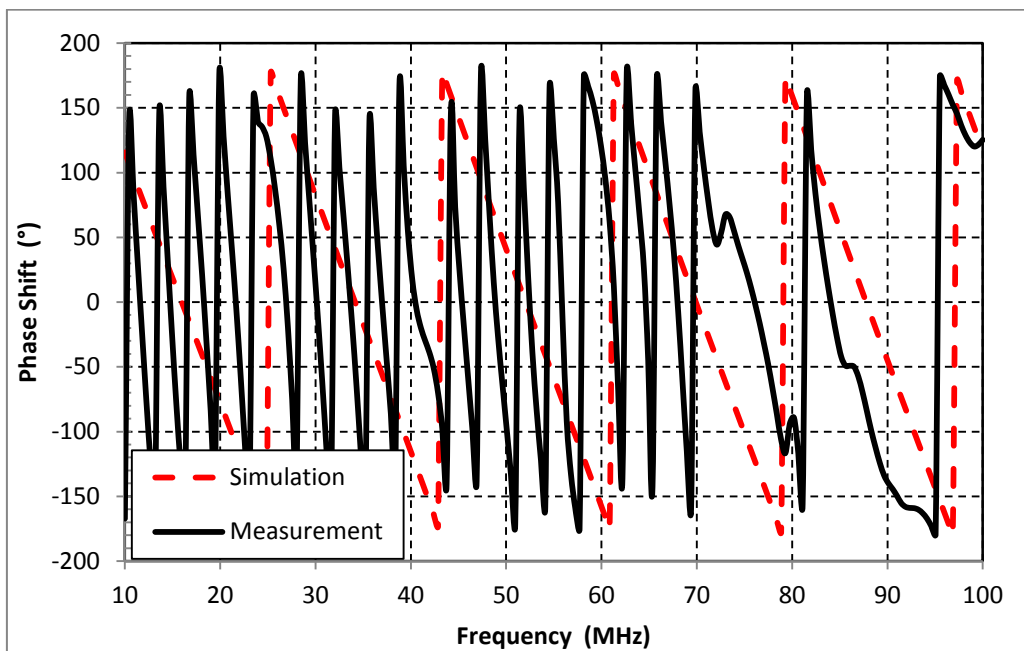


Figure 5.5-3: The phase shift of a bridged tap with the branches open-circuited.

5.6 Chapter Conclusion

In an attempt to validate the analytical framework developed in Chapter 3 and Chapter 4, the measurement data was a vital component of the work. Therefore, this chapter has been useful in the discussion of the measurements with respect to the so developed analytical model for powerline parameters especially the S and Z. The S-parameters were measured and stored from the network analyzer for further analysis. Z-parameters were derived in order to determine characteristic impedance and attenuation from open and short-circuit impedances. The specific attenuation for no-branch network powerline configuration is evaluated by comparing the Ahola model and the analytical model. Based on RMSE, the analytical model shows the least error of 0.10 dB/m while the Ahola model exhibits an RMSE error value of 0.186 dB/m for two-wire transmission line. In addition, for the bridged-taped/ two-branch network transmission line the analytical model shows the least error of 0.10 dB/m while Ahola model has 0.40 dB/m. Again, it can be seen from the measurements that the signal attenuation is directly proportional to the number of branches, and this is the ascertainment made by many previous researchers. The standard transmission matrix theory and two-port network models were applied as a modelling tool. The simulated and measured frequency responses were very close for frequencies up to 15 MHz. However, at higher signal frequencies, slightly higher differences between the two-port network model and the measurement results were similarly observed as reported by Ahola *et al.*, (2002) and Ahola *et al.*, (2003). The attenuation of the signal in the PLC channel is determined by the cable characteristics, cable length, network topology and electric appliances connected to the network.

A comparison between the measured values and the simulation results of the frequency response shows a very good agreement. The agreement demonstrates applicability of the models in a practical environment. The frequency response periodic ripples are caused by reflections in an open branch. A small frequency response ripple is due to unmatched impedance between the transmitter and receiver. Thus we conclude that the models developed do not require knowledge either of the link topology or the cable models but requires an extensive measurement campaign.

5.7 References

- Ahola J., T. Lindh, and J. Partanen, (2002), "Determination of Properties of Low Voltage Power Cables at Frequency Band 100 kHz – 30 MHz," ICEM 2002, Bruges, Belgium, August 26-28, 2002.
- Ahola J., (2003), "Applicability of Powerline Communications to Data Transfer of Online Condition Monitoring of Electrical Drives," PhD thesis, Lappeenranta University of Technology, Aug.

Chapter Six

Conclusions and Recommendation for Future Work

6.1 Conclusions

In Chapters four and five, the main results of this thesis work are summarised. The main scientific contribution in this research work is comprised of measurements, analysis and modelling of low voltage power cables (CABTYRE CABLE- FLEXIBLE WIRING CABLE (300/500 V)) in the frequency range 10 MHz – 100 MHz.

In Chapter four, we modelled the transmission line as one single element, by dividing its length into a grid of small areas, where each small area transmits an echo and the forward scattered response gets to receiver based on the validation of the assumption of a randomly spread multitude of scatterers in the vicinity of the channel that only requires a sufficient number impedance discontinuity points.

There are many factors that influence reliable high-speed data communication on single-phase low voltage (LV) networks. Among these, the distribution of scattering points that lead to signal attenuation is a critical one, which must be studied extensively. By knowing the amplitude distributions of the first path in the network, which followed a lognormal distribution, the scatterers distribution was derived. The input parameters N_t , μ , and σ were obtained by using Monte Carlo simulations with a corresponding number of branching nodes(x).

In Section 4.2, an analytical model of scattering size distribution and probability density distribution in broadband PLC channels is presented. The analysis performed show that there are more scattering points at lower diameter sizes of branches of indoor networks where the peak is reached at a mean diameter of 0.8 mm, which implies more reflections of the signal. In fact, there is extensive coupling and uncoupling of appliances connecting to the branches of this mean diameter in indoor single-phase networks. But on the high diameter range (above 2 mm), scattering points are smaller and the reflection is less. Also, the results show the independency of the distributions towards the indoor network topology.

In Section 4.3, a specific attenuation model of a powerline network using Mie scattering theory was developed at the nodes where mismatch occurs. The proposed model was estimated for different

number of branching nodes. By using the frequency range of 10 MHz to 100 MHz, we compared the proposed model with the theoretical attenuation. The results showed that the proposed model underestimates the attenuation at the frequencies below 20 MHz and overestimates the attenuation value at the frequencies above 50 MHz compared to the theoretical attenuation. Also, we developed a power law model that relies on the knowledge of the number of branching nodes in the network and thus, the attenuation can be predicted from this model. We also investigated the phase shift that occurs in the PLC channel due to a varying number of branches.

In chapter five, the characteristics of two low voltage power cables (CABTYRE CABLE- FLEXIBLE WIRING CABLE (300/500 V)) were measured and modelled in the frequency band 10 MHz – 100 MHz. From the measurements, the transmission line parameters of the cables were determined and the attenuation results obtained were very close to those obtained using the analytical model.

The characteristic impedances of the power cables used for measurements are low compared to those of conventional cables used for data transfer, and this is due to the dimensions of the conductor when compared to its layer of insulation. This arises from the design perspective of low voltage power cables, which is to carry low voltages and heavy currents. Generally, the characteristic impedances range between 5 to 50 ohms, and they are dependent on the type of the cable and the type of the signal coupling used.

The attenuation of the signal in the transmission line increases as a function of frequency. In the frequency band 10 MHz – 100 MHz, the main loss mechanism of the low voltage power cable is the dielectric loss of the PVC insulation material used. From the measurements, due to the fact that we recorded the lowest characteristic impedances at 80 MHz, the signal attenuation in the two bridge-taped transmission line is approximately 0.95 dB/m at the signal frequency of 80 MHz and it is approximately 0.60 dB/m for a transmission line without any branches at the same frequency. Thus, the attenuation is inversed proportional to the characteristic impedances.

The standard transmission matrix theory and two-port network models were applied as a modelling tool. The simulated and measured frequency responses were very close for frequencies up to 15 MHz. However, at higher signal frequencies, slightly higher differences between the two-port network model and the measurement results were observed. The attenuation of the signal in the PLC channel is determined by the cable characteristics, cable length, network topology and electric appliances connected to the network.

In the CENELEC frequency band 3-148.5 kHz, the losses in low voltage transmission line cable are low. Notches in the frequency responses of PLC channels may occur. These are caused by the serial

resonances of the electric appliances connected to the network. Due to the fact that the length of cabling is limited and the carrier frequencies are relatively low, the notches and peaks in the frequency response caused by the standing waves are rare. The phase response in the CENELEC band can be considered to be relatively linear due to the missing standing waves.

In the studied frequency range of 10 MHz – 100 MHz, for the measurements done, the attenuation of the signal in the PLC channels increases due to the increasing losses of the cabling. The length of the transmission line does not limit the formation of standing waves. Additionally, electric appliances connected to the network are mismatched loads in the whole frequency band. Hence, standing waves are formed which can be noticed in the frequency responses of the power-line channels as frequently repeating notches and peaks. Correspondingly, the phase response at the frequencies of notches and peaks is nonlinear and may cause problems in data transfer applications. Lastly, it is seen from the measurements that the signal attenuation is directly proportional to the number of branches, and this confirms the findings made by previous researchers in the same field.

In summary, this thesis puts forward a different class of modeling approach towards powerline communications. Much emphasis is made for the no-branch and two-branch network to validate the proposed framework. Overall, the measurement results show that both the analytical specific attenuation model so developed in this work and the channel transfer function are feasible novel ideas in PLC channel network characterization. A comparison between the measured values and the simulation results of the frequency response shows a very good agreement. Thus, we conclude that the models developed do not require knowledge either of the link topology or the cable models but requires an extensive measurement campaign.

6.2 Recommendation for Future work

Designs that incorporate multiple-branch network will provide more insight into the future of such modeling for powerline communications. Besides, the provably practical assumptions of the scattering point sizes may require more regression analysis if optimization is to be taken into account. Also, possible enhancements to improve on the performance of the PLC channels, like coding and modulation are worth exploring. Modeling and characterization of the channel noise through measurements also provide an avenue for possible future work.

References

Ahola J., T. Lindh, and J. Partanen, (2002), "Determination of Properties of Low Voltage Power Cables at Frequency Band 100 kHz – 30 MHz," *ICEM*, Bruges, Belgium, August 26-28.

Ahola J., (2003), "Applicability of Powerline Communications to Data Transfer of Online Condition Monitoring of Electrical Drives," PhD thesis, Lappeenranta University of Technology, Aug.

Amirshahi, P. and M. Kavehrad (2006), "High-Frequency Characteristics of Overhead Multiconductor Power Lines for Broadband Communications," *IEEE Journal on Selected Areas in Communications*, Vol. 24, No. 7, July, pp. 1292-1303.

Anatory, J., M.M. Kissaka and N.H. Mvungi, (2006), "Powerline Communications: The effects of Branches on the network performance", *IEEE-ISPLC2006*, Florida, USA, March. pp. 70-75.

Anatory, J., N. H. Mvungi, and M. M. Kissaka, (2004), "Analysis of Powerlinechannel Model for Communication from Primary Substation Node to End-Users" *Iranian journal of electrical and computer engineering*, vol. 3, No. 1, winter-Springer.

Anatory, J., N. Theethayi, R. Thottappillil, M.M. Kissaka and N.H. Mvungi, (2005), "The effects of Interconnections and Branched Network in the Broadband Power line Communications", *International Gathering of Radio Science*, India, 23rd –29th October.

Anatory, J., M. M. Kissaka and N. H. Mvungi, (2007a), "Channel Model for Broadband Power line Communication," *IEEE Trans. On Power Delivery*, January, No. 1, pp. 135-141.

Anatory, J., N. Theethayi, R. Thottappillil, M.M. Kissaka and N.H. Mvungi (2007b), "The Effects of Load Impedance, Line Length and Branches in the BPLC- Transmission Lines Analysis: A Case of Indoor Voltage Channel", *IEEE Trans. On Power Delivery, October*, Vol.22, No 4, pp 2150-2155.

Anatory, J., Nelson Theethayi, Rajeev Thottappillil, M.M. Kissaka and N.H. Mvungi, (2007c), "Broadband Power line Communications: Factors Influencing the Signal propagations in the Medium Voltage Lines", *IEEE ISPLC*, Pisa, Italy, 26-28, March.

Anatory, J., M.M. Kissaka and N.H. Mvungi, (2006), "Power line Communications: The effects of Branches on the network performance", *IEEE-ISPLC*, Florida, USA, March.

Barmada, S. and A. Musolini, (2006), “ Innovative Model for Time-Varying Power Line Communication channel Response Evaluation,” *IEEE Journal on Selected Areas in Communications*, Vol. 24, No. 7, July, pp1317-1326.

Biglieri, B. (2003), “Coding and Modulation for a Horrible Channel,” *IEEE Communications Magazine*, May, pp. 92-98.

Bohren, C. F and D. R. Huffman, (2004) “*Absorption and scattering of light particles,*” Wienheim, John Wiley.

Brown, P. A. (1995), “High frequency conditioned power networks,” in *UTC Annu. Conf. Proc.*, July/Aug.

Göran Lindell, (2001), “On Coding and Modulation for the PowerlineCommunication Channel”, *Proceeding of ISPLC channel*, Sep., pp. 14-17.

Chen, Y. and T.D. Chiueh, (2002), “Baseband Transceiver Design of a 128 kbps Powerline Modem for Household Applications,” *IEEE Trans. Power Delivery*, vol. 17, no.2, Apr. pp. 338-44.

Dlh'aň, Farkač (2008), “Impulsive Noise Cancellation in Systems with OFDM Modulation” *Journal of Electrical Engineering*, Vol. 59, No.6, pp310-316.

Dostert, K. (1997), "Telecommunications over power distribution grid: Possibilities and limitations," *ISPLC'1997*, Essen Germany.

Esmailian, T., P.G. Gulak, and F.R. Kschischang, (2000)“A discrete multitone power line communications system,” *Proc. of ICASSP'00*, vol. 5, pp. 2953-2956, Jun.

Feynman, R. P., Robert B. Leighton and M. Sands, (1964), “The Feynman Lectures on Physics”, *Vol. No.2*, Addison-Wesley.

Galli, S., A. Scaglione, and Z. Wang, (2011), “For the grid and through the grid: the role of power line communications in the smart grid,” *Proceedings of the IEEE*, vol. 99, no. 6, pp. 998–1027.

Guillet, V., G. Lamarque, P. Ravier and C. Leger, (2009), “Improving the power line communication signal-to-noise ratio during a resistive load commutation,” *Journal of Communications*, Vol. 4, No. 2, March, pp126-132.

Hudson, A. G., D. R. Beuerle and H. J. Fiedler, (1976), "SSB Carrier for utility control and communication," *Proc. of IEEE National Telecommunication Conf.*, pp. 2. 1.1-2.17.

Hooijen, O. G. (1998), "On the Relation between Network Topology and Power Line Signal Attenuation", *ISPLC'98, Tokyo, Japan*, March 24-26.

Liu, E., Y. Gao, G. Samdani, Omar Mukhtar, and T. Korhonen, (2005), "Broadband powerlinechannel and capacity analysis," *ISPLC channel 2005*, pp.7-11, April.

Lokken, G., N. Jagoda and R. J. D'Auteuil, (1976), "The Proposed Wisconsin Electric Power Company Load Management System Using Power Line Over Distribution Lines," *IEEE Proc. of IEEE National Telecommunication Conf.*, pp. 2.2.1-2.2.3.

Katayama, M., T. Yamazato, and H. Okada (2006) "A Mathematical Model of Noise in Narrowband Power Line Communication Systems," *IEEE Journal on Selected Areas in Communications*, Vol. 24, No. 7, July, pp1272-1280.

Malack, J.A. and J.R. Engstrom, (1976) "RF Impedance of United States and European Power Lines" *IEEE Trans. Electromagnetic Compatibility*, vol. EMC-18, pp. 36-38, February.

Markus Sebeck and Gerd Bumiller, (2000) "A Network Management System for PowerlineCommunication and its Verification by Simulation", *Proceeding of ISPLC channel, Limerick, Ireland*, April, pp.225-232.

Matov, A. (2001). "A Planning Tool for High Bit Rate Transmission over Power Line Communication Channels *Proceeding of ISPLC channel*, pp. 15-20. Malmö, Sweden, April.

Mätzler, C. (2002a), Effects of Rain on Propagation, Absorption And Scattering of Microwave Radiation Based on The Dielectric Model of Liebe, *IAP Res. Rep. No. 02-10*, University of Bern, June.

Mätzler, C. (2002b), MATLAB Functions for Mie Scattering and Absorption, Version 2, *IAP Res. Rep. No. 08*, University of Bern, Switzerland, June.

Meng, H., S. Chen, Y.L. Guan, C. Law, P.L. So, E. Gunawan and T.T. Lie, (2004), "Modeling of Transfer Characteristics for the Broadband Power Line Communication Channel," *IEEE Trans. Power Delivery*, Vol. 19, No. 3, July, pp. 1057-1064.

Mujčić, A., N. Suljanović, M. Zajc, J. F. Tasič, (2004) "Corona noise on the 400 kV overhead power line - Measurements and Computer Modelling," *Springer Journal of Electrical Engineering*, Vol. 86, No.2, January, pp61-67.

Mulangu, C.T and T. J. Afullo, (2009) "Variability of the Propagation Coefficients Due to Rain for Microwave Links in Southern Africa", *Radio Sci.*, Vol. 44.

Mulangu, C.T, T. J. Afullo and N. M. Ijumba, (2012a) "Scattering points Size Distribution for Indoor Broadband PLC channel Channels", *PIERS Progress In Electromagnetics Research Symposium. PIERS 2012*, ISSN: 1559-9450, Kuala Lumpur, Malaysia, March.

Mulangu, C.T., T. J. Afullo and N. M. Ijumba, (2012b) "Estimation of Specific Attenuation due to Scattering Points for Broadband PLC channel Channels", *PIERS Progress In Electromagnetics Research Symposium. PIERS*, , ISSN: 1559-9450, Kuala Lumpur, Malaysia, March.

Dostert, K. (1997), "Telecommunications over power distribution grid: Possibilities and limitations," *Proceeding of ISPLC channel*, Essen Germany.

Okada, M., S. Hara, and N. Morinaga, (1993) "Bit error rate performances of orthogonal multicarrier modulation radio transmission systems," in *IEICE Trans. Communications*, vol. E76-B, Feb. pp. 113–119.

Olsen, R. L., D. V. Rogers and D. B. Hodge, (1978), "The aR^b Relation in the Calculation of Rain Attenuation," *IEEE Trans. Antennas Propagat.*, AP-26(2), pp. 318-329.

Papaleonidopoulos, I. C., C. N. Capsalis, C. G. Karagiannopoulos and N.J. Theodorou, (2003), "Statistical Analysis and Simulation of Indoor Single-Phase Low Voltage PowerlineCommunication Channels on the basis of Multipath Propagation," *IEEE Trans. Consumer Electronics*, Vol.49, No. 1, pp. 89-99, February.

Papaleonidopoulos, I. C., C. N. Capsalis, C.G. Karagiannopoulos, N. J. Theodorou, C. E. Anagnostopoulos and I. E. Anagnostopoulos, (2002), "Modelling of Indoor Low-Voltage Cables in the High Frequency range," in *Proc. ISPLC'97*, pp. 267-271.

Papaleonidopoulos, I.C., C.G. Karagiannopoulos and N.J. Theodorou, (2002), "Modelling Of Indoor Low Voltage Powerline Cables In The High Frequency Range", in *Proc. Int. Symp. Power-lines Comm.*, Athens, Greece.

Pahlavan, K. and A.H. Levesque, (1995) "*Wireless Information Networks*", John Wiley & Sons, Inc.: New York, pp. 37-142.

Philippis, H. (1999). "Modelling of Powerline Communication Channels," in *Proc. ISPLC*, pp. 14-21.

Philippis, H., (1998). "Performance Measurements of Powerline Channels at High Frequencies", in *Proc. ISPLC*, Tokyo, Japan, March, p. 229-237.

Philippis, H., (2000), "Development of a Statistical Model for Power Line Communications Channels," *ISPLC*, Limerick, Ireland, April.

T. S. Rappaport, (1996). *Wireless Communications: Principles and Practice*. Upper Saddle River, NJ: Prentice-Hall.

R'oka and Urminsk', (2008) "Experimental Measurements for Verification of the Parametric Model For Reference Channels In the Real PLC channel Environment," *Journal of Electrical Engineering*, Vol. 59, No.3, pp. 146-152.

Güzelgöz, S., H. B., Çelebi, and H. Arslan,(2011)," Statistical Characterization of the Paths in Multipath PLC channel Channels", *IEEE Trans. On Power Delivary*, vol.26, No.1, January.

Tsuzuki, S., T. Takamatsu, H. Nishio and Y. Yamada, (2002) "An estimation method of the transfer function of indoor powerline channels for Japanese houses" in *Proc. Int. Symp. Power-lines Comm.*, Athens, Greece, pp.55-99.

Vandendorpe, L. (1993) "Multitone system in an unlimited bandwidth multipath rician fading environment," in *Proc., IEE Mobile and Personal Communications Conf.*, Dec. pp. 114–119.

Zimmermann, M., and K. Dostert, (1999). "A Multi-Path Propagation Model for the Power-Line channel in the High Frequency Range," in *Proc. ISPLC*, pp. 45-61.

Zimmermann, M. and K. Dostert, (2002), "A Multi-Path Model for the Powerline Channel," *IEEE Transactions on communications*, vol. 50, No. 4, April, pp. 553-539.